공학박사 학위논문

Critical Crack Path Dependent Shear Strength Models of Concrete Beams without Web Reinforcement

위험 파괴 균열 경로를 고려한

콘크리트 보 부재의 전단강도 모형

2012년 8월

서울대학교 대학원

건축학과

임 우 영

Critical Crack Path Dependent Shear Strength Models of Concrete Beams without Web Reinforcement

위험 파괴 균열 경로를 고려한

콘크리트 보 부재의 전단강도 모형

지도 교수 홍 성 걸

이 논문을 공학박사 학위논문으로 제출함

2012년 6월

서울대학교 대학원

건축학과

임 우 영

임우영의 공학박사 학위논문을 인준함

2012년 6월

위 원 장 _____ (인)

부위원장 _____ (인)

위 원 _____ (인)

위 원 _____ (인)

위 원 _____ (인)

Abstract

Critical Crack Path Dependent Shear Strength Models of Concrete Beams without Web Reinforcement

Lim, Woo Young

Department of Architecture and Architectural Engineering

The Graduate School

Seoul National University

This dissertation aims at estimating the critical crack path dependent shear strength of reinforced concrete beams without web reinforcement and investigating size effect by using the mixed mode fracture in linear elastic fracture mechanics (LEFM) approach. This approach has been supplied the theoretical basis for size effect in shear strength because the stress states at the crack tip can be expressed as a function of crack length.

Even though the efforts of numerous experimental and analytical studies for shear strength and size effect of reinforced concrete beams, a fundamental theory explaining the size effect and shear failure mode of slender and deep beams without web reinforcement considering critical crack path is still missing. Current code provisions and many existing models are based on empirical and statistical considerations.

To determine the shear strength and investigate the size effect of reinforced concrete beams, a failure mechanism based on the critical crack path and crack length was proposed. This study assumes biaxial stress fields at the diagonal critical crack tip in both diagonal tension failure and sliding failure modes. The transition area which is located from uniaxial stress states below the neutral axis of beams to biaxial stress states above the neutral axis requires the change of primary fracture mode. This failure is defined as material failure such as separation and sliding. To provide the deformation dependent strength model, the modified Mohr-Coulomb criteria was used and failure mechanism was investigated by using concrete failure criteria. For investigating the stress states at critical diagonal crack tip, size dependent critical stress intensity factors for mode-I and mode-II fracture expressed in terms of ultimate stresses determined by material failure criteria and crack length were proposed. From the relationship between the stress intensity factor and critical stress intensity factor, it is recognized that size effect is related to the crack length for both mode-I and mode-II fracture.

To obtain the shear strength of slender beams without web reinforcement, failure modes are classified into diagonal tension failure and sliding failure on the basis of critical crack path. And it is assumed that softening occurs at cracked section in the compression zone. In addition a newly flexural-shear behavior of reinforced concrete beams without web reinforcement based on the concrete strain for diagonal tension failure and sliding failure was proposed. The ultimate shear strength is determined at the intersection between flexural behavior curves and shear limit curves represented the softening.

To determine the shear strength of deep beams without web reinforcement, behavior of prismatic body of concrete subjected to uniaxial compression was investigated. Both normal stress and shear stress assume to exist in the prismatic body on the basis of theory of elasticity. As a result, deep beams also showed the size effect for effective depth.

Proposed models are to estimate the shear strength of reinforced concrete slender and deep beams without web reinforcement. The proposed theory accurately predicts the experimental results for the ultimate shear stress of slender and deep beams with various strengths of concrete, steel ratio, shear span-to-depth ratio and effective depth.

Finally, the proposed theoretical models based on the critical crack path and crack length are more reasonable to explain the size effect of reinforced concrete beams than existing models.

Keywords : critical crack path, shear strength, size effect, critical stress intensity factor, mixed mode fracture, failure mechanism

Student Number : 2007-30163

Table of Contents

Abstract ..... **i**

Table of Contents ..... **iv**

List of Figures ..... **viii**

List of Tables ..... **xiv**

Notations ..... **xv**

1. Introduction 1

1.1 Research Background and Problem Statements 1

1.2 Research Objectives and Scope 4

1.3 Organization of the Dissertation 5

2. Literature Review 6

2.1 Current Design Provisions 6

2.1.1 ACI 318-08 Building Code 6

2.1.2 CEB-FIP Model Code 1990 7

2.1.3 Eurocode 2 8

2.1.4 JSCE 10

2.2 Previous Researches 11

2.2.1 Fracture Mechanics Approach 11

2.2.2 Strut-and-Tie Model 16

2.2.3 Deformation based Design 18

2.2.4 Regression Analysis 21

2.3 Review 22

3. Behavior of Concrete 24

3.1 Uniaxial Compression 24
3.2 Uniaxial Tension 24
3.3 Biaxial Stress Behavior 26
3.4 Softening of Concrete 27
3.3 Summary 34
4. Fracture Mechanics of Concrete 35
4.1 Linear Elastic Fracture Mechanics 35
4.2 Stress Intensity Factor 37
4.3 Critical Stress Intensity Factor 42
4.4 Material Properties and Nonlinear Zone 43
4.4.1 Nonlinear Behavior of Concrete 43
4.4.2 Concrete Crack and Fracture Process Zone 45
4.6.3 Fracture Process zone for Mixed Mode Fracture 47
4.5 Size Dependent Critical Stress Intensity Factor 51
4.6 Size Effect 54
4.6.1 Size Effect of Linear Elastic Materials 54
4.6.2 Size Effect of Concrete Structures 55
4.7 Mixed-Mode Fracture of Concrete Beams 58
4.7.1 Introduction 58
4.7.2 Size Dependent Effective Stress Intensity Factors 61
4.8 Summary 67
5. Flexural Behavior of Reinforced Concrete Beams without Web Reinforcement 68
5.1 Introduction 68
5.2 Moment-Curvature Relationship 69
5.3 Depth of neutral axis 72

5.4 Moment Capacity 79
5.5 Summary 82
6. Critical Crack Path Dependent Shear Strength 83
6.1 Introduction 83
6.2 Crack Path Dependent Failure Mechanism 84
6.2.1 Characteristics of Critical Diagonal Crack 84
6.2.2 Failure Mechanisms 86
6.3 Diagonal Cracking Strength 88
6.3.1 General 88
6.3.2 Effective Stress Intensity Factor 88
6.3.3 Critical Stress Intensity Factor 91
6.3.4 Shear Strength of Flexural Tension Zone 96
6.4 Shear Strength for Diagonal Tension Failure 103
6.4.1 General 103
6.4.2 Failure Criteria 103
6.4.3 Effective Stress Intensity Factor 105
6.4.4 Shear Strength 108
6.4.5 Verification and Effect of Primary Parameters 114
6.5 Shear Strength for Sliding Failure 122
6.5.1 Introduction 122
6.5.2 Shear Transfer across a crack 123
6.5.3 Failure Criteria 127
6.5.4 Shear Strength 131
6.5.5 Verification 135
6.5.6 Summary 139
6.6 Shear Strength of Reinforced Concrete Short Beams without Web

Reinforcement 141
6.6.1 Introduction 141
6.6.2 Failure Mode of Diagonal Strut 142
6.6.3 Uniaxial Compression 143
6.6.4 Stress Concentrations 144
6.6.5 Concentrated Load at a Point of a Straight Boundary 144
6.6.6 Sliding Failure of Prismatic Body 148
6.6.7 Shear Strength of Short Beams 157
6.6.8 Verification 159
6.6.9 Summary 163
7. Summary and Conclusions 165
7.1 Summary 165
7.2 Conclusions 166

References 168
Appendix 176
초 록 184

List of Figures

Figure 1.1 Influence of various design parameters: (a) concrete strength, $f_c^{'}$; (b) reinforcement steel ratio, ρ; (c) shear span-to-depth ratio, a/d; (d) effective depth, d (data from Reineck et al. 2003) 1

Figure 1.2 Influence of member size and maximum aggregate size on shear stress at failure (Collins et al., 1996) 3

Figure 1.3 Size Effect of Reinforced Concrete: (a) tests by Leonhardt and Walther (1962); (b) comparing actual strength with failure load according to theory of plasticity. 3

Figure 2.1 Truss model and notation for shear reinforced members 9

Figure 2.2 Diagonal shear failure of longitudinal reinforced concrete beam proposed by Bazant and Kim (1984): (a) decomposition of shear loading capacity; (b) composite action; (c) arch action 13

Figure 2.3 Assumptions for modeling proposed by Gustafsson and Hillerborg: (a) Shear strength anlaysis; (b) Geometrical shapes of beams; (b) Bond stress τ_b versus bond slip s 13

Figure 2.4 Theoretical shear strength versus ratio d/l_{ch} 14

Figure 2.5 Theoretical failure mode proposed by Jenq and Shah (1989): (a) theoretical failure mode for modeling diagonal shear failure of reinforced concrete beam; (b) Balance condition for calculating value of P_s 15

Figure 2.6 Inclined compressive strut with reduced strut width: (a) ideal strut-and-tie model; (b) influence of flexure and bond; (c) reduced strut width 18

Figure 2.7 Failure due to splitting of concrete proposed by Zararis et al. (2001): (a) Distribution of normal stresses along line of second branch of critical crack; (b) Splitting failure of concrete 19

Figure 2.8 Shear strength of simply supported reinforced concrete beams subjected to concentrated load proposed by Muttoni et al. (2008) ... 21

Figure 2.9 Comparisons of shear strength recommended by code provisions for effective depth 23

Figure 3.1 Stress-strain curves for concrete cylinders loaded in uniaxial compression 25

Figure 3.2 Split-cylinder test for tensile strength 26

Figure 3.3 Combination of direct stress and shear causing failure of concrete . 27

Figure 3.4 Stress-strain relationship of concrete under uniaxial load [Elfgren (1989)]: (a) in uniaxial tension; (b) in uniaxial compression 28

Figure 3.5 Fictitious crack model: (a) test specimen under uniaixal tension; (b) influence of specimen length; (c) stress-train diagram for regions outside the fracture process zone; (d) stress-crack opening relationship of fictitious crack 29

Figure 3.6 Uniaxial compression: (a) test specimen; (b) influence of length; (c) stress-strain diagram proposed by Hognestad 30

Figure 3.7 Localized failure of concrete in uniaxial compression: Effect of specimen slenderness on (a) the complete stress-strain curve; (b) the postpeak stress-deformation cruve.(Van Mier, 1984, 2009) 32

Figure 3.8 Shear-band propagation in prismatic specimens subjected to plane strain [Van Geel (1998), Van Mier (2009)] 33

Figure 3.9 Influence of boundary conditions on the uniaxial load-displacement behavior in compression (Kotsovos 1983): (a) Load-displacement relationship obtained from tests; (b) Typical fracture modes of cylinders 33

Figure 4.1 Three basic pure fracture modes: (a) Mode I or pure opening mode (b) Mode II or in-plane shear mode (c) Mode III or anti-plane shear mode 36

Figure 4.2 A crack of length *2a* in an infinite plate subjected to a uniform stress σ_∞ at infinity 38

Figure 4.3 A crack of length *2a* in an infinite plate subjected to uniform in-plane shear stresses τ_∞ at infinity 41

Figure 4.4 Tensile stress-elongation curves: (a) linear elastic materials; (b) Quasi-brittle materials 43

Figure 4.5 Types of nonlinear zone in different types of materials: (a) Linear elastic; (b) Nonlinear plastic; and (c) Quasibrittle 44

Figure 4.6 Stress-displacement behavior under uniaxial tension: (a) Brittle; (b) Ductile; and (c) Quasi-brittle materials 44

Figure 4.7 Estimation of size of plastic zone at crack tip: (a) A first approximation; (b) Proposed by Irwin (1960) 46

Figure 4.8 Size of fracture process zone 48

Figure 4.9 Variation of size of fracture process zone for concrete strength..... 49

Figure 4.10 Size of fracture process zone: (a) for concrete strength and (b) for effective depth with test results 50

Figure 4.11 Dependence of the apparent fracture toughness on the specimen size: (a) Concrete (Di Leo's data, after Hillerborg 1984); (b) Mortar (after Ohgishi et al. 1986); (c) Hardened cement paste (after Higgins and Bailey 1976) 51

Figure 4.12 Load deflection diagram of ductile and brittle structures (ACI Committee 446, 1992) 55

Figure 4.13 Progressive nature of failure illustrated fro punching shear of a slab (ACI Committee 446, 1992) 56

Figure 4.14 Fracture mechanics size effect for geometrically similar structures of different sizes (ACI Committee 446, 1992) 57

Figure 4.15 Stress notation in region of crack tip: (a) Cartesian stress; (b) polar stresses 59

Figure 4.16 Failure loci for different mixed mode fracture criteria 60

Figure 4.17 Stress states for height of reinforced concrete beams: (a) reinforced concrete beams subjected to concentrated load; (b), (c), (d), (e) stress states at concrete cover zone, flexural tension zone, pure shear zone and compression zone, respectively..... 62

Figure 5.1 Stress-strain relationship of materials: (a) concrete in compression; (b) concrete in tension; and (c) reinforcement steel in tension..... 69

Figure 5.2 Moment-curvature relationship 69

Figure 5.3 Stress and strain distribution: (a) section; (b) crack propagation; (c) strain distribution and (d) stress distiribution 71

Figure 5.4 Depth of neutral axis 73

Figure 5.5 Normal stress distribution at the failure moment 74

Figure 5.6 Yield moment versus reinforcement degree 75

Figure 5.7 Stress-strain relationship 76

Figure 5.8 Stress and strain distribution of RC beams with rectangular section 77

Figure 5.9 Variation of *c/d* for concrete strain 78

Figure 5.10 Variation of normal stress and strain according to crack propagation 80

Figure 6.1 Final pattern of cracking of test beams: (a) without web reinforcement; (b) with web reinforcement [Karayiannis et al. (1999) and Zararis (2003)] 85

Figure 6.2 Height of single and diagonal cracks..... 85

Figure 6.3 Critical crack path dependent failure mechanism..... 86

Figure 6.4 Diagonal tension failure 87

Figure 6.5 Sliding failure 87

Figure 6.6 Stress states at the center and inclined cracks 89

Figure 6.7 Mode-I fracture in flexural tension zone: (a) mode-I fracture; (b) inclined crack and (c) stress states and Mohr's circle 91

Figure 6.8 Comparison of prediction with critical stress intensity factor proposed by Bazant and Oh (1983) 93

Figure 6.9 Critical stress intensity factor for mode-I fracture..... 94

Figure 6.10 Variation of diagonal crack angle in flexural tension zone: (a) for normal stress and (b) for the ratio of shear stress to normal stress... 96

Figure 6.11 Variation of the ratio of shear stress to normal stress for concrete strength 99

Figure 6.12 Cracking strength for concrete strength 99

Figure 6.13 Comparison of prediction with experimental results 100

Figure 6.14 Comparison of prediction of ACI 318-08 with experimental results101

Figure 6.15 Comparison of prediction of Hong et al. with experimental results 102

Figure 6.16 Stress state of compression zone and Mohr's circle 104

Figure 6.17 Variation of shear stress for normal stress at the crack tip 105

Figure 6.18 Mode-I fracture in compression zone: (a) mode-I fracture; (b) inclined crack and (c) stress states and Mohr's circle 106

Figure 6.19 Initial and effective crack length..... 107

Figure 6.20 Failure condition of diagonal tension failure 109

Figure 6.21 Proposed flexural-shear behavior..... 112

Figure 6.22 Analysis results for diagonal tension failure 113

Figure 6.23 Ultimate shear strength for effective depth: (a) proposed model and (b) ACI 318-08 115

Figure 6.24 Comparison of predictions with experimental results: (a) for shear span-to-depth ratio, (b) effective depth 118

Figure 6.25 Comparison of predictions with experimental results: (c) for concrete strength, (b) longitudinal reinforcement ratio 119

Figure 6.26 Comparison of ACI 318-08 with experimental results: (a) for shear span-to-depth ratio, (b) effective depth 120

Figure 6.27 Comparison of ACI 318-08 with experimental results: (a) for shear span-to-depth ratio, (b) effective depth 121

Figure 6.28 Forces transferring shear across an inclined crack..... 123

Figure 6.29 Components of shear resistance obtained by Taylor (1970) 124

Figure 6.30 Walraven's crack model: (a) no contact; (b) growing contact and (c) maximum contact 125

Figure 6.31 Variation of shear stress for normal stress in case of sliding failure130

Figure 6.32 Variation of the ratio of shear stress to normal stress for concrete strength 130

Figure 6.33 Stress states and Mohr's circle: (a) pure shear and (b) biaxial stress132

Figure 6.34 Critical stress intensity factor K_{IIc} for mode-II fracture..... 133

Figure 6.35 Initial and effective crack length for sliding failure mode 134

Figure 6.36 Proposed flexural-shear behavior for sliding failure..... 135

Figure 6.37 Comparison of predictions with experimental results for a/d 136

Figure 6.38 Two different failure mechanism of concrete strut: (a) General

compressive failure mechanism; (b) Compressive sliding failure mechanism..... 143

Figure 6.39 Stress distributions near the end of a bar of rectangular cross section subjected to a concentrated load *P* acting over a small area (Gere, 2001)..... 145

Figure 6.40 Concentrated force at a point a straight boundary: (a) Concentrated vertical force P acting on a horizontal straight boundary AB of an infinitely large plate; (b) Distribution of the load along the thickness of the plate (Timoshenko, 1970)..... 146

Figure 6.41 Distribution of normal and shear stresses 147

Figure 6.42 Sliding failure of a prismatic body: (a) Dimensions; (b) Normal and shear stresses; (c) Distribution of stresses; (d) Inclined crack. 148

Figure 6.43 Maximum shear stresses..... 151

Figure 6.44 Normalized compressive force: (a) Size effect of compressive force; (b) Degradation of compressive force for angle..... 153

Figure 6.45 Single strut 154

Figure 6.46 Strut-and-tie model for deep beam..... 158

Figure 6.47 Diagonal single strut of deep beams..... 159

Figure 6.48 Test results and size effect obtained by Walraven et al.(1994) 161

Figure 6.49 Comparison of shear stress between test data and predictions 162

Figure 6.50 Comparisons of size effect between proposed model based on concrete softening and theory of plasticity..... 163

List of Tables

Table 2-1 Experimental results by Kani (1967) 23

Table 6-1 Experimental results by Chana (1981) 94

Table 6-2 Dimensions and properties of test specimen 116

Table 6-3 Dimensions and material properties of test specimens 137

Table 6-4 Examples for estimation of size effect 152

Table 6-5 Information of test data obtained by Walraven et al.(1994) 160

Table 6-6 Comparison of ultimate shear strength between test results and predictions 162

Notations

a	shear span length
a_c	crack length
a_{eff}	effective crack length
A_s	area of reinforcement
b	width
c	depth of neutral axis
C	resultant compression force
d	effective depth
D	size
E_c	Young's modulus of concrete
E_s	Young's modulus of steel
f_s	stress of reinforcing steel
f_{ct}	tensile strength of concrete
f_y	yield strength of reinforcing steel
$f_c^{'}$	concrete compressive strength
G_f	fracture energy
h	overall height
jd	moment arm
K	stress intensity factor

K_{Ic}	critical stress intensity factor for mode-I fracture
K_{IIc}	critical stress intensity factor for mode-II fracture
M	bending moment
v_u	ultimate shear stress
V	applied shear force
ε_c	strain of concrete
ε_0	strain of concrete at maximum stress
ε_{cu}	ultimate concrete strain at failure
ρ	longitudinal reinforcement ratio
σ_1	principal tensile stress
σ_2	principal compressive stress
σ_x	normal stress at crack tip
τ_{xy}	shear stress at crack tip
τ_u	ultimate shear stress
φ_0	crack angle at pure bending zone
φ_1	crack angle at flexural tension zone
φ_2	crack angle at compression zone

1. Introduction

1.1 Research Background and Problem Statements

Shear strength of reinforced concrete beams is affected by various design parameters, concrete strength $f_c^{'}$, reinforcement steel ratio ρ, shear span-to-depth ratio a/d, and effective depth, d as shown in Fig. (1.1). Generally as increasing with the reinforcement steel ratio the normalized shear stress increases. (Fig. 1.1(b)) And normalized shear stress decreases as shear span-to-depth ratio and effective depth increases. (Fig. 1.1 (c), (d))

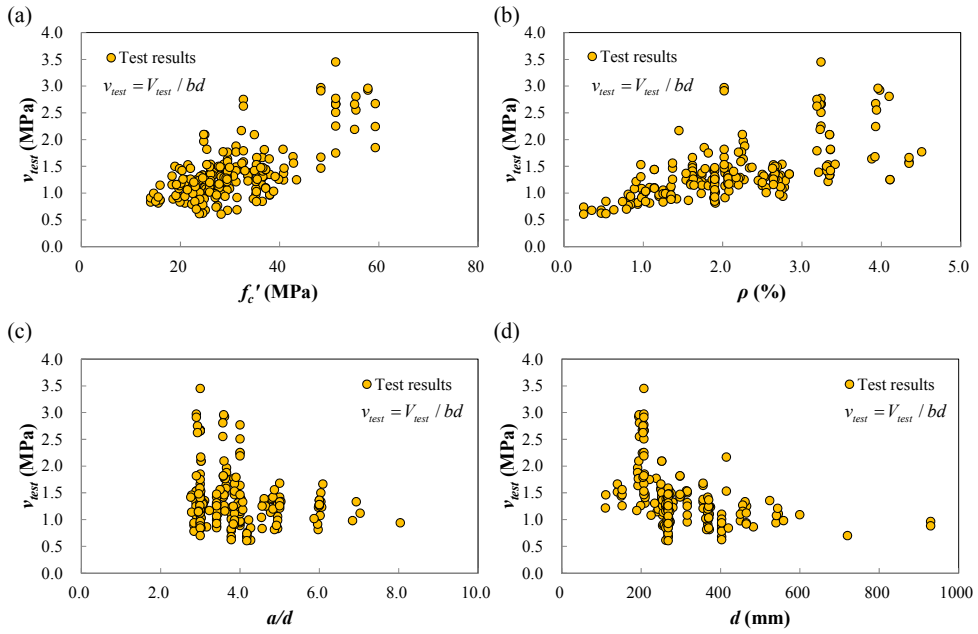

Figure 1.1 Influence of various design parameters: (a) concrete strength, $f_c^{'}$; (b) reinforcement steel ratio, ρ; (c) shear span-to-depth ratio, a/d; (d) effective depth, d (data from Reineck et al. 2003)

For these reasons, despite the numerous experimental and analytical studies over the decades, the problem of how shear failures occur in reinforced concrete beams still remains. Thus, it is fact that international codes, such as ACI code (ACI 318-08) or Eurocode 2, are based on semi- or empirical considerations.

Many reinforced concrete structural members, especially slender and deep beams without web reinforcement, showed that the shear stress decrease with increase in the size of members.

Many design code provisions, ACI 318-08, CEB-FIP, Eurocode, and JSCE are more or less the result of statistical analysis of experimental results. Kani (1967) showed that such a procedure may be dangerous because test specimens used in laboratory experiments are usually smaller than structural members in reality. Kani (1967) investigated the size effect of concrete for shear strength and after that, Collins et al. (1996), Collins and Kuchma (1997), and Collins and Mitchell (1997) showed the influence of member size and maximum aggregate size on shear stress at failure as shown in Fig. (1.2). Walraven et al. (1994) found that crack propagation beam quicker as the specimen size became larger.

The reinforced concrete beams are classified into three types depending on shear span-to-depth ratio (*a/d*) on the basis of failure mechanism. In slender beams having *a/d* from about 2.5 to about 6, the beam fails at the inclined cracking load. Very slender beams, with *a/d* greater than about 6, will fail in flexure prior to the formation of inclined cracks. Fig. (1.3) presents several tests performed by Leonhardt and Walther (1962) where *a/d* was varied from 1.5 to 8.0 and shows the influence of *a/d* on shear strength. For small values of *a/d*, the cracks practically do not develop through the inclined strut and thus the flexural strength can be reached. For larger values of *a/d*, cracks develop through the inclined struts, consequently decreasing the shear strength of the member. (Muttoni et al., 2008)

Consequentially, the shear strength of RC beams without web reinforcement appears to be affect by the beam depth and the shear span-to-depth ratio.

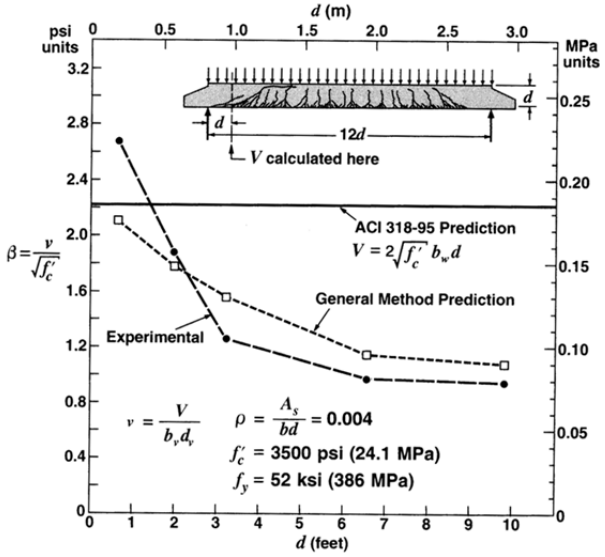

Figure 1.2 Influence of member size and maximum aggregate size on shear stress at failure (Collins et al., 1996)

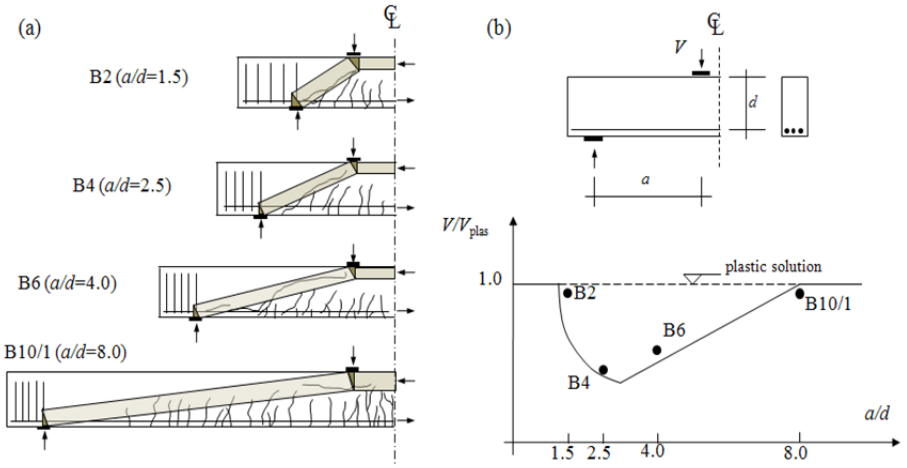

Figure 1.3 Size Effect of Reinforced Concrete: (a) tests by Leonhardt and Walther (1962); (b) comparing actual strength with failure load according to theory of plasticity.

1.2 Research Objectives and Scope

The main objectives of this dissertation are to provide theoretical formula for shear strength of reinforced concrete beams without web reinforcement based on critical crack path and to evaluate the size effect in linear elastic fracture mechanics approach. Specific objectives are as follows:

(1) To provide a rational failure mechanism of reinforced concrete structural members subjected to bending moment and shear on the basis of critical crack path.
(2) To determine size dependent critical stress intensity factors for mode-I and mode-II fracture, K_{Ic} and K_{IIc}.
(3) To present an appropriate strength evaluation of the prismatic body for sliding failure considering a size effect.
(4) To develop a theoretical formula for shear strength of reinforced concrete beams without web reinforcement.

To achieve these objectives, effective stress intensity factor in linear elastic fracture mechanics which can be expressed the stress state at the crack tip and crack length is used.

Based on these results, rational and theoretical formulas for shear strength of reinforced concrete beams without web reinforcement were developed considering the interaction between normal stress and shear stress at critical diagonal crack tip. The proposed models were verified by the comparisons with the results of code provisions and existing experimental results.

1.3 Organization of the Dissertation

In chapter 2, current design provisions such as ACI 318-08, CEB-FIP model code 1990, Eurocode 2, and JSCE are reviewed. Recent code provisions for shear strength of reinforced concrete members considering size effect are summarized. Also, other previous researches on the shear strength regarding the size effect of RC slender beams are presented.

In chapter 3, behavior of concrete under uniaxial tension and uniaxial compression is introduced. And softening of concrete is investigated on the basis of fracture mechanics.

In chapter 4, fracture mechanics of concrete are reviewed. Size dependent stress intensity factor and critical stress intensity factor for mode-I and mode-II fracture are investigated. And to calculate the shear strength of reinforced concrete beams, mixed mode fracture and size effect in linear elastic fracture mechanics are reviewed.

In chapter 5, flexural behavior of reinforced concrete slender beams without web reinforcement is investigated. To find the location where a critical diagonal crack occurs in compression zone, primary parameters in flexural behavior of concrete beams are investigated based on the concrete strain.

In chapter 6, shear strength of reinforced concrete members without web reinforced concrete is evaluated on the basis of failure mechanism which depends on the critical diagonal crack. And theoretical predictions and experimental results are compared.

Summary and conclusions are presented in chapter 7.

2. Literature Review

2.1 Current Design Provisions

2.1.1 ACI 318-08 Building Code

ACI 318-08 building code (ACI, 2008) specifies the empirical design method for shear strength of reinforced concrete members. The shear strength is based on an average shear stress on the full effective cross section bd. In a member without shear reinforcement, shear is assumed to be carried by the concrete web. In a member with shear reinforcement, a portion of the shear strength is assumed to be provided by the concrete and the remainder by the shear reinforcement.

The nominal shear strength of beam is as follows.

$$V_n = V_c + V_s \tag{2.1}$$

where V_n is the nominal shear strength, V_c is nominal shear strength provided by concrete, and V_s is nominal shear strength provided by shear reinforcement.

The nominal shear strength provided by concrete is computed by as follows.

$$V_c = 0.17\lambda\sqrt{f_c'}bd \tag{2.2}$$

or

$$V_c = \left(0.16\lambda\sqrt{f_c'} + 17\rho_w \frac{V_u d}{M_u}\right)bd \tag{2.3}$$

Equation (2.3) is basic expression for shear strength of members without shear reinforcement.

The shear strength provided by concrete V_c is assumed to be the same for beams with and without shear reinforcement and is taken as the shear causing significant inclined cracking.

The nominal shear strength provided by shear reinforcement is

$$V_s = \frac{A_v f_{yt} d}{s} \tag{2.4}$$

where A_v is the area of shear reinforcement within spacing s.

The current ACI Code (318-08) base its design on the diagonal cracking strength of the normal strength concrete (NSC) beams, with the depth less than 400mm, without considering the influence of beam size.

2.1.2 CEB-FIP Model Code 1990

CEB-FIP model code (1990) suggests a more sophisticated empirical formula based on Zsutty's (1971) equation and adding an extra term to account for the size effect as following Eq. (2.5).

If shear cracking would occur in the serviceability limit state the amount of shear reinforcement controlling the opening of diagonal crack may be very small and the criteria of serviceability may be violated. In the absence of a more precise calculation the shear force causing shear cracking may be estimated as follows.

$$V_{cr} = 0.15\left(\frac{3d}{a_v}\right)^{1/3}\left(1+\sqrt{\frac{200}{d}}\right)\left(100\rho f_c'\right)^{1/3} b_{red} d \tag{2.5}$$

where

a_v is the distance from major load to support

ρ is the ratio of flexural tensile reinforcement (A_s / bd) anchored at the support

b_{red} is the reduced web breadth

$(3d / a_v)^{1/3}$ is an empirical expression allowing for the influence of the transverse compression from the loads and support reaction

2.1.3 Eurocode 2

In Eurocode 2, shear stress depends on concrete strength, effective depth and longitudinal reinforcement steel ratio.

The recommended design value for the shear resistance $V_{Rd,c}$ is given by

$$V_{Rd,c} = \left[C_{Rd,c} k \left(100 \rho_1 f_{ck}\right)^{1/3} + k_1 \sigma_{cp} \right] bd \tag{2.6}$$

with a minimum of

$$V_{Rd,c} = \left(v_{\min} + k_1 \sigma_{cp}\right) bd \tag{2.7}$$

where

$k = 1 + \sqrt{\frac{200}{d}} \le 2.0$ with d in mm

$\rho_1 = \frac{A_{si}}{bd} \le 0.02$

A_{sl} is the area of the tensile reinforcement

b is the smallest width of the cross section in the tensile area [mm]

$\sigma_{cp} = N_{Ed} / A_c < 0.2 f_{cd}$ [MPa]

N_{Ed} is the axial force in the cross section due to loading or prestressing

A_c is the area of concrete cross section [mm^2]

The recommended value for $C_{Rd,c}$ is $0.18 / \gamma_c$ and k_1 is 0.15.

The shear strength of concrete without axial force or presstressing is as follow

$$V_{Rd,c} = \frac{0.18}{\gamma_c}\left(+\sqrt{\frac{200}{d}}\right)\left(100\rho_1 f_c^{'}\right)^{1/3} bd \tag{2.8}$$

where γ_c is the partial safety factor for concrete $\gamma_c = 1.0$

The design of members with web reinforcement is based on truss model called by variable strut inclination method as shown in Fig. (2.1)

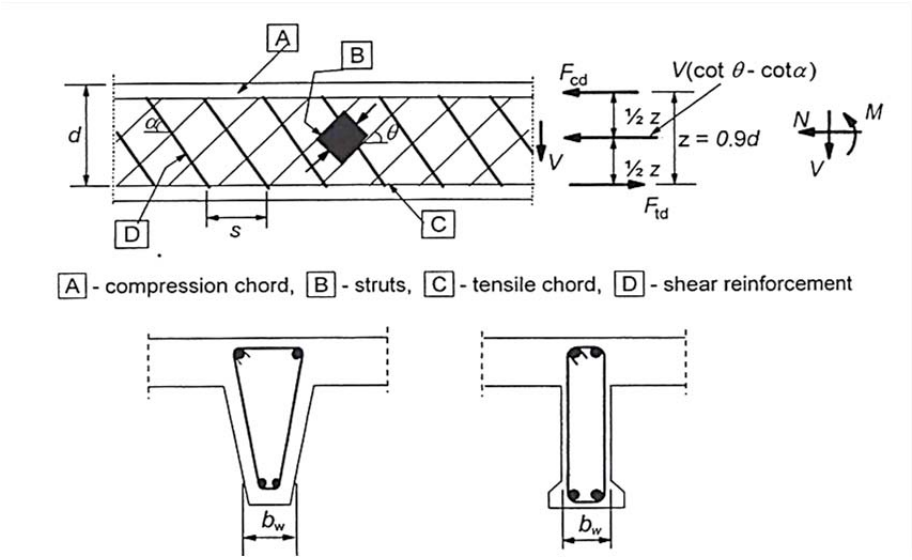

Figure 2.1 Truss model and notation for shear reinforced members

where α is the angle between shear reinforcement and the beam axis perpendicular to the shear force, θ is the angle between the concrete compression strut and the beam axis, F_{td} is the design value of the tensile force in the longitudinal reinforcement, F_{cd} is the design value of the concrete compression force in the direction of the longitudinal member axis, b is the minimum width between tension and compression chords and z is the inner lever arm, for a member with constant depth.

In Eurocode 1 the designer should choose an appropriate angle θ (the angle between the assumed concrete compression strut and the tension chord) to use in the model. The limits on $\cot\theta$ are between 1 and 2.5. Thus, the maximum shear capacity depends on θ as following equation.

$$V_{Rd,s} = \frac{A_{sw}}{s} z f_{ywd} \cot\theta \tag{2.9}$$

where A_{sw} is the cross-sectional area of the shear reinforcement, s is the spacing of the stirrups and f_{ywd} is the design yield strength of the shear reinforcement.

2.1.4 JSCE

The design shear capacity of a member V_{yd} may be obtained using Eq. (2.10). When both bent longitudinal bars and stirrups are arranged as shear reinforcement, it should be ensured that the stirrups provided carry at least 50% of the shear force provided by shear reinforcement.

$$V_{yd} = V_{cd} + V_{sd} + V_{ped} \tag{2.10}$$

where V_{cd} is the design shear capacity of linear members without shear reinforcement steel calculated by

$$V_{cd} = \beta_d \cdot \beta_p \cdot \beta_n \cdot f_{vcd} \cdot b_w \cdot d / \gamma_b \tag{2.11}$$

$f_{vcd} = 0.20\sqrt{f'_{cd}}$ [MPa] where $f_{vcd} \le 0.72$ [MPa]

$\beta_d = \sqrt[4]{1/d}$ [d : m] when $\beta_d > 1.5$ β_d is taken as 1.5.

$\beta_p = \sqrt[3]{100 p_w}$ when $\beta_p > 1.5$ β_p is taken as 1.5.

$\beta_n = 1 + M_0 / M_d \left(N_d^{'} \geq 0 \right)$ when $\beta_n > 2$ β_n is taken as 2.

$\beta_n = 1 + 2M_0 / M_d \left(N_d^{'} < 0 \right)$ when $\beta_n < 0$ β_n is taken as 0.

$p_w = A_s / bd$

γ_b is 1.3 in general

2.2 Previous Researches

2.2.1 Fracture Mechanics Approach

Bazant and Kim (1984) have proposed the size effect model that combined the existing code formulas for diagonal failure of longitudinally reinforced concrete beams without web reinforcement.

It is assumed that the end segment of a beam shown in Fig. (2.2), in which a constant shear force V acts throughout the shear span a. And bending moment at any distance x from the support expressed as $M = Tjd$ where $T = T(x)$ is tensile force resultant acting at the centroid of longitudinal reinforcement, and $j = j(x)$ is variable coefficient. The shear force expressed as $V = dM / dx$, and the derivative is written as a sum of two terms

$$V = V_1 + V_2, \; V_1 = \frac{dT}{dx} jd, \; V_2 = \frac{dj}{dx} Td \tag{2.12}$$

By empirically selecting values of T and j,

$$V_1 = k_1 \rho^{1/2-m} f_c^{'q} bd, \qquad V_2 = c_2 \frac{\rho^{1-m}}{\left(a / d \right)^r} bd \tag{2.13-a, b}$$

where k_1, q, m and c_2 are empirical constants.

As a result, total shear stress is expressed as

$$v = k_1 \rho \left(f_c^{'q} + k_2 \frac{\sqrt{\rho}}{(a/d)^r} \right) \left(1 + \frac{d}{\lambda_0 d_a} \right)^{-1/2} \tag{2.14}$$

Proposed equation has been compared to essentially all important experimental evidence, both that with regard to the effect of steel ratio, shear span, and concrete strength, and the more limited on with regard to the effect of size.

The several required empirical constants were obtained by statistically analysis. As a result of all statistical comparisons, the following formula is proposed for the mean ultimate nominal shear strength.

$$v_u = \frac{10\sqrt[3]{\rho}}{\sqrt{1 + d/25d_a}} \left(\sqrt{f_c^{'}} + 3000\sqrt{\rho/(a/d)^5} \right) \tag{2.15}$$

Gustafsson and Hillerborg (1988) proposed a finite analysis for longitudinally reinforced concrete beams based on a nonlinear fracture mechanics model called the fictitious crack model as shown in Fig. (2.3).

Concrete and steel are assumed to be linear elastic materials. And a single diagonal crack is assumed.

Shear stress across the fracture zone carried by aggregate interlocking between the fracture surface was not considered nor was the shear force carried by dowel action of the reinforcement steel considered.

In Fig. (2.4) , normalized calculated shear strength f_v / f_t are shown versus d / l_{ch}. This figure indicates a significant decrease in shear strength with decreased characteristic length and with increased beam size.

Consideration of the characteristic length of the concrete may be equally important a consideration of beam size and might thus reduce the apparently large scatter in shear strength test data.

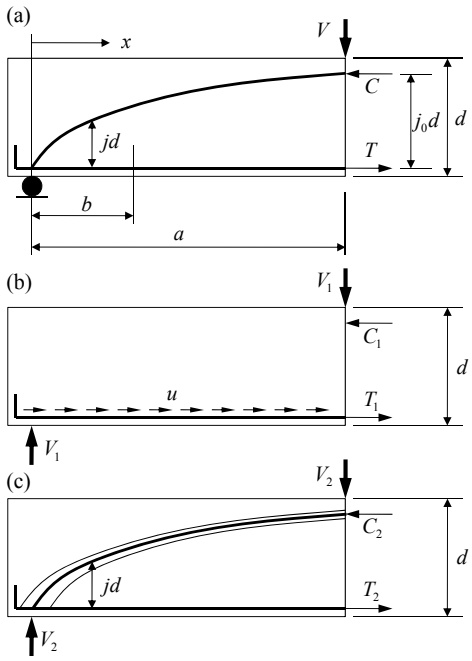

Figure 2.2 Diagonal shear failure of longitudinal reinforced concrete beam proposed by Bazant and Kim (1984): (a) decomposition of shear loading capacity; (b) composite action; (c) arch action

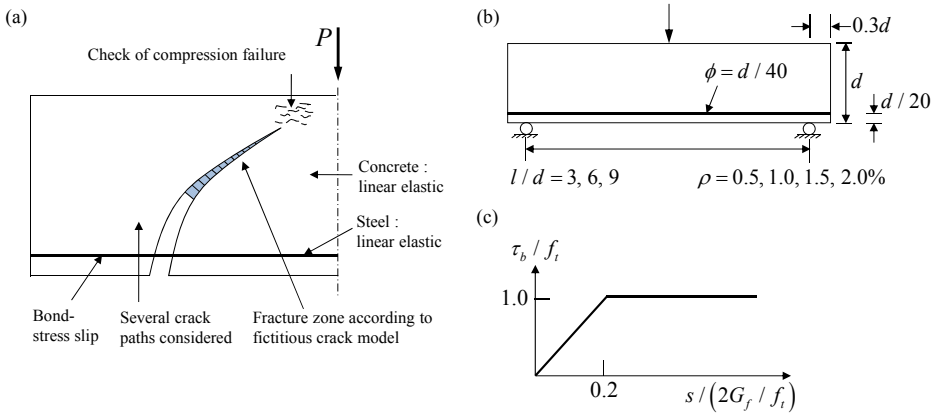

Figure 2.3 Assumptions for modeling proposed by Gustafsson and Hillerborg: (a) Shear strength anlaysis; (b) Geometrical shapes of beams; (b) Bond stress τ_b versus bond slip s

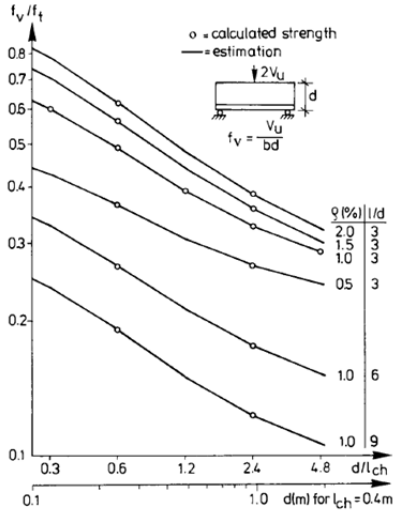

Figure 2.4 Theoretical shear strength versus ratio d / l_{ch}

Gustafsson and Hillerborg have suggested that it should be possible to achieve consideration of l_{ch} in existing empirical shear strength formulas simply by replacing the measure of beam size d in the actual size reduction factor by the ratio d / l_{ch}.

An approximate relation for simple analysis of the influence of ratio d / l_{ch} was proposed as follows.

$$\frac{f_v}{f_t} = k\left(\frac{d}{l_{ch}}\right)^{-0.25} \tag{2.16}$$

where k is proportional constant.

Jenq and Shah (1989) have proposed a model based on their two-parameter fracture model. A diagonal failure of a longitudinally reinforced concrete beams is assumed in Fig. (2.5), where a single diagonal linear crack is assumed to be responsible for shear failure of the beam and the value $\theta \approx 45^{\circ}$ was used. It was assumed that any

crack growth in the concrete take place when the stress intensity factor at the crack tip attains the mode-I fracture toughness K_{Ic}^{s}. It is assumed that the steel force along the beam, $F_s(x)$, is represent by a power law as follow

$$F_s(x) = F_{s,\max}\left(\frac{2x}{S}\right)^{N_1} \le A_s f_y \tag{2.17}$$

where $F_{s,\max}$ is the maximum steel force at the mid-span ($x = S/2$), and the value of N_1 is a constant whose value will be adopted after numerical experimentation based on a bilinear approximation to the bond slip and frictional pullout behavior of the reinforcing bars. Based on the test data reported by Ferguson and Thompson, Jenq and Shah proposed that

$$F_{s,\max} = 2.509 S f_t \left(\frac{\rho}{b}\right)^{1/2} \tag{2.18}$$

where the tensile strength $f_t = 1.4705\left(K_{Ic}^{s}\right)^2 / E\ CTOD_c$ based on the two parameter fracture mode.

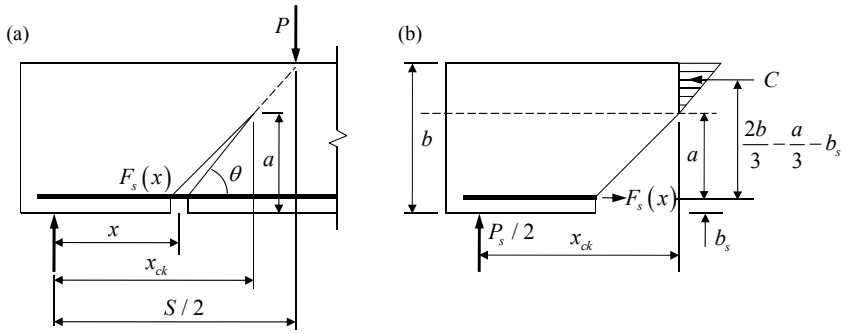

Figure 2.5 Theoretical failure mode proposed by Jenq and Shah (1989): (a) theoretical failure mode for modeling diagonal shear failure of reinforced concrete beam; (b) Balance condition for calculating value of P_s

Based on LEFM,

$$K_{Ic}^{s} = K_I = \sigma_N \sqrt{\pi a} g_1\left(\frac{a}{b}\right) \tag{2.19}$$

where σ_N is the nominal stress at the section x and $g_1(a/b)$ is the geometric function. For three-point bending beams with $S/b = 4$, $\sigma_N = (3P_m x)/(b^2 t)$, and $g_1(a/b)$ is given by

$$g_1\left(\frac{a}{b}\right) = \frac{1.99 - (a/b)(1 - a/b)\left[2.15 - 3.93(a/b) + 2.70(a/b)^2\right]}{\sqrt{\pi}(1 + a/b)(1 - a/b)} \tag{2.20}$$

As a result, the total shear strength of the beam, v_u is given as

$$v_u = \frac{P}{bt} = \frac{P_m + P_s}{bt} \tag{2.21}$$

where P_m is the force resisted by the concrete and P_s is the force resisted by the longitudinal steel.

2.2.2 Strut-and-Tie Model

Reinforced concrete beam theory is based on equilibrium, compatibility, and the constitutive behavior of the materials, steel and concrete. It is assumed that the strain varies linearly through the depth of a member and this assumption is validated by St. Venant's principle.

However this principle does not apply in the discontinuity regions within reinforced concrete members near concentrated loads, openings, or changes in cross section.

Because of their geometry, the full volume of deep beams and column brackets qualify as discontinuity regions.

When concrete cracks, the strain field is disrupted, causing a redistribution of the internal forces. So it is possible to represent the internal forces within D-regions using a statically determinate truss, referred to as a strut-and-tie model.

Strut-and-tie model are based on a lower bound solution in the theory of plasticity.

Basic assumptions for this model are assumed as perfectly plastic behavior of the material and small deformation of the structure.

Hong and Ha (2012) have proposed model that is suitable for estimating the shear strength of RC beams with an intermediate a/h, as their governing diagonal failure modes. They study considers that the mechanism of diagonal cracking reduced the width of a concrete strut and hence causes a reduction in the capacity of the concrete strut as shown in Fig. (2.6).

The reduced width of concrete strut can be defined as follows.

$$\frac{w_s'}{h} = \zeta^2 \sqrt{1 + \left(\frac{1-\zeta}{\alpha}\right)^2} \tag{2.22}$$

where w_s' means the reduced width of concrete strut, α represent the ratio of the shear span to the overall depth of the member ($\alpha = a/h$), ζ means the ratio of the flexural compression depth to the overall depth of the members, $\zeta = c_n / h = 1.53\sqrt[3]{\rho}$. ρ represents the longitudinal reinforcement ratio.

The proposed shear strength model is as follows

$$v = \frac{3}{4} f_c' \frac{\zeta^2 (1-\zeta)\left(1+\zeta-\zeta^2\right)}{\alpha} \tag{2.23}$$

The derived equation for the shear strength is expressed in terms of the strength of concrete f_c', the ratio of the flexural compression depth to the overall depth of the member ζ.

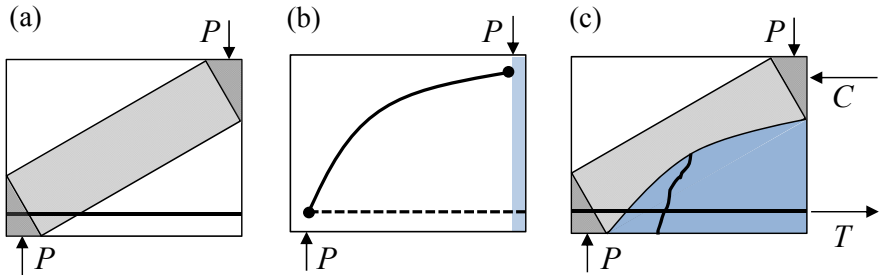

Figure 2.6 Inclined compressive strut with reduced strut width: (a) ideal strut-and-tie model; (b) influence of flexure and bond; (c) reduced strut width

2.2.3 Deformation based Design

Zararis and Papadakis (2001) have proposed the very simple formulation of shear strength of reinforced concrete beams without web reinforcement to take into account the size effect as follows.

$$v_u = \frac{V_u}{bd} = \left(1.2 - 0.2\frac{a}{d}d\right)\frac{c}{d}f_{ct} \tag{2.24}$$

where $1.2 - 0.2\dfrac{a}{d}d \geq 0.65$ (d in meters)

To define the failure criteria of the compression zone it is assumed that splitting of concrete occurs at the second branch of critical crack. Split-cylinder tensile tests reported by Hasegawa et al. (1985) were used to explain the size effect of the above formulation. The factor $\left(1.2 - 0.2a\right)f_{ct}$ means the size effect on the diagonal shear failure of slender beams, with a minimum value of 0.65.

Finally, they have suggested that shear strength is related to the tensile strength of concrete at the compression zone.

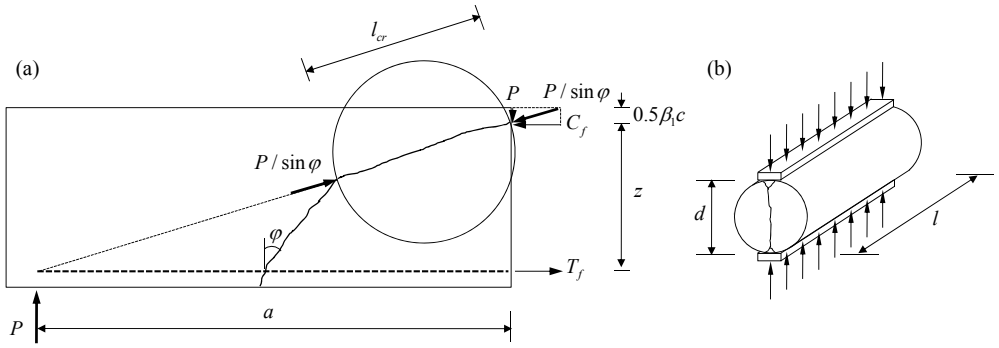

Figure 2.7 Failure due to splitting of concrete proposed by Zararis et al. (2001): (a) Distribution of normal stresses along line of second branch of critical crack; (b) Splitting failure of concrete

Park and Choi (2006) have proposed the strain-based shear strength model. To define the failure mechanism of the compression zone subjected to the combined stresses, Rankine's failure criteria were used. A concrete failure occurs then the principal stress resulting from the combined stresses reaches the material strength. When the principal compressive stress reaches the compressive strength of concrete $-f_c^{'}$, failure controlled by compression occurs, and when principal tensile stress reaches the tensile strength concrete $f_c^{'}$ failure controlled by tension occurs. The failure criteria of the compression is defined as follows.

For failure controlled by compression :

$$\sigma_1 = -\frac{\sigma_u}{2} - \sqrt{\left(\frac{\sigma_u}{2}\right)^2 + v_u^2} \geq -f_c^{'} \qquad (2.25\text{-a})$$

For failure controlled by tension :

$$\sigma_2 = -\frac{\sigma_u}{2} - \sqrt{\left(\frac{\sigma_u}{2}\right)^2 + v_u^2} \le f_t' \tag{2.25-b}$$

Mottoni and Ruiz (2008) have suggested the critical shear crack theory which is assumed that the shear strength is checked in a section where the width of the critical shear crack represented by the strain at a depth of $0.6d$ from the compression face and the critical crack width w is proportional to the longitudinal strain as shown in Eq. (2.26).

$$w \propto \varepsilon d \tag{2.26}$$

where ε means the strain in the control depth $0.6d$ derived based on the bending moment M in the critical section.

The shear strength considering the effects of the critical crack width, the aggregate size and the concrete compressive strength have been proposed as following equations.

$$\frac{V_R}{b_w d\sqrt{f_c}} = \frac{1}{6}\frac{2}{1+120\dfrac{\varepsilon d}{16+d_g}} \quad \text{[MPa, mm]} \tag{2.27}$$

where d_g represents the aggregate size for high-strength concrete ($f_c' > 60$ MPa) or light-weight concrete d_g should be taken equal to zero because the crack surface develops through the aggregates as proposed by Angelakos et al. (2001), and Bentz et al. (2006).

Fig. 2.8 shows the degradation of shear strength as increasing the effective depth or deformation.

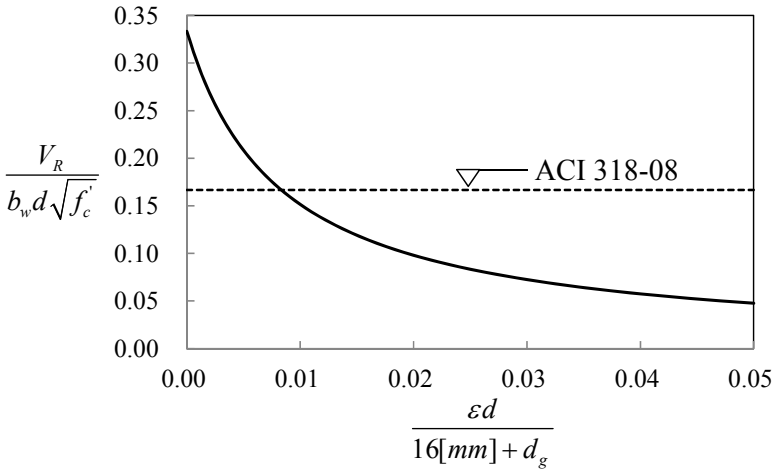

Figure 2.8 Shear strength of simply supported reinforced concrete beams subjected to concentrated load proposed by Muttoni et al. (2008)

2.2.4 Regression Analysis

Zsutty (1968) have proposed the shear strength by using an empirical method which combines the techniques of dimensional analysis and statistical regression analysis as follows.

$$\frac{V_{cr}}{bd} = 2.2\left(f_c' \rho \frac{d}{a} \right)^{1/3} \tag{2.28}$$

where ρ represents the ratio of reinforcement steel.

Zsutty's equation took into account the influence of the compression strength of the concrete and the longitudinal reinforcement ratio. When the steel ratio is small, flexural cracks extend higher into the beam and open wider.

2.3 Review

Shear resistance of reinforced concrete beams has been studied extensively over the last few decades. Nevertheless, most theoretical and experimental researches even the current design codes are based on empirical and statistical method to express the size effect especially. In this chapter, current code provisions and previous researches for shear strength reinforced concrete beams with or without web reinforcement were studied.

Only ACI 318-08 based on empirical formulations does not provide the size effect. On the other hand CEB-FIP model code, Eurocode 2, and JSCE based on empirical and statistical method take into account the size effect in their formula directly as shown in Eq. (2.5), Eq. (2.8), and Eq. (2.10). Fig. (2.9) and Table (2-1) show the comparisons of shear strength recommended by code provisions for effective depth. For comparisons, four simply supported prototype reinforced concrete beams subjected concentrated load tested by Kani (1967) were used. Material properties and geometry of specimens such as concrete strength $f_c^{'} = 27\text{MPa}$, width of beams $b = 152.3\text{mm}^2$, ratio of reinforcement $\rho = 2.8\%$, and shear span-to-depth ratio $a/d = 4.0$ are same. All of code provisions except ACI 318-08 show the degradation of shear strength as an effective depth increases and represent very rational accuracy. However, ACI 318-08 shows constant values regardless of effective depth of specimen.

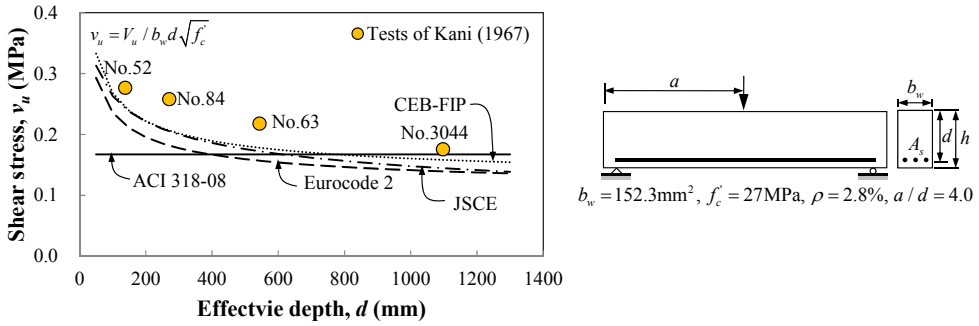

Figure 2.9 Comparisons of shear strength recommended by code provisions for effective depth

Table 2-1 Experimental results by Kani (1967)

Author	Beam	f_c' [MPa]	b [mm]	d [mm]	h [mm]	a/d	ρ [%]	V_t [kN]	v_t [MPa]
Kani (1967)	52	24.8	152	138	152	3.93	2.69	28.9	0.28
	84	27.5	151	271	305	4.01	2.83	55.4	0.26
	63	26.2	154	543	610	4.00	2.77	93.2	0.22
	3044	29.5	152	1097	1220	3.97	2.73	159.1	0.18
Mean value		27.0	152.3			4.00	2.80		

3. Behavior of Concrete

3.1 Uniaxial Compression

The compressive strength of concrete is usually obtained from cylinders with a height to diameter ratio of 2. The standard cylinder is 300mm high by 150mm in diameter, and the resulting compressive cylinder strength is termed f_c'.

Concrete is a mixture of cement paste and aggregate, each of which has an essentially linear and brittle stress-strain relationship in compression. Brittle materials tend to develop tensile fractures perpendicular to the direction of the largest tensile strain. When concrete is subjected to uniaxial compressive loading, cracks tend to develop parallel to the maximum compressive stress.

Fig. ( ) represents typical stress-strain curves obtained from concrete cylinders loaded in uniaxial compression in a test. The curves are almost linear up to about one-half the compressive strength. The peak of the curve for high-strength concrete is relatively sharp, but for low-strength concrete the curve has a flat top. The strain at the maximum stress is approximately 0.002.

After peak stress the curves softening of concrete occurs due to the gradual formation of microcracks within the structure of concrete.

3.2 Uniaxial Tension

The tensile strength of concrete, which is 8 and 15 percent of the compressive strength, can be obtained directly from tension specimens. However, because of the difficulties of holding the specimens to achieve axial tension the direct tension test is infrequently used.

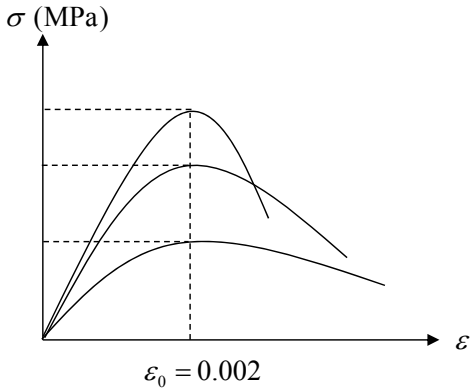

Figure 3.1 Stress-strain curves for concrete cylinders loaded in uniaxial compression

Two types of tests are widely used. The first of these is the modulus of rupture in which a plain concrete beam, generally 150mm×150mm×750mm long, is loaded in flexure at the 3-points of a 600mm span until it fails due to cracking on the tension face. The modulus of rupture f_r is calculated from the following equation.

$$f_r = \frac{6M}{bh^2} \tag{3.1}$$

where M is flexural moment, b is width of specimen, and h means the overall depth of specimen.

The second tensile test is the split cylinder test. In case of this test, the tensile strength of concrete may be measured indirectly in terms of the computed tensile stress at which a cylinder placed horizontally in a testing machine and loaded along a diameter will split. From the theory of elasticity, the splitting tensile strength, f_{ct} is computed as follows.

$$f_{ct} = \frac{2P}{\pi ld} \tag{3.2}$$

where P is the maximum applied load, l is the length of specimen, and d is the diameter of specimen.

Fig. (3.2) shows the split-cylinder test for tensile strength. The split cylinder tensile strength usually ranges from 50 to 75% of the modulus of rupture. The difference is mainly due to the stress distribution in the concrete of the flexural member.

According to ACI 318 code provisions, for normalweight concrete, the average splitting tensile strength f_{ct} is approximately equal to $f_{ct} = 0.56\sqrt{f_c'}$.

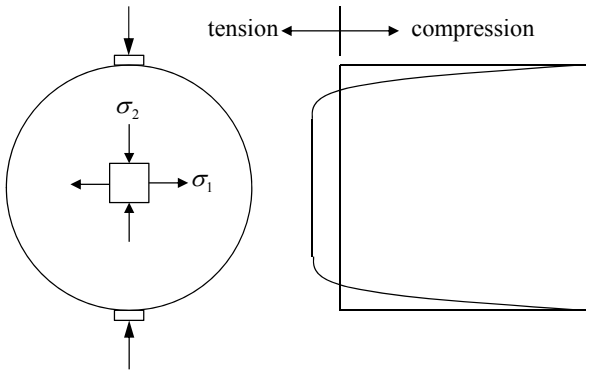

Figure 3.2 Split-cylinder test for tensile strength

3.3 Biaxial Stress Behavior

A biaxial stress condition occurs if the principal stresses act only in two directions. A failure curve for elements with direct stress in one direction combined with shear stress, as found by Bresler and Pister (1958), appears in Fig. (3.3). The curve indicates that the compressive strength of concrete is reduced in the presence of shear stress. This action may influence the strength of concrete in the compression zone of beams.

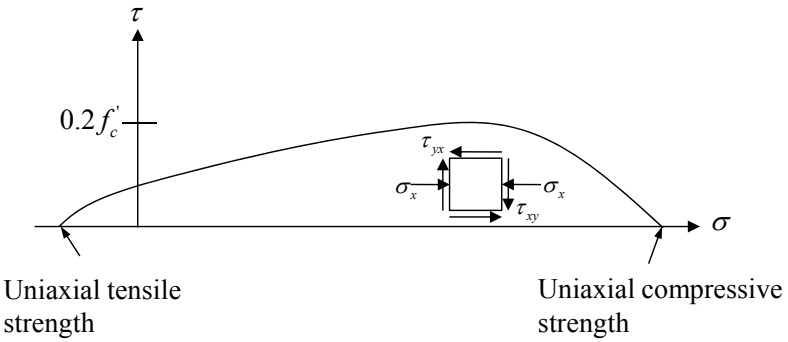

Figure 3.3 Combination of direct stress and shear causing failure of concrete

3.4 Softening of Concrete

Softening is a gradual decrease of resistance from the peak load due to the continuous increase of deformation. Softening is found in stress-deformation relationship as shown in Fig. (3.4). It is characterized by the descending branch of the stress-strain or deformation curve. Due to the heterogeneity of concrete the material is gradually weakened and this cause progressive failure of internal bonds when concrete is subjected to progressive deformation [Hsu et al. (1963)].

Vonk (1992) introduced the softening of concrete as following. Initially, the cracking starts as microcracking. They are stable, which means that they grow only when the load is increased. At the peak load, the macrocrack starts. They are unstable, which means that the load has to decrease to avoid an uncontrolled growth. In a deformation-controlled test, this macrocrack growth results in softening and localization of deformation. Localization of deformation means that all further deformation concentrate in the macrocracks, while the concrete parts in series with these macrocracks show decreasing deformation due to unloading.

Softening and localization of deformation show the concrete in tension as well as under compression.

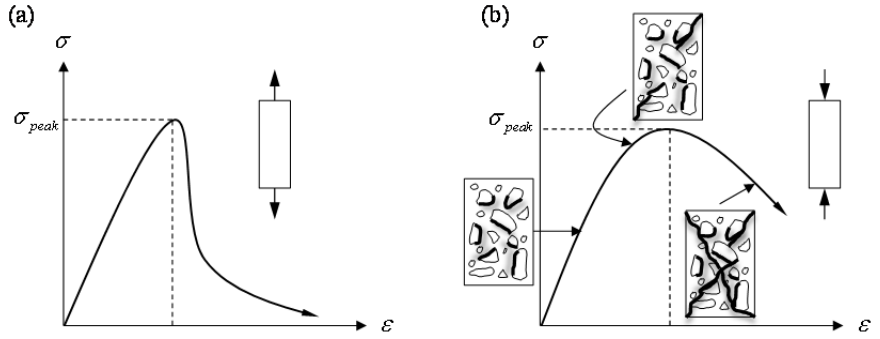

Figure 3.4 Stress-strain relationship of concrete under uniaxial load [Elfgren (1989)]: (a) in uniaxial tension; (b) in uniaxial compression

Though concrete is normally is used in compression, its fracture behavior in tension is very important as well as fracture under compression. Unfortunately only few experiments on concrete subjected to uniaxial tension are presented.

Hillerborg et al. (1976) introduced the "fictitious crack model" which is capable of describing the failure of concrete in tension. A typical stress-elongation curve for a concrete plate subjected to uniaxial tension is shown in Fig. (3.5).

It is assumed that strain localization appears only after the maximum load is reached. The area under the entire softening stress-elongation curve, $\sigma(w)$, is denoted as G_f, which is given by

$$G_f = \int_0^{w_c} \sigma(w)\,dw \tag{3.3}$$

where w_c is the critical crack separation displacement when the softening stress is equal to zero. The material fracture toughness G_f represents the energy absorbed per unit area of crack and is regarded as a material fracture parameter.

In the fictitious crack model, the softening stress-separation curve $\sigma(w)$ is assumed to be a material property that is independent of structural geometry and size. It is noted that the softening curve $\sigma(w)$ can be completely determined if the material tensile strength f_{ct}, the fracture toughness G_f, and the shape of the $\sigma(w)$ curve are known. f_{ct} is a standard tensile strength measured on specimens of specified size and cured and tested in a specified way. The tensile strength is not always known. The main reason is that concrete is cracked, and cracking reduces the strength of concrete.

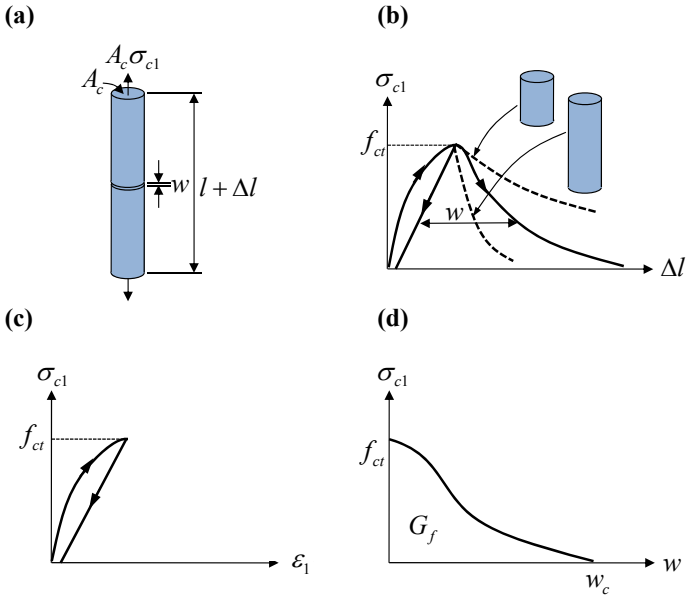

Figure 3.5 Fictitious crack model: (a) test specimen under uniaixal tension; (b) influence of specimen length; (c) stress-train diagram for regions outside the fracture process zone; (d) stress-crack opening relationship of fictitious crack

(1) Compression Failure controlled by Principal Stresses

A common representation of the stress-strain curve for concretes with strengths up to about 40MPa is the modified Hognestad stress-strain curve shown in Fig.(3.6). This consists of a second-degree parabola with apex at a strain of $1.8f_c^{"}/E_c$, where $f_c^{"}=0.9f_c^{'}$ followed by a downward-sloping line terminating at a stress of $0.85f_c^{'}$ and limiting strain of 0.038.

$$f_c = f_c^{"}\left[\frac{2\varepsilon_c}{\varepsilon_0}-\left(\frac{\varepsilon_c}{\varepsilon_0}\right)^2\right], \quad \varepsilon_0=\frac{1.8f_c^{"}}{E_c} \tag{3.4}$$

For normal-weight concrete ACI Section 8.5.1 gives the modulus of elasticity as

$$E_c = 4700\sqrt{f_c^{'}} \quad \text{[MPa]} \tag{3.5}$$

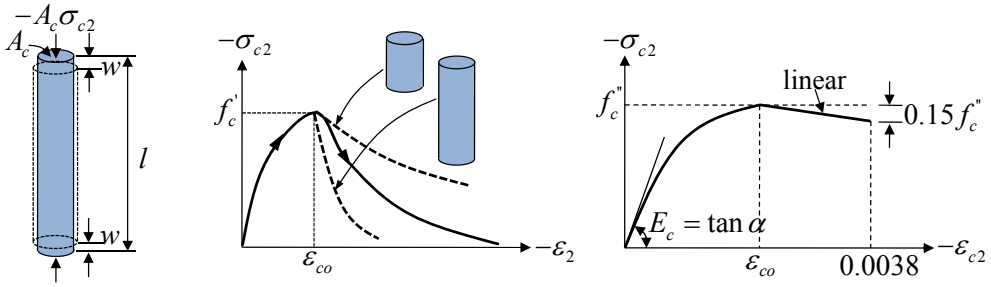

Figure 3.6 Uniaxial compression: (a) test specimen; (b) influence of length; (c) stress-strain diagram proposed by Hognestad

Several prisms with varying height (H=50, 100 and 200mm) and constant cross-sectional area (A=100×100mm^2) were loaded between brushes.

In Fig. (3.6-b) the axial stress-strain curves for three specimens with different height are plotted. Note that the stress axis made dimensionless with respect to the peak stress measured in each separate experiment. The peak stress measured in the three

tests is same. In the pre-peak region the stress-strain curve is the same for all heights, however, in the descending branch, the slope of the softening branch decreases when the height of the specimen decreases. When the post-peak curves are drawn as load-displacement curves as shown in Fig. (3.6-c) the differences in post-peak behavior disappear almost completely.

A localized deformation is smeared over different specimen heights, leading to the observed decrease of the softening slope in terms of stress and strain. In fact it is shown that failure in uniaxial compression is similar to the localized fracture mode observed in uniaxial tension. Only the location and orientation of the macroscopic fracture plane is different. In uniaxial tension, a localized macroscopic fracture plane develops perpendicular to the tensile direction and in uniaxial compression a shear type fracture plane develops which takes the form of a zig-zag band when the specimen height is decreased.

(2) Compression Failure controlled by Sliding Failure Mode

The occurrence of localization of deformation during softening of concrete subjected to uniaxial compression was for the first time shown by Van Mier (1984). As shown in Fig. (3.7), the curves for specimens of different slenderness $\left(h/d = 0.5 \sim 2.0\right)$, where h is a height and d represents width of specimen, were observed to fall in a narrow bundle. It should be mentioned that for the considered specimen slenderness the maximum stress varied only slightly.

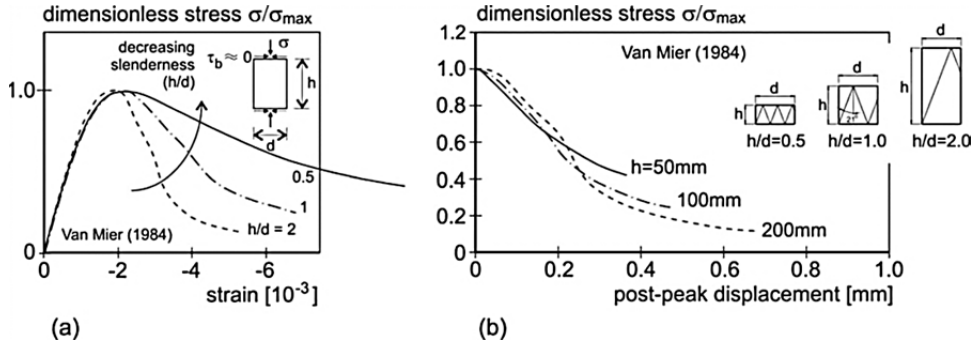

Figure 3.7 Localized failure of concrete in uniaxial compression: Effect of specimen slenderness on (a) the complete stress-strain curve; (b) the postpeak stress-deformation cruve.(Van Mier, 1984, 2009)

Fig. (3.8) shows the various stages of localized crack growth. Before the peak (Stage **a**) no cracking Beyond peak, at state **b**, inclined cracks appear to develop from three corners of triaxially loaded specimens are the reason for crack initiation in the corners. The cracks at Stage **b** are critical cracks according to the definition given above. At Stage **c**, well in the softening regime, the cracks from two positive corners propagate toward the center of the specimen. At Stage **d**, **e**, and f the shear band grows to cross the entire specimen cross section.

An interesting result which is explained the influence of boundary constraint on the fracture behavior of uniaxial compressed cylinders tested by Kotsovos (1983). The results are shown in Fig. (3.6). Tests were carried out under varying boundary conditions with different frictional characteristics. When the friction at the specimen-loading platen interface was reduced, the slope of the softening branch became increasingly steep. The various observed fracture modes are shown in the same figure. It must be concluded that material, specimen and testing machine characteristics are interacting, and have a considerable influence on the observed stress-deformation response.

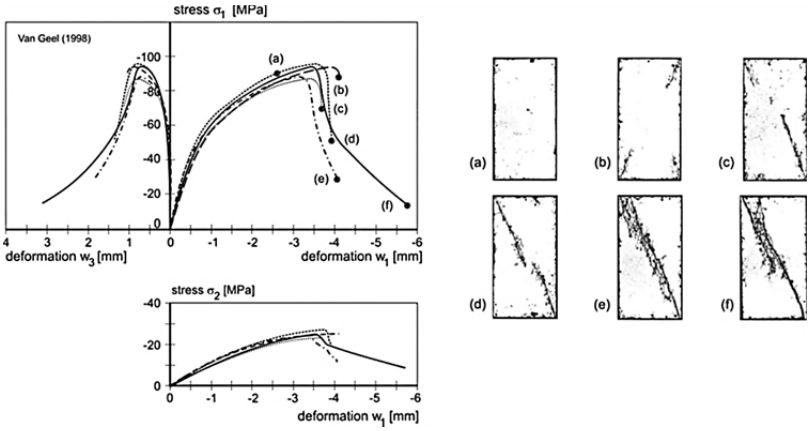

Figure 3.8 Shear-band propagation in prismatic specimens subjected to plane strain [Van Geel (1998), Van Mier (2009)]

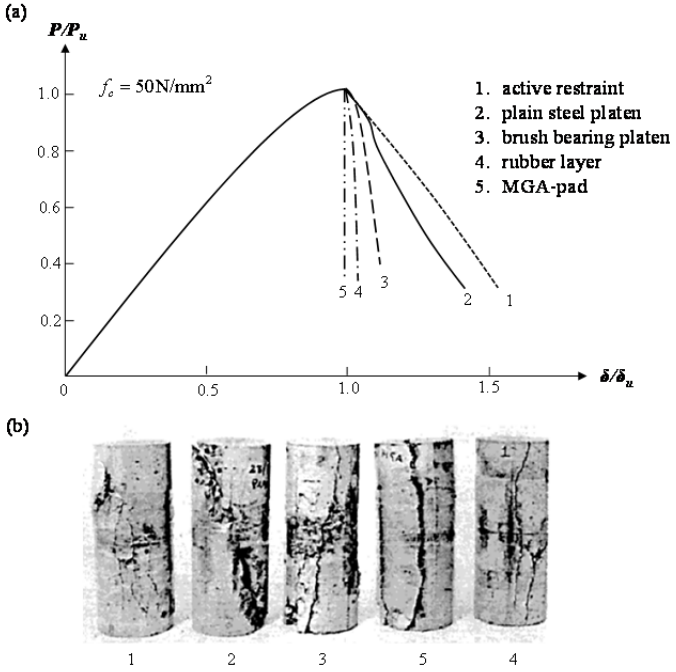

Figure 3.9 Influence of boundary conditions on the uniaxial load-displacement behavior in compression (Kotsovos 1983): (a) Load-displacement relationship obtained from tests; (b) Typical fracture modes of cylinders

3.3 Summary

This section presented the behavior of concrete and softening of concrete. From the study of uniaxial tension and compression behavior of concrete, the main points can be summarized as follows.

The same as the tensile failure, the compression failure of concrete exhibits a size effect. Unfortunately, to date the compressive response of concrete and its contribution to the post-peak response of a reinforced concrete beam has still not been clearly understood.

Failure mechanism of concrete under uniaxial tension and compression is classified into the general compression failure and sliding failure. Not only the general compression failure but also sliding failure shows the size effect.

4.Fracture Mechanics of Concrete

4.1 Linear Elastic Fracture Mechanics

For many years fracture mechanics has been used to study the crack propagation of mechanical components. It has been used methods of analytical solid mechanics to calculate the force on a crack and those of experimental solid mechanics to characterize the material's resistance to fracture.

Linear elastic fracture mechanics (LEFM) is the basic theory of fracture, originated by Griffith (1921, 1924) and completed in its essential aspects by Irwin (1957, 1958) and Rice (1968). This assumes that the material is isotropic and linear elastic. Based on these assumptions, the stress field near the crack tip is calculated by using the theory of elasticity.

LEFM is applicable to any material as long as certain conditions are met. These conditions rely on the presence of all basic ideal conditions analyzed in LEFM in which all materials are elastic except in a vanishingly small region (a point) at the crack tip. In fact, the stress near the crack tip is so high that some kind of inelasticity must take place in the immediate vicinity of the crack tip.

The theory of Linear Elastic Fracture Mechanics (LEFM) has been developed using a stress intensity factor determined by the stress analysis, and expressed as a function of stress and crack size i.e. $(\text{stress}) \times (\text{length})^{1/2}$. The strain energy release rate, or the stress intensity at the crack tip (K_C), eventually, will inevitably reach a critical value.

In this LEFM, fracture mode is classified into three types as shown in Fig. (4.1).

(1) Opening mode, Mode I

The crack surfaces separate symmetrically with respect to the planes *xy* and *xz*.

(2) Sliding mode, Mode II

The crack surfaces slide relative to each other symmetrically with respect to the plane *xy* and skew-symmetrically with respect to the plane *xz*.

(3) Tearing mode, Mode III

The crack surfaces slide relative to each other skew-symmetrically with respect to both planes *xy* and *xz*.

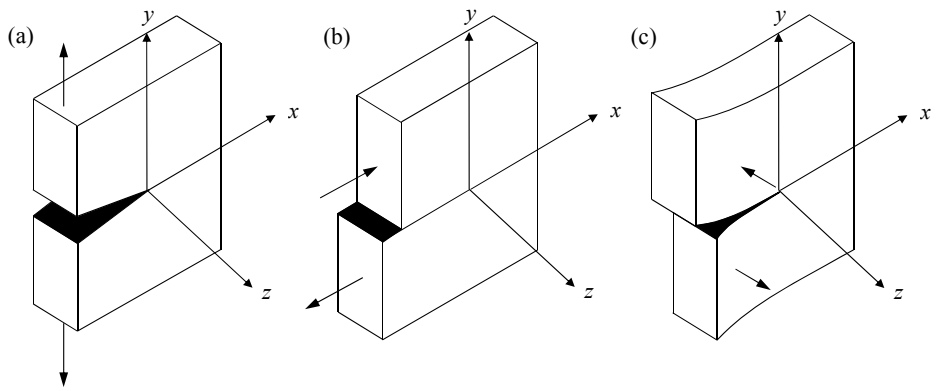

Figure 4.1 Three basic pure fracture modes: (a) Mode I or pure opening mode (b) Mode II or in-plane shear mode (c) Mode III or anti-plane shear mode

The stress and deformation fields associated with each of these three deformation modes will be determined for the cases of plane strain and generalized plane stress.

$$u = u(x, y), \quad v = v(x, y), \quad w = 0 \tag{4.1}$$

where u, v and w represent the displacement components along the axes x, y and z, respectively. Thus, the strains and stresses depend only on the variables x

and y. In crack problems, plane strain conditions are approximated in plates with large thickness relative to the crack length.

A generalized plane stress state parallel to the xy plane is defined by

$$\sigma_z = \tau_{zx} = \tau_{zy} = 0 \tag{4.2}$$

$$\sigma_x = \sigma_x(x,y), \quad \sigma_y = \sigma_y(x,y), \quad \tau_{xy} = \tau_{xy}(x,y) \tag{4.3}$$

where σ_x, σ_y, σ_z and τ_{xy}, τ_{zx}, τ_{zy} mean the normal and shear stresses associated with the system xyz. Generalized plane stress conditions are realized in thin flat plates with traction-free surfaces. In crack problems, the generalized plane stress conditions are approximated in plates with crack lengths that are large in relation to the plate thickness.

4.2 Stress Intensity Factor

To predict the stress state near the crack tip a stress intensity factor has been used in fracture mechanics. From the linear elastic theory Irwin showed that the stresses in the vicinity of a crack tip take the form as follows.

$$\sigma_{ij} = \frac{K}{\sqrt{2\pi r}} f_{ij}(\theta) + \cdots \tag{4.4}$$

where r, θ are the cylindrical polar co-ordinates of a point with respect to the crack tip.

K is a quantity which gives the magnitude of elastic stress field. It is called the stress intensity factor. Dimensional analysis shows that K must be linear related to stress and directly related to the square root of a characteristic length.

The general form of the stress intensity factor is given by

$$K = \sigma\sqrt{\pi a} f\left(\frac{a}{W}\right) \tag{4.5}$$

where $f(a/W)$ is a dimensionless parameter that depends on the geometries of the specimen and crack, and σ is the remotely applied stress. For an infinite plate with a central crack with length $2a$, $f(a/W)=1$ and thus $K=\sigma\sqrt{\pi a}$.

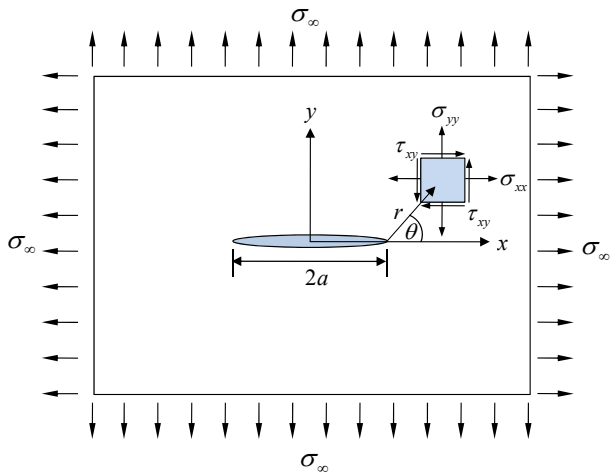

Figure 4.2 A crack of length *2a* in an infinite plate subjected to a uniform stress σ_∞ at infinity

Fig. (4.2) shows that a crack of length $2a$ which occupies the element $-a \le x \le a$ along the x-axis in an infinite plate subjected to uniform equal stresses σ_∞ along the y and x directions at infinity. The boundary conditions of the problem may be stated as follows

$$\sigma_y + i\tau_{xy} = 0 \quad \text{for} \quad y = 0,\ -a < x < a \tag{4.6}$$

And

$$\sigma_x = 0,\ \sigma_y = \sigma_\infty,\ \tau_{xy} = 0 \quad \text{for} \quad \sqrt{x^2 + y^2} \to \infty \tag{4.7}$$

The function defined by

$$Z_I = \frac{\sigma_\infty z}{\sqrt{z^2 - a^2}} \tag{4.8}$$

Satisfies the boundary condition Eqs.(4.6) and (4.7) and therefore is the Westergaard function for the problem shown in Fig. (4.2)

If we place the origin of the coordinate system at the crack tip $z = a$ through the transformation

$$\zeta = z - a \tag{4.9}$$

Equation (4.8) takes the form

$$Z_1 = \frac{\sigma_\infty (\zeta + a)}{\sqrt{[\zeta(\zeta + 2a)]}} \tag{4.10}$$

Expanding Eq. (4.10) we obtain

$$Z_1 = \frac{\sigma_\infty (\zeta + a)}{\sqrt{2a\zeta}} \left[1 - \frac{1}{2}\frac{\zeta}{2a} + \frac{1}{2}\frac{3}{4}\left(\frac{\zeta}{2a}\right)^2 - \frac{1}{2}\frac{3}{4}\frac{6}{5}\left(\frac{\zeta}{2a}\right)^3 + \cdots \right] \tag{4.11}$$

For small $|\zeta|$, this is near the crack tip at $x = a$, Equation (4.11) may be written

$$Z_1 = \frac{K_I}{\sqrt{2a\zeta}} \tag{4.13}$$

where $K_I = \sigma_\infty \sqrt{\pi a}$

Using polar coordinate, r, θ we have

$$\zeta = re^{i\theta} \tag{4.14}$$

And the stresses near the crack tip are determined as follows.

$$\sigma_{xx} = \frac{K_I}{\sqrt{2\pi r}} \cos\left(\frac{\theta}{2}\right)\left[1 - \sin\left(\frac{\theta}{2}\right)\sin\left(\frac{3\theta}{2}\right)\right] \tag{4.15}$$

$$\sigma_{yy} = \frac{K_I}{\sqrt{2\pi r}} \cos\left(\frac{\theta}{2}\right)\left[1 + \sin\left(\frac{\theta}{2}\right)\sin\left(\frac{3\theta}{2}\right)\right] \tag{4.16}$$

$$\tau_{xy} = \frac{K_I}{\sqrt{2\pi r}} \cos\left(\frac{\theta}{2}\right)\sin\left(\frac{\theta}{2}\right)\cos\left(\frac{3\theta}{2}\right) \tag{4.17}$$

Similarly, for mode-II crack in an infinite cracked plate subjected to plane shearing, as shown in Fig. (4.3), the stress components near the crack tip are as follows.

$$\sigma_{xx} = -\frac{K_{II}}{\sqrt{2\pi r}} \sin\left(\frac{\theta}{2}\right)\left[2 + \cos\left(\frac{\theta}{2}\right)\cos\left(\frac{3\theta}{2}\right)\right] \tag{4.18}$$

$$\sigma_{yy} = \frac{K_{II}}{\sqrt{2\pi r}} \sin\left(\frac{\theta}{2}\right)\cos\left(\frac{\theta}{2}\right)\cos\left(\frac{3\theta}{2}\right) \tag{4.19}$$

$$\tau_{xy} = \frac{K_{II}}{\sqrt{2\pi r}} \cos\left(\frac{\theta}{2}\right)\left[1 - \sin\left(\frac{\theta}{2}\right)\sin\left(\frac{3\theta}{2}\right)\right] \tag{4.20}$$

where the stress intensity factor for mode-II fracture K_{II} is given by

$$K_{II} = \tau\sqrt{\pi a} \tag{4.21}$$

The values of K_I and K_{II} account for singularity of the stress field at the crack tip and are function of load, specimen geometry, boundary condition, and crack size. Stress intensity factors can serve as a fracture criterion. A crack propagates whenever K_I or K_{II} is equal to

$$K_I = K_{Ic}, \qquad K_{II} = K_{IIc} \tag{4.22}$$

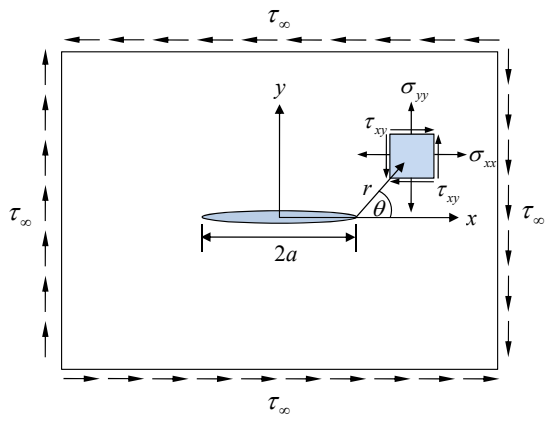

Figure 4.3 A crack of length *2a* in an infinite plate subjected to uniform in-plane shear stresses τ_∞ at infinity

where K_{Ic} and K_{IIc} are the critical stress intensity factors for mode-I and mode-II cracks, respectively. The values of K_{Ic} and K_{IIc} are regard as material fracture properties based on linear elastic fracture mechanics.

Stress intensity factors can also be used to characterize structures. Based on how stress intensity factors change with crack lengths, structures can be classified as positive and negative geometries. The stress intensity factor increases with the increasing crack length for the positive-geometry structures. On the other hand, the stress intensity factor initially decreases and then increases with the crack propagation for the negative-geometry structures. Therefore, based on linear elastic solutions, any propagation of the crack means a catastrophic failure for positive-geometry structures. [Shah et al. (1995)]

4.3 Critical Stress Intensity Factor

Mode-1 fracture is uniquely determined by K_I since the stress state of the material surrounding a very small fracture process zone, crack tip, the crack will propagate until this stress intensity factor reaches a certain critical value K_{Ic}, called critical stress intensity factor or fracture toughness. K_{Ic} for the given material may be determined performing a fracture test and determining the K_I value that provoked failure. Because the energy fracture criterion must also hold, and indeed does according to the fundamental relationship, is related to the fracture energy G_f by

$$K_{Ic} = \sqrt{EG_f} \tag{4.23}$$

With this definition, the local fracture criterion for pure mode 1 may be stated in analogy to the energy criterion

if $K_I < K_{Ic}$ then : No crack growth (stable)

if $K_I = K_{Ic}$ then : Quasi-static growth possible

if $K_I > K_{Ic}$ then : Dynamic growth (unstable)

For loadings that are not pure mode 1, the problem becomes more difficult because, in general, an initially straight crack kinks upon fracture and the criteria must give not only the loading combination that produces the fracture, but also the kink direction.

The early researches on concrete fracture often attempted to apply LEFM directly to evaluate the fracture tests. In this case, the fracture toughness is calculated from the

peak load P_u (or nominal strength σ_{Nu}) using the LEFM formula for a propagating crack in a specimen. If the geometry is so-called

4.4 Material Properties and Nonlinear Zone

4.4.1 Nonlinear Behavior of Concrete

Concrete, rocks, most ceramics and sintered metals contain defects, such are pores and cracks even in the virgin state. These defects reduce their tensile capacity.
Fig. (4.4) shows the typical tensile stress-elongation curves for quasi-brittle material. Initially, randomly distributed microcracks are formed. At some point before the peak stress, microcracks begin to localize into a macrocrack that propagates at the peak stress. Strain softening is observed under steady-state propagation of this crack.

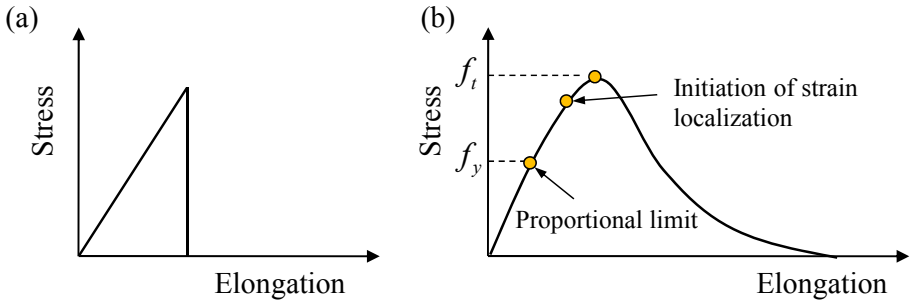

Figure 4.4 Tensile stress-elongation curves: (a) linear elastic materials; (b) Quasi-brittle materials

The basic difference between fracture principles applied to different kinds of material is shown in Fig. (4.5). A nonlinear zone ahead of the crack tip is composed of fracture process zone and hardening plasticity. LEFM is applied to the material in which the zone is very small in case of Fig. (4.5-a). Fig. (4.5-b) shows the nonlinear behavior for ductile material in which the zone with nonlinear material behavior or

hardening plasticity is large and the fracture zone is small. The third case is applicable to nonlinear behavior of cementitious materials in which the fracture zone is large and hardening plasticity is small.

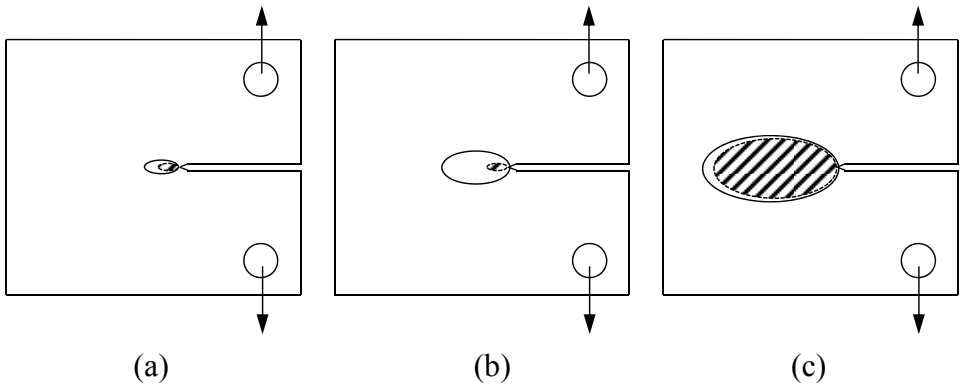

Figure 4.5 Types of nonlinear zone in different types of materials: (a) Linear elastic; (b) Nonlinear plastic; and (c) Quasibrittle

In the other way, the nonlinear behavior of three different types of materials subjected to uniaxial tension can be shown using stress-deformation relationship as illustrated in Fig. (4.6).

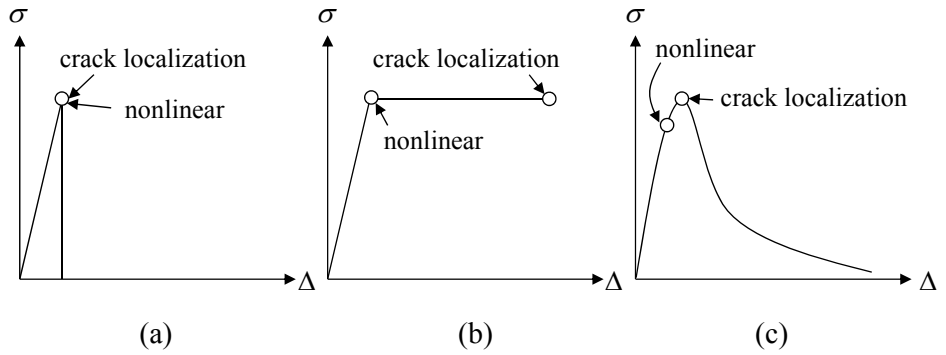

Figure 4.6 Stress-displacement behavior under uniaxial tension: (a) Brittle; (b) Ductile; and (c) Quasi-brittle materials

The brittle material shows a linear elastic behavior almost up to the peak load, and a crack will propagates through the specimen just after the peak. The ductile material behavior shown in Fig. (4.6-b) is characterized by a pronounced yield plateau and the nonlinear behavior starts much behavior the onset of crack localization. In the quasibrittle material, the nonlinear behavior starts before the peak load and then upon arrival at the peak load, crack localization will occur.

4.4.2 Concrete Crack and Fracture Process Zone

In this section, the equations for a crack tip based on linear elastic region were obtained. These equations result in infinite stresses at the crack tip, therefore, there is a stress singularity. This solution assumes the size of the inelastic zone at the crack tip is zero. However, real materials have some finite size R. This limits the stresses at the crack tip. More importantly, structural materials deform plastically above the yield stress and so in reality there will be a plastic zone surrounding the crack tip.

Fig. (4.7) shows the estimation of size of plastic zone at crack tip. The distribution of σ_y ahead of the crack tip will be as shown in Fig. (4.7-a). The value of σ_y is greater than the material yield stress σ_{ys} for the region $r < r_{p0}$. The distance r_{p0} indicates the size of plastic zone at crack tip and its value can be estimated from the condition of $\sigma_y = \sigma_{ys}$ at $r = r_{p0}$.

$$r_{p0} = \frac{K_I^2}{2\pi\sigma_{ys}^2} = \frac{a}{2}\left(\frac{\sigma}{\sigma_{ys}}\right)^2 \tag{4.24}$$

Fig. (4.7-b) shows the size of plastic zone at crack tip proposed by Irwin (1960). For the analysis there are several restrictions.

1) The plastic zone shape is considered to be circular.
2) Only the situation along the x-axis is analyzed.
3) The material behavior is considered to be elastic-perfectly plastic.
4) A plane stress state is considered.
5) Assuming that the area of A is equal to the area of B, the size of plastic zone r_p is obtained as follows.

$$r_p = \delta a + r_{p0} = a\left(\frac{\sigma}{\sigma_{ys}}\right)^2 = \frac{1}{\pi}\left(\frac{K_I}{\sigma_{ys}}\right)^2 \tag{4.25}$$

It is seen that the size of the plastic zone, r_p, based on the above second-order estimation is twice as large as the first-order estimation, r_{p0}.

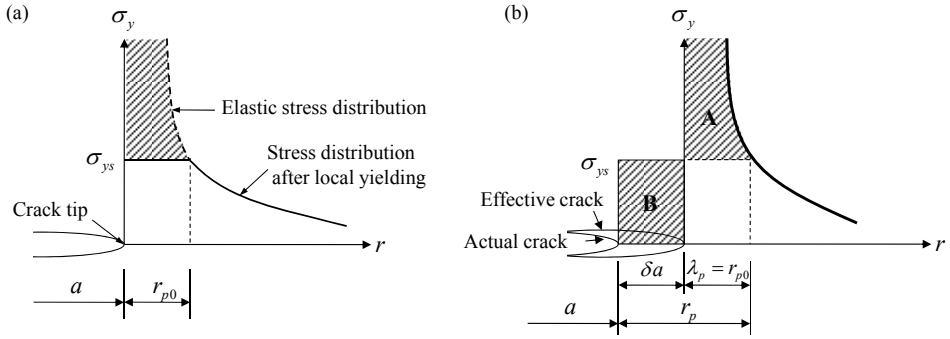

Figure 4.7 Estimation of size of plastic zone at crack tip: (a) A first approximation; (b) Proposed by Irwin (1960)

Consequentially, it should be noted that since LEFM assumes the size of fracture process zone is zero, that is, there is singularity at the crack tip, in other words, it is impossible to apply the LEFM directly, it is necessary to determine the fracture process zone to resolve the singularity.

4.6.3 Fracture Process zone for Mixed Mode Fracture

The mechanical behavior of structure is greatly influenced by the materials used. Generally, based on tensile stress-deformation relationship, structural failure is classified brittle, ductile and quasi-brittle as shown in Fig. (4.6). When a brittle failure occurs, the stress drops to zero suddenly. On the other hand, stress stays a constant when ductile failure takes place. In case of quasi-brittle materials, after peak stress, the stress decreases gradually as shown in Fig. (4.6-c). In this case, an inelastic zone develops at the location of the maximum stress when fracture occurs. This inelastic zone is often referred to a fracture process zone. Generally, the normal tensile stress decreases toward the crack tip within the fracture process zone. The development of fracture process zone usually causes a softening behavior in the load-deformation relationship. This happens for concrete, rock, cemented sands etc. When concrete is subjected to a large compression parallel to the crack plane (as in splitting fracture), the fracture process zone may be large.

Fig. (4.8) shows the three types of fracture process zone which explain how the softening influences. Irwin proposed that the presence of the crack tip plastic zone reduces the stiffness of the structure, and this is equivalent to that of a structure containing a longer crack. The distribution of stress σ_1 (principal tensile stress at compression zone) at the tip of the effective crack is given in Fig. (4.8-a). The stress over the length of r_1 and at the tip of the effective crack is limited to f_{ct}.

Further analysis shows that if the progressive softening is concave upward, instead of linear, one can get much larger sizes of the fracture process zone for quasi-brittle materials.

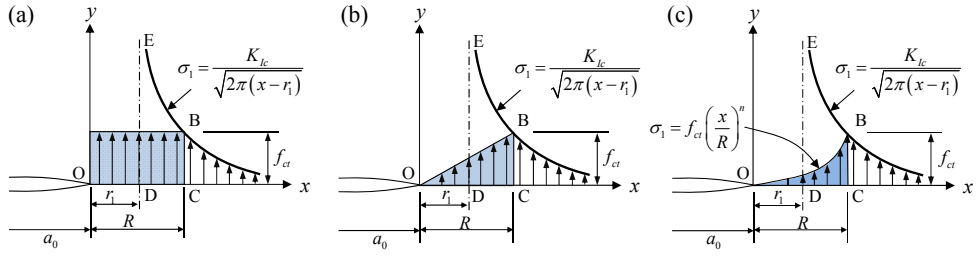

Figure 4.8 Size of fracture process zone

To prove this result, take the case shown in Fig. (4.8-c), in which the stress profile along the fracture zone is parabolic of degree n. The areas OBCDO and DEBCD to be equal.

$$\int_{r_1}^{R} K_{Ic}\left[2\pi\left(x-r_1\right)\right]^{-1/2} dx = \int_{0}^{R} f_{ct}\left(\frac{x}{R}\right)^n dx = \frac{1}{n+1} R f_{ct} \tag{4.26}$$

This equation leads to the following solution.

$$R = \frac{n+1}{\pi}\left(\frac{K_{Ic}}{f_{ct}}\right)^2 \tag{4.27}$$

This shows that the nonlinear zone size may be many times Irwin's estimate for metal. The values of n for concrete may be of the order of 7 and as large as 14.

To sum up, one may state that the nonlinear zone ahead of the crack tip at the critical state for a very large structure may be written as

$$R = \eta\left(\frac{K_{Ic}}{f_{ct}}\right)^2 = \eta\frac{E^{'}G_f}{f_{ct}^2} \tag{4.28}$$

where η is dimensionless constant taking the value $1/\pi$ for Irwin's estimate for metal. While, for quasi-brittle materials, this value is roughly between 2 and 5 for

concrete. Consequentially the fracture process zone is proportional to η. Hillerborg et al. (1976) called the right-hand side of the above equation the characteristic length l_{ch}.

If the critical stress intensity factor for mode-I fracture K_{Ic} is constant, the size of fracture process zone R decreases with increasing the tensile strength of concrete as shown in Fig. (4.9). Equation (4.28) shows that the size of fracture process zone is inversely proportional to the square of tensile strength of concrete. Because the tensile strength f_{ct} is function of compressive strength of concrete $f_c^{'}$, the value of R is reduced as the compressive strength increases.

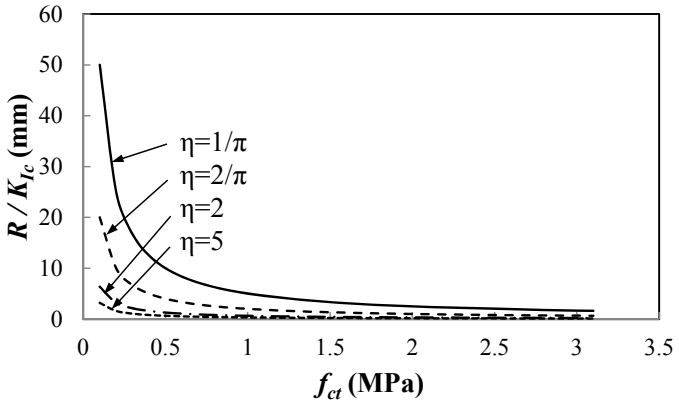

Figure 4.9 Variation of size of fracture process zone for concrete strength

Fig. (4.10) represents the size of fracture process zone for compressive strength of concrete. Because the critical stress intensity factor is function of elastic modulus of concrete E_c and fracture energy G_f.

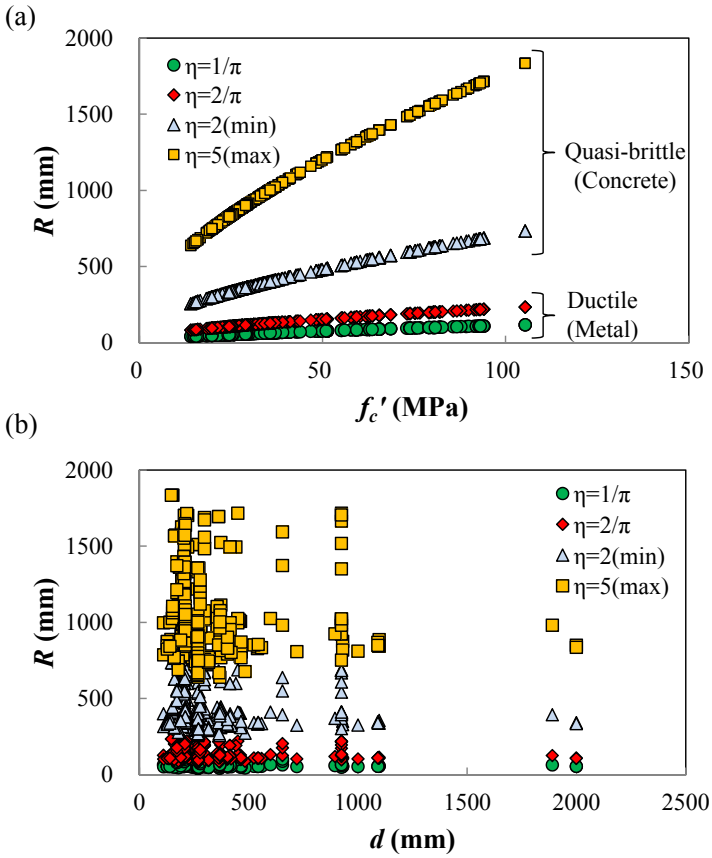

Figure 4.10 Size of fracture process zone: (a) for concrete strength and (b) for effective depth with test results

4.5 Size Dependent Critical Stress Intensity Factor

The critical stress intensity factor or fracture toughness of cement paste, mortar and concrete has been measured by many investigators.

Ohgishi et al. (1986) performed the experimental study to investigate the dependency on test parameter of critical stress intensity factor, K_{Ic} of cement paste and mortar. According to test results of cement paste K_{Ic} is not constant for the beam depth as shown in Fig. (4.11). As the depth of beam increases, K_{Ic} increases.

Higgins et al. (1976) investigated the fracture behavior of hardened cement paste. As a result of three point-bending tests critical stress intensity factor varies with beam depth. And Hillerborg (1984) reported that according to the Bologna tests as a function of the beam depth, K_{Ic} increases as the depth of beam increases.

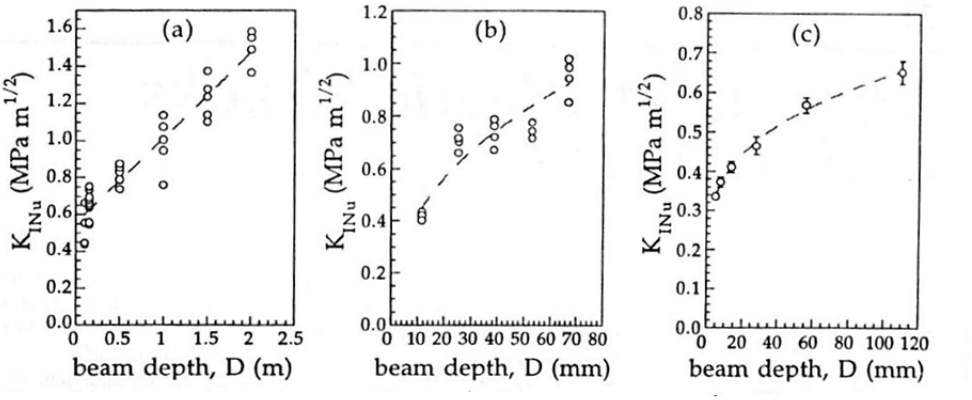

Figure 4.11 Dependence of the apparent fracture toughness on the specimen size: (a) Concrete (Di Leo's data, after Hillerborg 1984); (b) Mortar (after Ohgishi et al. 1986); (c) Hardened cement paste (after Higgins and Bailey 1976)

Critical stress intensity factors also depend on the crack length. The effect of crack length on a critical stress intensity factor is comparable to the effect of specimen dimensions. In both cases the condition of applicability of linear elastic fracture mechanics claims independence of fracture toughness of the respective variable. The experimental results on the effect of crack length are rather contradictory.

The decrease of fracture toughness with increasing crack length is explained by Hillemeier and Hilsdorf. They conducted an analytical and experimental investigation on hardened cement paste. Their results show that the value of K_{Ic} decreases with increasing crack length. Shah and McGarry reported increasing K_{Ic} with increasing notch depth. However, since the failure in their experiments seem to be catastrophic.

However many tests have ignored the effect of crack growth on K_{Ic}. Hardened cement paste is generally brittle, and it is difficult to restrict and control crack growth, particularly in flexural tests. Therefore, The value of K_{Ic} would be expected to be independent of crack growth in cement paste. However, both notched beam and DCB tests show that fracture toughness decreases with crack growth.

Based on these experimental results, Bazant (1998) has proposed that the apparent fracture toughness K_{INu} is defined as the value of K_{IN} at peak load as follows.

$$K_{INu} = \sigma_{Nu}\sqrt{D}k(\alpha_0) \tag{4.29}$$

where σ_{Nu} represents the peak load, D is size of specimen and α_0 means the relative crack length calculated by a_c / D.

It should be noted that critical stress intensity factor is dependent on the size, depth of beam.

For mode-I fracture, the critical stress intensity factor K_{Ic} is defined as $K_{Ic} = \sqrt{EG_{f(I)}}$ and also for mode-II facture, critical stress intensity factor can be expressed as $K_{IIc} = \sqrt{EG_{f(II)}}$, where $G_{f(I)}$ and $G_{f(II)}$ represent the fracture energy for pure mode-I and mode-II fracture, respectively. Generally, it is said that these factors should be determined by experiment.

For mixed modes, Bazant says in his book that the critical stress intensity factor for mode-II or mode-III fractures should be determined by using phenomenological approach like ellipsoidal failure locus or maximum principal stress criterion. Following equation shows the ellipsoidal failure locus.

$$\frac{K_I^2}{K_{Ic}^2} + \frac{K_{II}^2}{K_{IIc}^2} - 1 = 0 \tag{4.30}$$

where K_{Ic} and K_{IIc} are material parameter to be determined by experiment.

This pure phenomenological approach may prove practically useful, but gives no insight into the way fracture proceeds. Moreover, according to Eq. (4.30), critical stress intensity factor for mode-II fracture depends on the mode-I fracture. Thus, In this formula there is no evidence to explain the critical stress intensity factor itself.

As mentioned above that the critical stress intensity factors can be obtained by using ultimate values at the crack tip. The main difference is that conventional critical stress intensity factor based on energy approaches is constant always regardless of geometry but the latter is not constant in accordance with size of beams.

Thus, in this study, critical stress intensity factors by ultimate stress at crack tip were used as follows.

$$\text{Mode-I fracture : } K_{Ic} = \sigma_u \sqrt{\pi a_0} \tag{4.31}$$

$$\text{Mode-II fracture : } K_{IIc} = \tau_u \sqrt{\pi a_0} \tag{4.32}$$

where σ_u and τ_u are ultimate stress causing the mode-I and mode-II fracture, respectively.

4.6 Size Effect

4.6.1 Size Effect of Linear Elastic Materials

Consider the cracked plane loaded in mode-I fracture. Let a_0 be the initial crack length and α_0 the initial relative crack length. From the Eq. (4.13), crack growth condition $K_I = K_{Ic}$ is fulfilled when σ_N reaches a maximum given by

$$K_I = \frac{P}{b_w\sqrt{d}}\hat{k}(\alpha) = \sigma_N\sqrt{d}\,k(\alpha) \tag{4.33}$$

where $\hat{k}(\alpha)$ and $k(\alpha)$ are dimensionless functions, $\alpha = a_c / d$ is relative crack length, where a_c means the crack length and d represents the size of specimen.

$$\sigma_{Nu} = \frac{K_{Ic}}{\sqrt{d}\,k(\alpha)} \text{ for } \alpha > \alpha_0 \tag{4.34}$$

If $k(\alpha)$ increase with α, then σ_{Nu} decreases. On the other hand, if $k(\alpha)$ decrease σ_{Nu} increases and reaches a maximum when $k(\alpha)$ is minimum.

In any case, since both α_0 is constant for geometrically similar structures, it turns out that the nominal strength is always inversely proportional to the square root of the size as following equation.

$$\sigma_{Nu} = \sigma_{Nu1}\sqrt{\frac{d_1}{d}} \tag{4.35}$$

where σ_{Nu1} and d_1 are nominal strength and size of geometrically similar structure, respectively.

Thus, it has been generally proved that geometrically similar structures following LEFM exhibit the inverse square root size effect.

4.6.2 Size Effect of Concrete Structures

Based on the load-deflection relationship two basic types, ductile and brittle, are distinguished as shown in Fig. (4.12)

If load-deflection diagram does not have such a plateau, the failure is not plastic but brittle shown in Fig. (4.12-b) If there no significant geometric effects such as the $P-\Delta$ effect in buckling, the absence of a plateau implies the existence of softening in the material due to fracture.

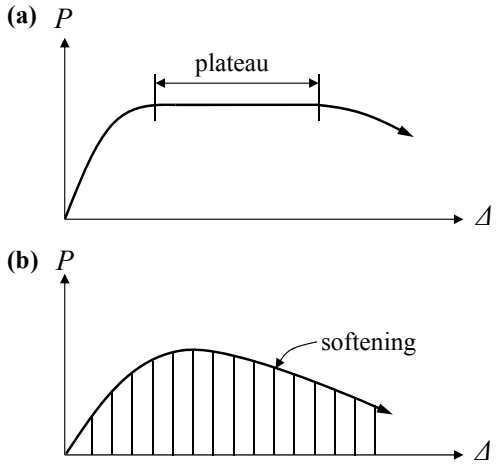

Figure 4.12 Load deflection diagram of ductile and brittle structures (ACI Committee 446, 1992)

Consider a punching shear failure in a slab as shown in Fig. (4.13). In part (a) is shown the failure surface. A plastic material response is shown in Fig. (4.13-b). The

cross section gradually plasticizes until all its points are at the yield limit. If the material exhibits softening the stress peak moves across the failure zone as shown in parts (c) and (d). For the cast of the structure is large the stress profile develops a steep stress drop behind the peak-stress point. This effect depends on the relative size of the process zone versus the size of the structure.

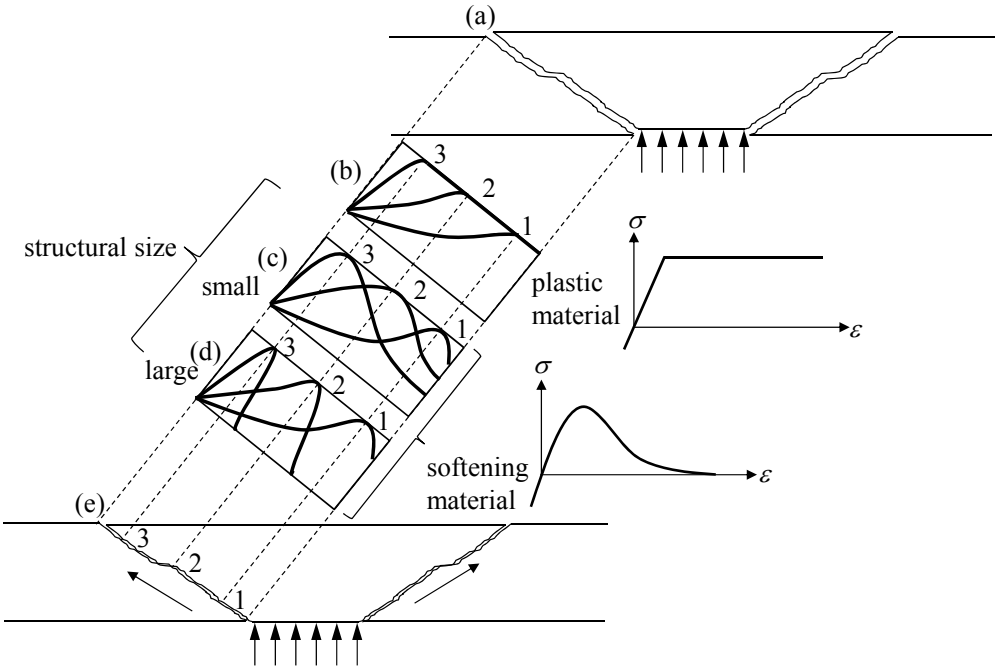

Figure 4.13 Progressive nature of failure illustrated fro punching shear of a slab (ACI Committee 446, 1992)

By general convention, the load capacity predicted by plastic limit analysis or an theory in which the material failure criterion is expressed in terms of stress or strain (or both) are said to exhibit no size effect as shown in Fig. (4.14).

The size effect is defined through a comparison of geometrically similar structures of different sizes. It is conveniently characterized in terms of the nominal strength, σ_{Nu}, representing the value of the nominal stress, σ_N, at maximum (ultimate) load,

P_u . The nominal stress represent any actual stress in the structure and may be defined simply as $\sigma_N = P / bD$; b is the thickness of a two-dimensional structure, and D is the characteristic dimension of the structure, which may be chosen as any dimension, e.g., the depth of the beam.

According to the classical failure theories, such as the elastic analysis with allowable stress, plastic limit analysis, or any other theory that uses some type of a strength limit or failure surface in terms of stress or strain σ_{Nu} is constant, i.e., independent of structural size.

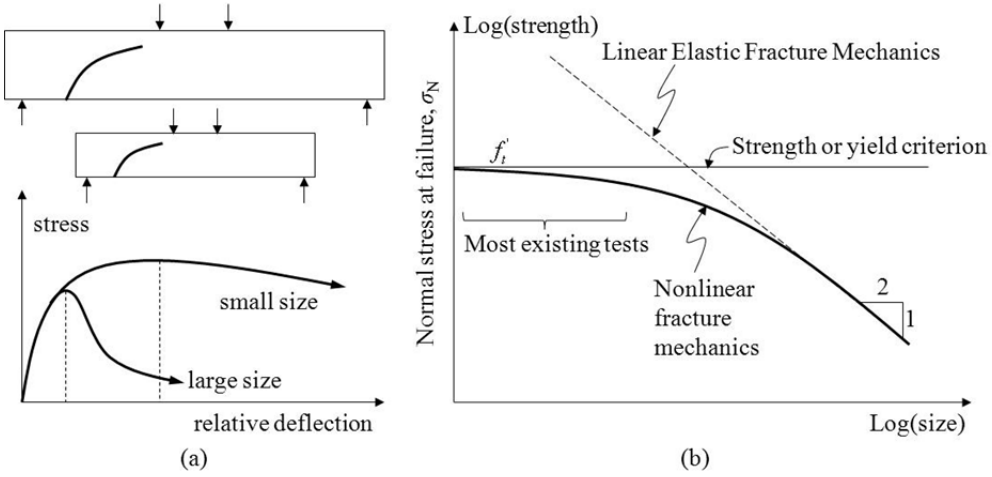

Figure 4.14 Fracture mechanics size effect for geometrically similar structures of different sizes (ACI Committee 446, 1992)

4.7 Mixed-Mode Fracture of Concrete Beams

4.7.1 Introduction

In reality, mixed mode fracture combined by mode-I fracture (opening) and mode-II fracture (shearing) is observed in reinforced concrete structures. Many researchers have studied the mixed mode fracture concrete. Ingraffea and Gerstle (1985) reported that the finial failure load is very sensitive to the material constants, i.e., tensile strength, fracture energy and shape of the stress-separation curve) used in the fictitious crack model proposed by Hillerborg et al. (1976). It has been reported that it is very difficult to accurately determine these material properties from laboratory tests. Therefore, a trial and error method or numerical analysis has to be used to determine the appropriate material properties for the particular experimental results. Therefore, it is necessary to evaluate the mixed mode fracture more accurately based on theoretical background. In this section, mixed-mode fracture will be discussed for proposed newly failure mechanism of reinforced concrete slender beams.

Erdogan and Shi (1963) proposed maximum principal stress criterion for in-plane mixed mode crack growth will happen along the direction for which the initial normal stress across the possible crack path is tensile, principal and maximum.

Consider a crack in a mixed-mode stress field governed by the values of the opening-mode K_I and sliding-mode K_{II} stress intensity factors, the singular polar stress components (Fig. 4.15) near the crack tip are expressed by

$$\sigma_{\theta\theta} = \frac{1}{\sqrt{2\pi r}}\left[K_I \cos^3\frac{\theta}{2} - 3K_{II}\cos^2\frac{\theta}{2}\sin\frac{\theta}{2} \right] \tag{4.36}$$

$$\sigma_{r\theta} = \frac{1}{\sqrt{2\pi r}}\left[K_I \cos^2\frac{\theta}{2}\sin\frac{\theta}{2} + K_{II}\cos\frac{\theta}{2}\left(\cos^2\frac{\theta}{2} - 2\sin^2\frac{\theta}{2}\right)\right] \qquad (4.37)$$

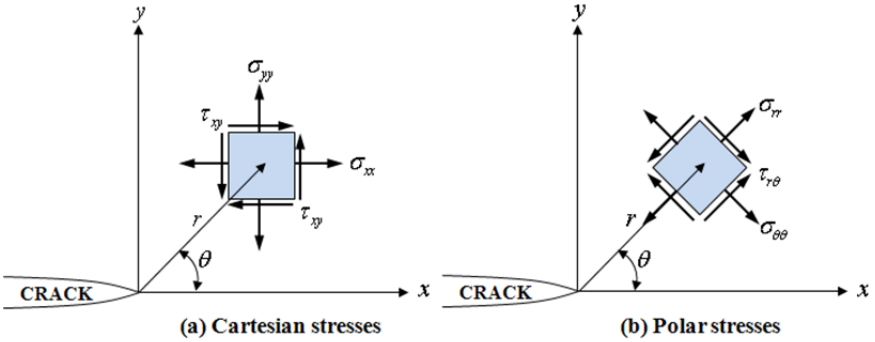

Figure 4.15 Stress notation in region of crack tip: (a) Cartesian stress; (b) polar stresses

The assumptions made in the criterion for crack extension in brittle materials may be stated as

(a) The crack extension starts from its tip along the radial direction $\theta = \theta_c$ on which σ_θ becomes the maximum.

(b) Fracture stats when that maximum of σ_θ reaches a critical stress σ_c equal to the fracture stress in uniaxial tension.

(c) The magnitude $\sqrt{\sigma_{\theta\theta}^2 + \sigma_{r\theta}^2}$ of the traction vector is the maximum with respect to θ.

Observe that the circumferential stress σ_θ in the direction of crack extension is a principal stress, and the shear stress $\tau_{r\theta}$ for that direction vanishes. The crack extension angle θ_c is calculated by

$$K_I \cos^2\frac{\theta}{2}\sin\frac{\theta}{2} + K_{II}\cos\frac{\theta}{2}\left(\cos^2\frac{\theta}{2} - 2\sin^2\frac{\theta}{2}\right) = 0 \tag{4.38}$$

Dividing the above equation by $\cos^3(\theta/2)$ one gets a second degree equation in $\tan(\theta/2)$ which gives the cracking directions as a function of the ratio K_I / K_{II}

$$\tan\left(\frac{\varphi_1}{2}\right) = \frac{1}{4}\left[\frac{K_I}{K_{II}} \pm \sqrt{\left(\frac{K_I}{K_{II}}\right)^2 + 8}\right] \tag{4.39}$$

For opening-mode loading ($K_I \neq 0, K_{II} = 0$), Equations (4.38) and (4.39) yield $\theta_c = 0$, $K_I = K_{Ic}$, while for sliding-mode loading they give

$$\theta_c = -\cos^{-1}\frac{1}{3} = -70.6^\circ,\ K_{II} = K_{IIc} = \sqrt{\frac{3}{4}}K_{Ic} \tag{4.40}$$

Eliminating θ_c in equation and gives the fracture locus in $K_I - K_{II}$ coordinates shown in Fig. (4.16).

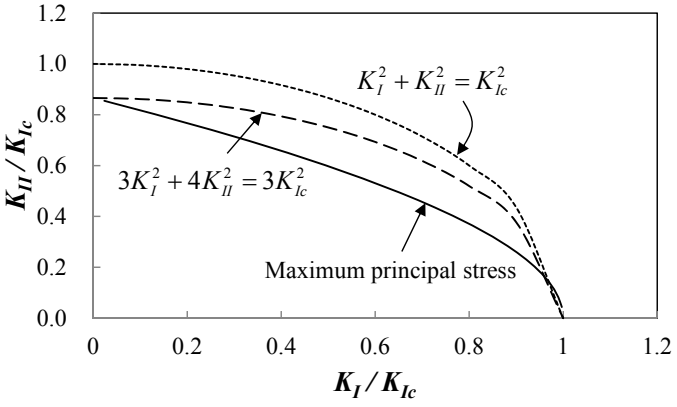

Figure 4.16 Failure loci for different mixed mode fracture criteria

4.7.2 Size Dependent Effective Stress Intensity Factors

Stress intensity factor is defined as function of stress at the crack tip and crack length as mentioned in Section 4.2. If the crack length is identical, the stress intensity factor for mode-I fracture can be expressed as normal stress at the crack tip and it can be given as shear stress in case of mode-II fracture. Both cases are assumed that only normal stress or shear stress exists at the crack tip for pure bending or pure shear.

However, both the normal and shear stress exist at the tip of diagonal crack. In this case, mixed-mode fracture occurs due to those combined stresses.

Consider the reinforced concrete beam with rectangular section as shown in Fig. (4.17). It is assumed that failure mechanisms are divided into four regions with crack growth, that is, pure bending zone, flexural tension zone, pure shear zone and compression zone.

When a RC beam is subjected to bending moment the pure flexural cracks occur in the pure bending zone perpendicularly up to reinforcement steel at distance x_a. And then, the inclined crack is developed from reinforcement steel indicated point A to neutral axis denoted point B with the angle φ_1 in the flexural tension zone. The second branch which is another inclined crack with the φ_2 occurs toward the load point crossing the compression zone.

Based on the crack growth, the failure mechanism of concrete can be divided into two fracture mode. If the failure is controlled by tension, in other words, a principal tensile stress reaches a tensile stress, diagonal tension failure occurs. On the other hand, if the failure is controlled by friction, that is, the stress intensity factor is equal to the critical stress intensity factor for mode-II fracture, sliding failure takes place. Since stress intensity factors can be used to characterized structures, that is, stress

intensity factors change with crack lengths, shear strength can be expressed by stress intensity factor based on crack growth.

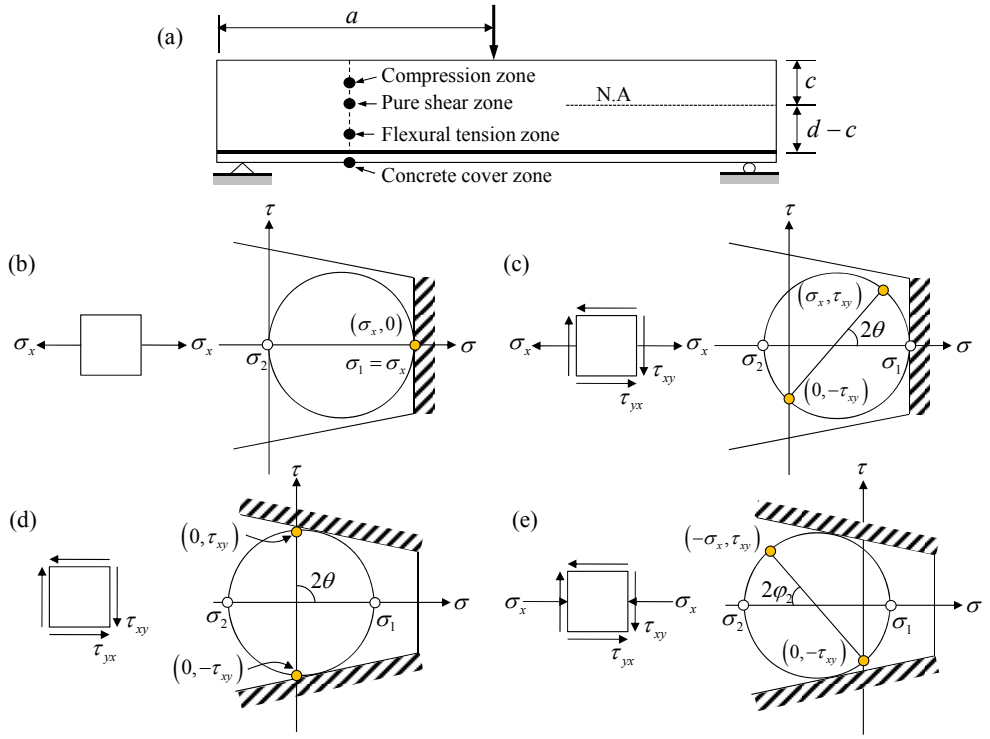

Figure 4.17 Stress states for height of reinforced concrete beams: (a) reinforced concrete beams subjected to concentrated load; (b), (c), (d), (e) stress states at concrete cover zone, flexural tension zone, pure shear zone and compression zone, respectively.

(1) Effective stress intensity factor in flexural tension zone

After propagation of flexural cracks in the concrete cover zone, the inclined crack occurs due to combined stresses with normal stress and shear stress. This crack propagates from the reinforcement steel to the neutral axis. Because the variation of

principal stresses depends on the depth of the beam, thus stress intensity factor will vary throughout the beam depth.

In flexural tension zone, the crack tip is subjected to combined stresses, horizontal normal stress and shear stress, both mode-I (opening) and mode-II (sliding) components exist in this zone.

The principal tensile stress and shear stress with respect to $x_1 - y_1$ axis are

$$\sigma_{x1} = \frac{\sigma_x}{2} + \frac{\sigma_x}{2}\cos 2\varphi_0 + \tau_{xy}\sin 2\varphi_0 \tag{4.41}$$

$$\tau_{x1y1} = -\frac{\sigma_x}{2}\sin 2\varphi_0 + \tau_{xy}\cos 2\varphi_0 \tag{4.42}$$

where φ_0 represent the angle of inclined crack in pure bending zone as illustrated in Fig. (4.17).

Thus, the stress intensity factors for mode-I and mode-II fracture can be expressed in terms of principal stress and crack length as follows.

$$K_I = \sigma_{x1}\sqrt{\pi a_c}, \qquad K_{II} = \tau_{x1y1}\sqrt{\pi a_c} \tag{4.43}$$

where σ_{x1} means the principal tensile stress, τ_{x1y1} represents the shear stress acting on the cracked plane, and a_c is the length of the newly inclined crack developed from initial crack tip which assumes the flexural crack in pure bending zone.

Jenq and Shah (1988) have proposed the effective stress intensity factor for mixed mode fracture of concrete with combining K_I and K_{II} as follows.

$$K_{eff} = \sqrt{K_I^2 + K_{II}^2} \tag{4.44}$$

As shown in Fig. (4.17), concrete fracture is governed by mode-I facture as same as separation failure in modified Mohr-Coulomb criterion in flexural tension region (Fig. 4.17–c). Thus, the effective stress intensity factor for mixed mode fracture in flexural tension zone is obtained as follows.

$$K_{eff} = \sigma_x \sqrt{\pi a_{eff}} \sqrt{\left[\cos\varphi_0 \left(\cos\varphi_0 + 2\frac{\tau_{xy}}{\sigma_x}\sin\varphi_0\right)\right]^2 + \left[\frac{\tau_{xy}}{\sigma_x}\left(2\cos^2\varphi_0 - 1\right) - \sin\varphi_0\cos\varphi_0\right]^2} \quad (4.45)$$

Because the initial crack angle φ_0 can be considered as zero, the effective stress intensity factor in flexural tension zone is obtained as follows..

$$K_{eff} = \sigma_x \sqrt{\pi a_{eff}} \sqrt{1 + \left(\frac{\tau_{xy}}{\sigma_x}\right)^2} \quad (4.46)$$

As you can see Eq. (4.46), effective stress intensity factor in flexural tension zone depends on the ratio of shear stress to normal stress and the angle of initial crack.
In this zone inclined crack will propagate when a principal tensile stress reaches the maximum value. Therefore, the effective stress intensity factor in flexural tension zone should be equal to K_{Ic}.

(2) Effective stress intensity factor in pure shear zone

The stress intensity factors for mode-I and mode-II fracture in pure shear zone are given by

$$K_I = \sigma_{x1}\sqrt{\pi a_c}, \qquad K_{II} = \tau_{x1y1}\sqrt{\pi a_c} \quad (4.47)$$

To determine the stress intensity factor, it is assumed that the only shear stress acts on the plane. Thus, the principal tensile stress and shear stress acting on cracked plane can be expressed as follows.

$$\sigma_{x1} = \tau_{xy} \sin 2\varphi_1 \tag{4.48}$$

$$\tau_{x1y1} = \tau_{xy} \cos 2\varphi_1 \tag{4.49}$$

where φ_1 means the angle of inclined crack which is developed from the flexural crack tip as shown in Fig. (4.17). Substituting Eq.(4.48) and Eq. (4.49) into Eq.(4.47) yields

$$K_I = \tau_{xy} \sin 2\varphi_1 \sqrt{\pi a_c} \tag{4.50}$$

$$K_{II} = \tau_{xy} \cos 2\varphi_1 \sqrt{\pi a_c} \tag{4.51}$$

Since an effective stress intensity factor can be expressed by Eq.(4.44), inserting Eq. (4.50) and Eq.(4.51) into Eq. (4.44) and organizing yields

$$K_{eff} = \tau_{xy} \sqrt{\pi a_{eff}} \tag{4.52}$$

(3) Effective stress intensity factor in compression zone

In the compression region of reinforced concrete beams, compressive stress and shear stress act on the plane simultaneously as shown in Fig. (4.17-b, c).
The stress intensity factor for mode-I and mode-II fracture is obtained as follows.

$$K_I = \sigma_{x1} \sqrt{\pi a_c}, \qquad K_{II} = \tau_{x1y1} \sqrt{\pi a_c} \tag{4.53}$$

Here, the stress intensity factor for mode-I fracture appears negative value. This means that closing failure mode occurs in this zone due to compressive stress.

From Fig. (4.17-c), principal tensile stress and shear stress is

$$\sigma_{x1} = -\sigma_x \cos^2 \varphi_2 + 2\tau_{xy} \sin \varphi_2 \cos \varphi_2 \tag{4.54}$$

$$\tau_{x1y1} = \sigma_x \sin \varphi_2 \cos \varphi_2 + \tau_{xy} \left(2\cos^2 \varphi_2 - 1\right) \tag{4.55}$$

where φ_2 means the angle of inclined crack in pure shear zone as illustrated in Fig. (4.17).

Inserting Eq.(4.54) and Eq.(4.55) into Eq.(4.53) yields

$$K_I = \tau_{xy} \sqrt{\pi a_c} \cos \varphi_2 \left(2\sin \varphi_2 - n\cos \varphi_2\right) \tag{4.56}$$

$$K_{II} = \tau_{xy} \sqrt{\pi a_c} \left[\left(2\cos^2 \varphi_2 - 1\right) + n \sin \varphi_2 \cos \varphi_2\right] \tag{4.57}$$

where n is the ratio of compressive stress and shear stress $\left(= \sigma_x / \tau_{xy}\right)$.

An effective stress intensity factor for mixed mode in compression zone is obtained as follows.

$$K_{eff} = \tau_{xy} \sqrt{\pi a_{eff}} \sqrt{n^2 \cos^2 \varphi_2 - 2n \sin \varphi_2 \cos \varphi_2 + 1} \tag{4.58}$$

Since it is assumed that failure mechanism of compression zone is governing by sliding failure (mode-II fracture), the effective stress intensity factor in compression zone should be equal to critical stress intensity factor for mode-II fracture.

4.8 Summary

In this chapter, linear elastic fracture mechanics based on linear elastic stress field in cracked bodies, with emphasis on the problem of a single crack in an infinite plate was studied. The principal findings are summarized as follows.

1) Concrete Fracture mode is classified into the mode-I (opening), mode-II (shearing), and mode-III (out-of-plane shearing).
2) Stress intensity factors for mode-I and mode-II fracture in linear elastic fracture mechanics represent the stress state at the crack tip. These factors are consisted of stress at the crack tip and length of crack. And stress intensity factor for mixed mode fracture contains both of these factors.
3) Critical stress intensity factors represent the material properties and are related to the fracture energy G_f. Crack will propagates when this stress intensity factors reach a certain critical values K_{Ic} or K_{IIc}, called fracture toughness.
4) Geometrically similar structures following linear elastic fracture mechanics exhibit the size effect law.
5) It is assumed that concrete is the quasi-brittle material which shows the post peak behavior due to uniaxial tension and compression localization.
6) To resolve the singularity at the crack tip, the size of fracture process zone is needed.
7) Stress intensity factors K_I, K_{II} for mode-I and mode-II fracture are determined as function of ultimate stress at the crack tip and are dependent on the size of specimen.

5. Flexural Behavior of Reinforced Concrete Beams without Web Reinforcement

5.1 Introduction

Generally, reinforced concrete slender beams without web reinforcement with $a/d > 2.5$ subjected to concentrated load appear the flexural behavior.

Flexural capacity is assessed on the basis of the plane sections theory. The theory describes analytically the relationship between flexural capacity and geometric characteristics by considering the equilibrium conditions at critical cross section.

Determinations of this chapter are depth of neutral axis c_x, above the critical diagonal crack, distance x_A where the location of critical diagonal crack from the support, diagonal crack angle at compression zone φ_2, resultant compressive forces C_f and moment arm jd_x.

Four basic assumptions are made when deriving a general theory for the flexural strength of reinforced concrete sections.

(1) Plane Sections before bending remain plane after bending. This means that the unit strains in a beam above and below the neutral axis are proportional to the distance from the axis.

(2) The stress-strain curve is known. The bending stress σ at any point depends on the strain at that point in a manner given by the stress-strain diagram of the material

(3) The stress-strain curve for concrete, defining the magnitude and distribution of compressive stress, is known (Fig. (5.1))

(4) Tension stiffening effect of reinforcement steel is neglected as shown in Fig. (5.1 -c)

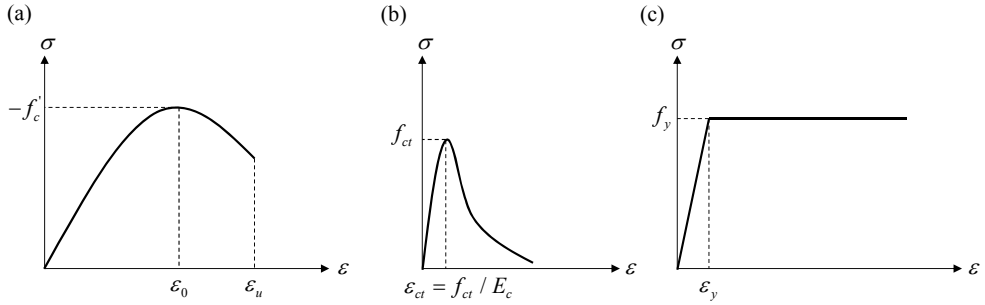

Figure 5.1 Stress-strain relationship of materials: (a) concrete in compression; (b) concrete in tension; and (c) reinforcement steel in tension

5.2 Moment-Curvature Relationship

When the load is gradually increased from zero to the magnitude that will cause the beam to fail, several different stages of behavior can be distinguished as shown in Figs. (5.2) and (5.3).

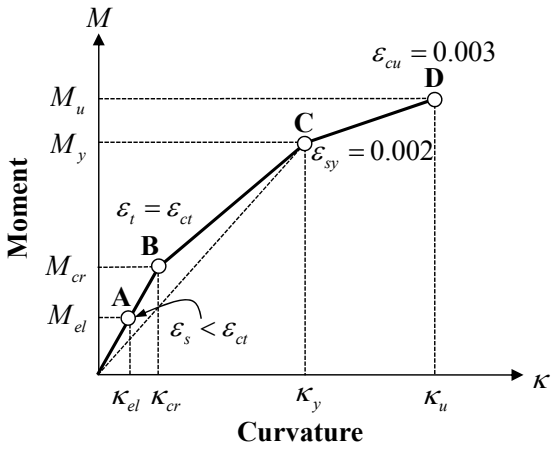

Figure 5.2 Moment-curvature relationship

At low loads, as long as the maximum tensile stress in the concrete is smaller than the modulus of rupture f_r, the entire concrete is effective in resisting stress, in compression on one side and in tension on the other side of the neutral axis. The strains at this stage are very small, and the stress distribution was essentially linear in this stage. The moment and curvature are shown by point A in Fig. (5.2). The moment-curvature diagram for this stage is linear. At this stage, the tensile strain of concrete $\varepsilon_{ct} = f_{ct} / E_c$ is and the tensile strain of reinforcement steel is smaller than the yield strain.

When the applied load is further increased, flexural tensile crack occurs and propagates upward to the level of the neutral plane. After the initial flexural cracking, the tensile force in the concrete was transferred to the longitudinal reinforcement steel. As a result, less of the concrete section was effective in resisting moments. At stage C, it is assumed that longitudinal reinforcement steel reaches yield strain $\varepsilon_{sy} = 0.002$. The compressive stress is still closed to being linear.

Eventually, the ultimate capacity of the beam is reached. Failure can be caused in one of two ways. When relatively moderate amounts of reinforcement are employed, at some value of the load the steel will reach its yield point. Diagonal tension failure may occur after yielding of the reinforcement.

If large amounts of reinforcement or normal amounts of steel of very high strength are employed, the compressive strain of the concrete may be reached the ultimate strain ε_{cu}. If the concrete strain in the compression zone increases to the ultimate strain that causes crushing of the concrete before not yielding of the reinforcement, the compression failure occurs in the compression zone. Exact criteria for this compression occurrence are not yet known, but it has been observed that rectangular beams failure in compression when the concrete strains reach values of about 0.003

to 0.004. ACI Section 10.2.3 specifies a limiting compressive strain, ε_{cu}, equal to 0.003. In Europe, the CEB Model Codes uses a limiting strain $\varepsilon_{cu} = 0.0035$ for beams.

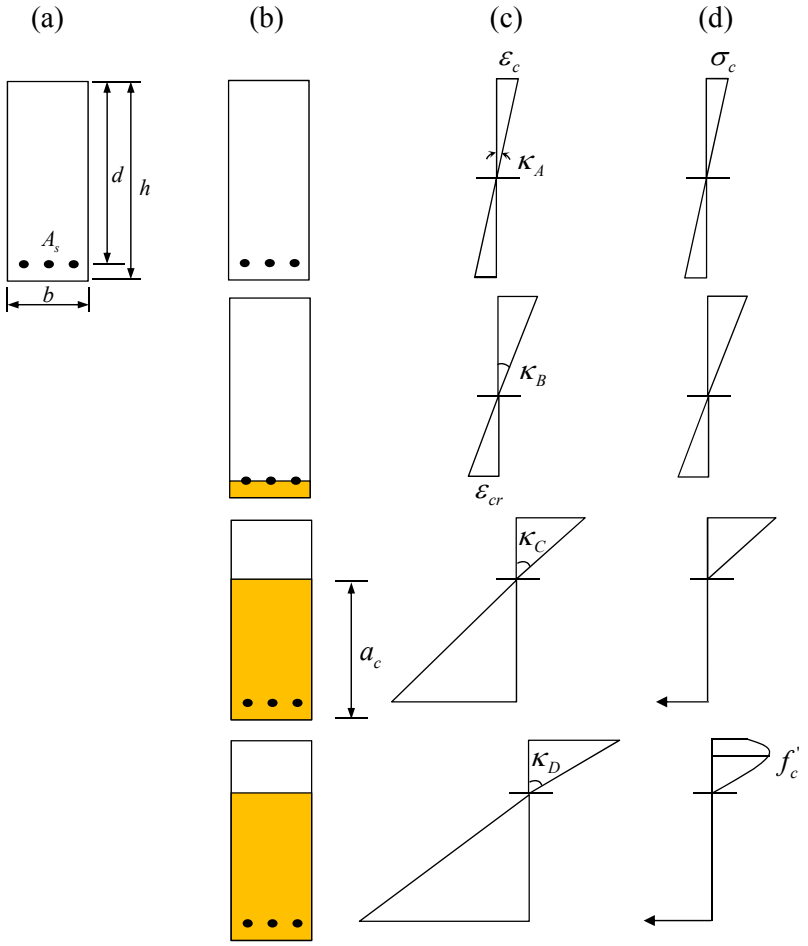

Figure 5.3 Stress and strain distribution: (a) section; (b) crack propagation; (c) strain distribution and (d) stress distiribution

5.3 Depth of neutral axis

When the tensile stress f_{ct} exceeds the modulus of rupture, cracks form. If the steel stress has not reached the yield point, both materials continue to behave elastically as shown in Fig. (5.4). The distance to the neutral axis, in this stage, is conventionally expressed as a fraction kd of the effective depth d . To determine the depth of the neutral axis, one can proceed from basic principles by accounting directly for the forces that act on the cross section. the concrete stress is distributed linearly. Thus, the total compression force C and the total tension force T are

$$C_c = \frac{f_c}{2} bkd, \quad T = A_s f_s \tag{5.1}$$

where f_c means concrete strength, b is the width, A_s and f_s are the area and strength of longitudinal reinforcement, respectively.

Equilibrium requires that the couple constituted by the two forces C and T be equal to the external bending moment . Hence, taking moments about C gives

$$M = Tjd = A_s f_s jd \tag{5.2}$$

Where jd is the internal lever arm between C and T and is given as follows·

$$jd = d - \frac{kd}{3} \tag{5.3}$$

Using the triangles in Fig. (5.4) and substituting $\rho = A_s / bd$ and $n = E_s / E_c$ give a quadratic equation solution for c / d as follows

$$\frac{c}{d} = \sqrt{(n\rho)^2 + 2n\rho} - n\rho \tag{5.4}$$

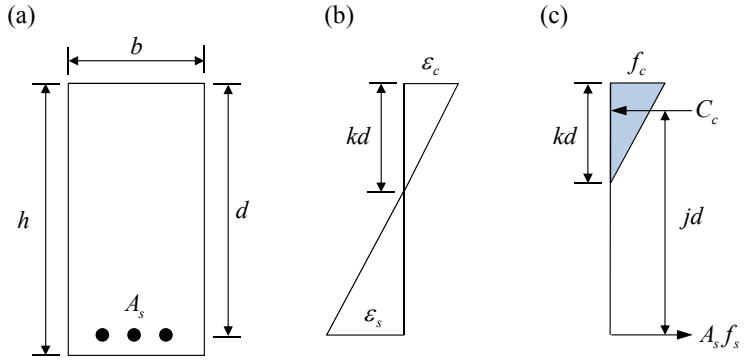

Figure 5.4 Depth of neutral axis

In limit theory of plasticity, fully rectangular stress block for whole compression zone is used as shown in Fig. (5.5). Consider the case of a beam with a rectangular cross section having height h and width b subjected to pure bending. The reinforcement is a tensile reinforcement with area A_s. The effective depth is d. If the strength of tensile reinforcement reaches the yield strength f_y, the stress distribution at failure will be as shown in Fig. (5.5). From the equilibrium,

$$A_s f_y = f_{ce} bc \tag{5.5}$$

where f_{ce} is an effective strength of concrete.

Thus, the depth of neutral axis is obtained as follows.

$$\frac{c}{d} = \frac{f_y}{f_{ce}} \rho \tag{5.6}$$

where ρ is the ratio of reinforcement.

The c/d can be expressed as follows.

$$\frac{c}{d} = \omega \tag{5.7}$$

where ω is the degree of reinforcement and is obtained by

$$\omega = \frac{A_s f_y}{b d f_{ce}} = \frac{f_y}{f_{ce}} \rho \tag{5.8}$$

The yield moment in pure bending M_p can then be determined as follows.

$$M_p = A_s f_y \left(d - 0.5c\right) = \left(1 - \frac{1}{2}\omega\right) \omega b d^2 f_{ce} \tag{5.9}$$

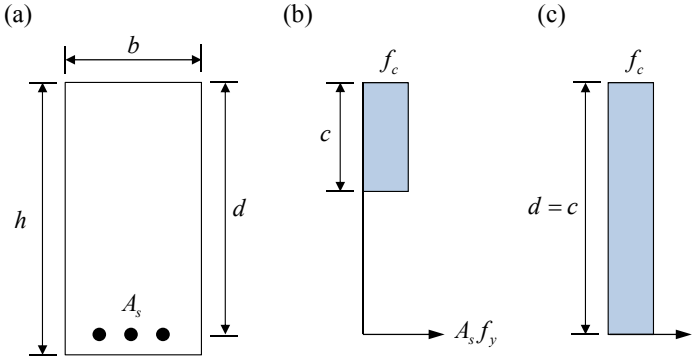

Figure 5.5 Normal stress distribution at the failure moment

The solution described above is valid only when $c \le d$, that is $\omega \le 1$. If $\omega > 1$, the stress distribution at failure will be as shown in Fig. (5.5-c). In this case $c = d$ and reinforcement will not yield. The failure moment will be

$$M_p = \frac{1}{2} b d^2 f_{ce} \tag{5.10}$$

Beams with $\omega \le 1$ are called normally reinforced beams and beams with $\omega > 1$ are called overreinforced beams. Fig. (5.6) shows the yield moment versus reinforced degree in theory of plasticity.

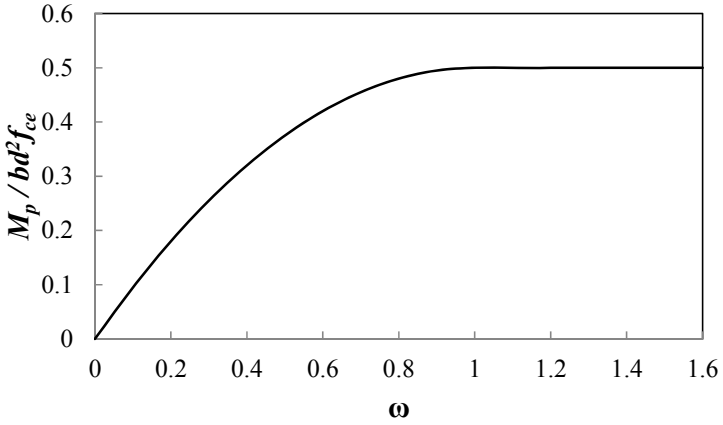

Figure 5.6 Yield moment versus reinforcement degree

To obtain the more realistic simulation of the stress-strain relationship of concrete, compressive normal stress was assumed to be parabolically distributed in the compression zone because no explicit stress-strain curve for concrete under compression based on fracture mechanics was available. (See Fig. (5.7))

$$\sigma_c(\varepsilon_c) = f_c^{'}\left[2\left(\frac{\varepsilon_c}{\varepsilon_o}\right) - \left(\frac{\varepsilon_c}{\varepsilon_o}\right)^2\right] \tag{5.11}$$

$$\text{or } \sigma_c(z) = f_c^{'}\left[2\left(\frac{z}{c}\right) - \left(\frac{z}{c}\right)^2\right] \tag{5.12}$$

According to ACI 318-08, the modulus of elasticity is defined as the slope of the line drawn from a stress of zero to a compressive stress of $0.45f_c^{'}$. The ACI 318-08 code provision is provided the modulus of elasticity for normal-weight concrete and high strength concrete as follows.

For normal-weight concrete, ACI 318-08 gives the modulus of elasticity as

$$E_c = 4700\sqrt{f_c'} \quad [\text{MPa}] \tag{5.13}$$

ACI Committee 363 proposed the following equation for high-strength concrete

$$E_c = 3320\sqrt{f_c'} + 6895 \quad [\text{MPa}] \tag{5.14}$$

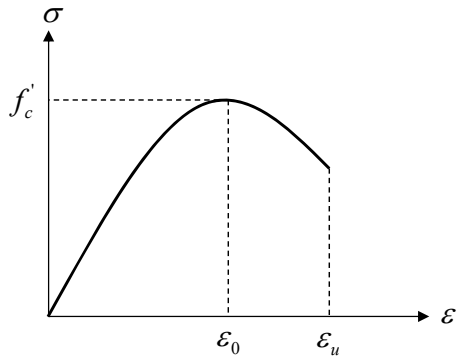

Figure 5.7 Stress-strain relationship

Since resultant compressive forces C_c and tensile forces T_s are acting on the cross section, the horizontal equilibrium of the forces as shown in Fig. (5.8) is formulated as follows. Resultant compressive forces are obtained by integrating the stress distribution along the compression zone.

$$\rho bdE_s\varepsilon_s = b\int_0^c \sigma_c(z)dz \tag{5.15}$$

where $\varepsilon_s = \varepsilon_c(d-c)/c$

If the strain is distributed linearly, steel strain can be expressed concrete strain by using similar triangles and replacing, E_s/E_c and A_s/bd with n and ρ, respectively. A following equation for c/d is function of n, ρ, f_c', and ε_c.

$$\frac{c}{d}=\frac{-\rho E_s\varepsilon_c+\sqrt{\left(\rho E_s\varepsilon_c\right)^2+\frac{8}{3}f_c^{'}\left(\rho E_s\varepsilon_c\right)}}{\frac{4}{3}f_c^{'}} \tag{5.16}$$

The depth compression zone c_x and moment lever arm jd_x of cracked section are defined as function of ε_c.

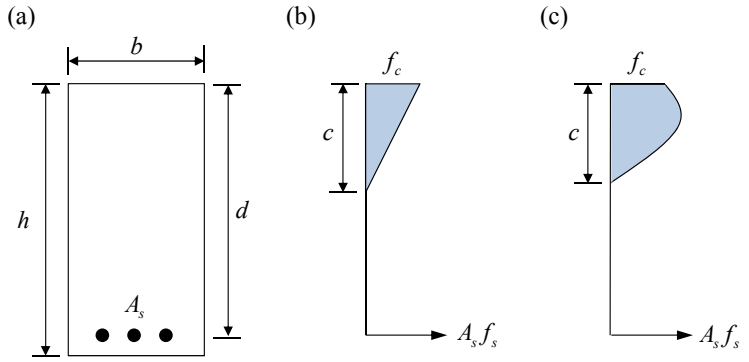

Figure 5.8 Stress and strain distribution of RC beams with rectangular section

To compare the value of c/d, an following example was used. The example which is a reinforced concrete beams with rectangular cross section has values of $f_c^{'}=40\,\text{MPa}$, ρ=0.02, n=6.7, $f_y=400\text{MPa}$, and $E_s=200\text{GPa}$. Fig. (5.9) shows the variation of the c/d for concrete strain.

It is seen that the value of c/d obtained from the Eq. (5.16) varies with increasing the normal strain ε_c. However the depth of neutral axis obtained from Eq. (5.4) and Eq. (5.7) does not depend on the deformation.

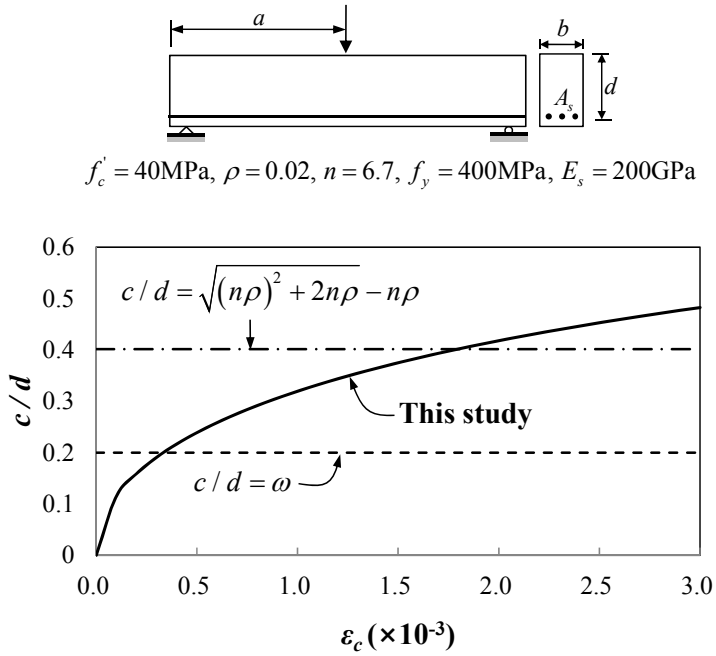

Figure 5.9 Variation of *c/d* for concrete strain

5.4 Moment Capacity

Fig. (5.10) shows the variation of normal stress and strain according to crack propagation. The x_A and x_B represent the position which occur the initial flexural crack and diagonal crack at flexural tension zone, respectively. The ε_{ca} and ε_{cb} are the concrete strain at loading point and distance x_B, respectively. It is assumed that a critical diagonal crack propagates with angle φ_1 after initial crack at distance x_A.

In case of simple beam subjected to concentrated load, shear strength is identical at any point within the whole shear span. Thus the moment at loading point can be expressed as follows.

$$M_a = \left(\int_0^{c_a} \sigma(z)\, dz \right) b \times jd_a = \frac{2}{3} f_c^{'} \times b \times c_a \times jd_a \tag{5.17}$$

where $jd_a = \dfrac{\int_0^{c_a} z\sigma(z)\, dz}{\int_0^{c_a} \sigma(z)\, dz} + d - c_a = d - \dfrac{3}{8} c_a$

According to experimental study performed by MacGregor et al. (1960), inclined crack will propagate rapidly up to the neutral axis due to the additional applied load in case of simple beam subjected to concentrated load. From the previous researches (Park and Choi, 2006), it can be assumed that additional applied load $0.05\sqrt{f_c^{'}}bd$ (MPa) is required to make the inclined crack reach the neutral axis.

From the moment at distance x_B from the support, $M_B = \left(\int_0^{c_B} \sigma(z)\, dz \right) b \times jd_B$ the distance x_A can be obtained as follows. The c_B and jd_B mean the depth of neutral axis and moment arm at distance x_B.

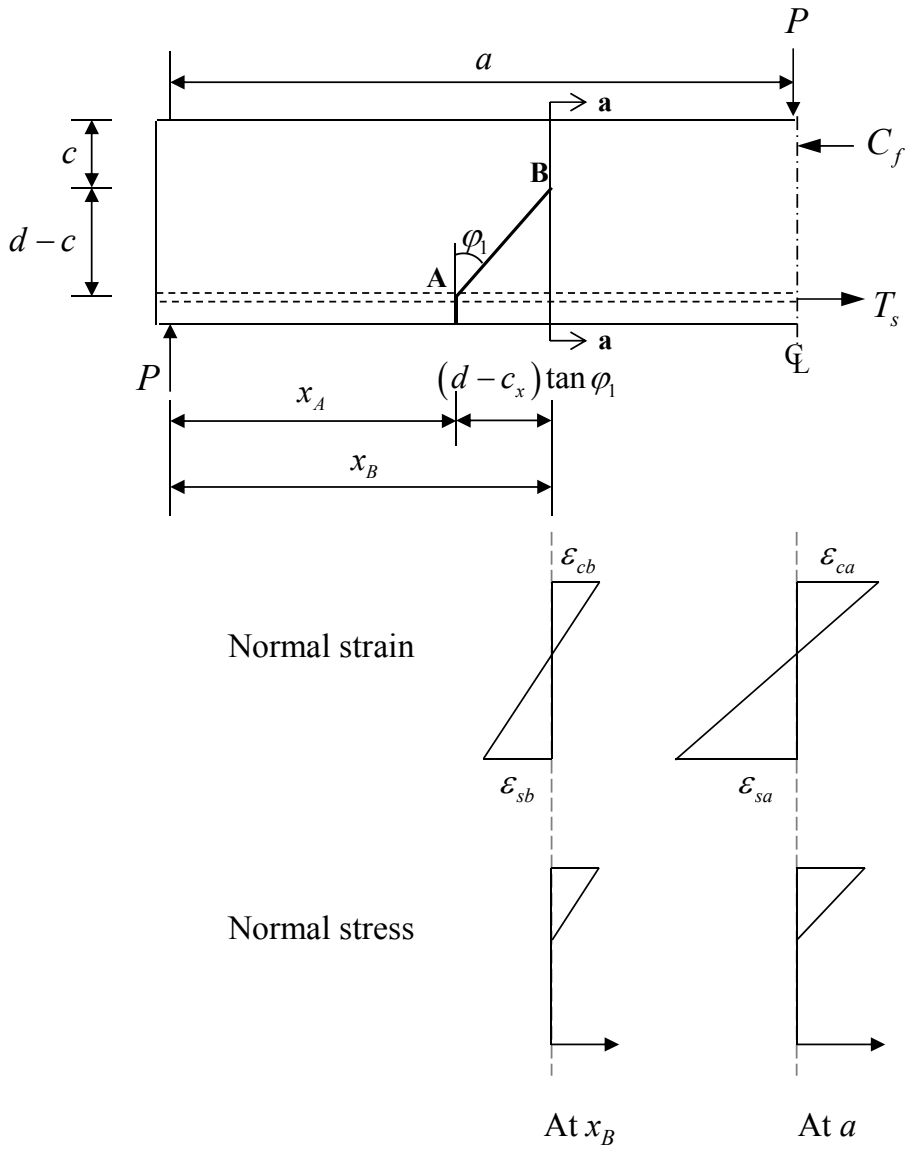

Figure 5.10 Variation of normal stress and strain according to crack propagation

$$\frac{M_A}{x_A} + 0.05\sqrt{f_c^{'}}bd = \frac{M_a}{a} \tag{5.18}$$

where $M_A = M_{cr} = f_r \frac{bh^2}{6}$ and f_r is modulus of rupture $f_r = 0.62\sqrt{f_c^{'}}$

As a result, x_A can be obtained as follows.

$$x_A = \frac{0.62\sqrt{f_c^{'}}\frac{bh^2}{6}}{M_a / a - 0.05\sqrt{f_c^{'}}bd} \tag{5.19}$$

As we assumed that the shear strength or stress is identical at any point within the shear span ε_x can be defined. In this study, to calculate the normal strain the ratio of shear stress to normal stress was used as follows.

$$\frac{\tau_{xy}}{\sigma_x} = \frac{1}{2xy}\left(\frac{d^2}{4} - y^2\right) \tag{5.20}$$

where σ_x and τ_{xy} are normal and shear stress at crack tip, respectively. And x represents the distance from the support for horizontal axis and y means the vertical distance with respect to neutral axis. Thus, the ratios of shear stress to normal stress at section a-a and at loading point is obtained.

$$\frac{\tau_B}{\sigma_B} = \frac{1}{2x_B y}\left(\frac{d^2}{4} - y^2\right), \qquad \frac{\tau_a}{\sigma_a} = \frac{1}{2ay}\left(\frac{d^2}{4} - y^2\right) \tag{5.21}$$

where σ_B and τ_B are normal stress and shear stress at section a-a and σ_a and τ_a present the normal stress and shear stress at the loading point.

Because the shear stresses τ_B and τ_a is identical, the normal strain at section a-a is defined as follows.

$$\varepsilon_{cB} = \varepsilon_{ca} \frac{x_B}{a} \tag{5.22}$$

where ε_{cB} means the concrete strain at section a-a.

As a result, the normal strain at any point within the shear span varies linearly from the any point to the loading point.

The moment at distance x_B from the support can be calculated by assuming that the strain and stress of extreme fiber vary linearly

$$M_x = \frac{1}{2} E_c \varepsilon_{cx} b c_x \left(d - \frac{c_x}{3} \right) \tag{5.23}$$

where ε_{ca} is the strain of extreme fiber and c_x is the depth of neutral axis at distance x.

5.5 Summary

In this chapter, flexural behavior of reinforced concrete slender beams based on concrete strain was investigated. The principal findings can be summarized as follows.

1) The depth of neutral axis was obtained by assuming that the distribution of concrete and which is a function of the concrete strain. Thus, the proposed depth of neutral axis increases with increasing the concrete strain.
2) Stress and strain of the cracked concrete at the cracked section could be determined by using the fact that shear strength is identical along the shear span.
3) Moment carrying capacity at loading point was determined as function of concrete strain.

6. Critical Crack Path Dependent Shear Strength

6.1 Introduction

Generally shear strength of reinforced concrete members in flexure depends on the failure mode of concrete, i.e. diagonal tension failure, diagonal compression failure and sliding failure.

Most previous theoretical and experimental studies have concentrated on beams with and without web reinforcement. These theories have been assumed that if principal tensile stress in the diagonal struts reaches the tensile strength of concrete diagonal tension failure occurs (Park and Choi, 2006). In the strut-and-tie model based on plasticity theorem (Hong and Ha, 2004, 2012), principal compressive stress in the diagonal struts reaches the compressive strength of concrete diagonal compression failure occurs. Based on these studies, many useful and reasonable results have been obtained. Especially, to obtain the precise and rational analysis results, Bazant and Kim (1984) and Zsutty (1971) established the several required empirical constants by using the statistical method and regression analysis, respectively.

However, shear strength obtained by equilibrium condition and failure criteria cannot explain size effect. And it has been known that statistical or regression method cannot present the evidence or theoretical basis strictly.

Therefore, it is necessary to evaluate the formula of shear strength of reinforced concrete structures which is capable of explaining the size effect theoretically.

In this chapter, based on the critical crack path and crack propagation, shear strength of reinforced concrete beams without web reinforcement considering the size effect is proposed.

6.2 Crack Path Dependent Failure Mechanism

6.2.1 Characteristics of Critical Diagonal Crack

In reinforced concrete beams without web reinforcement under 4-point loading, the critical crack typically involves two branches. Normally these two branches are formed at different time instants and are due to different causes.

Fig. (6.1) shows the final crack pattern of reinforced concrete beams without web reinforcement under 4-point loading. The first branch is an inclined shear crack which develops after the onset of nearby flexural cracking. The first branch is usually formed at the end of the flexural cracks. Generally, the height of the first branch is similar to that of the flexural cracks. The failure is caused by the formation of the second branch of the critical crack, which initiates from the tip of the first branch and propagates, abruptly or gradually, toward the loading point crossing the compression zone. This mode of failure is conventionally called diagonal tension failure, and it occurs only in slender beams with a shear span to depth ratio $a/d > 2.5$.

The height of first inclined cracks is assumed same as the height of flexural cracks as shown in Fig. (6.2). To obtain the height of first inclined cracks equilibrium condition is considered as follows.

$$\frac{\varepsilon_c}{\varepsilon_s} = \frac{c}{d-c} \tag{6.1}$$

where c is the depth of compression zone, d is effective depth, ε_c is the concrete strain at extreme fiber, and ε_s is the strain of reinforcement steel. Zararis et al. (2001) have proposed that inclined cracks propagate at the end of the bottom of compression zone. This means that tensile strength of concrete is neglected to

obtain flexural moment capacity simply. But in this study tensile strength concrete is considered at the flexural tensile zone so it is assumed that inclined cracks propagate from the bottom of the beam toward the concrete tension zone as illustrated in Fig. (6.1).

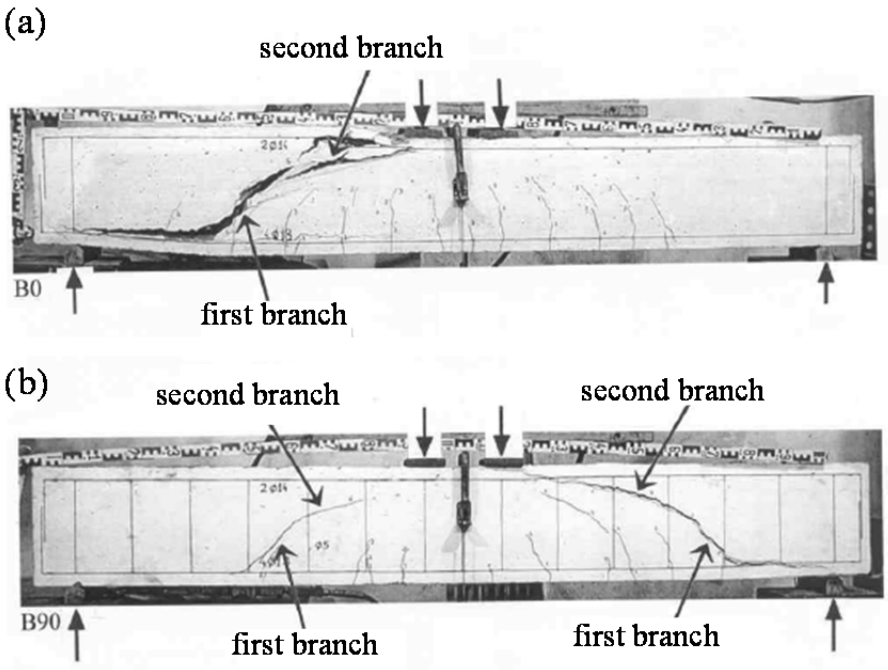

Figure 6.1 Final pattern of cracking of test beams: (a) without web reinforcement; (b) with web reinforcement [Karayiannis et al. (1999) and Zararis (2003)]

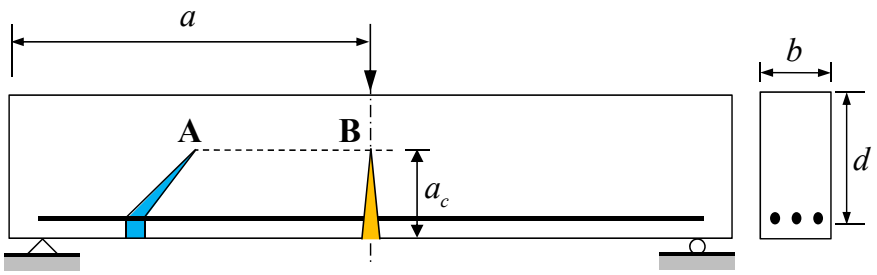

Figure 6.2 Height of single and diagonal cracks

6.2.2 Failure Mechanisms

Generally shear failure may be classified into three types, diagonal tension failure, diagonal compression failure and true shear failure. The diagonal crack, once formed, spreads toward and partially into the compression zone but stop short of penetrating to the compression face. The failure load may be significantly higher than that at which the diagonal crack first formed. Fig. (6.3) shows the critical crack path dependent failure mechanism. If the crack propagates from B to C diagonal tension failure may occur. On the other hand, the critical crack grows from B to C' sliding failure may take place due to the resultant compressive strength, C_f .

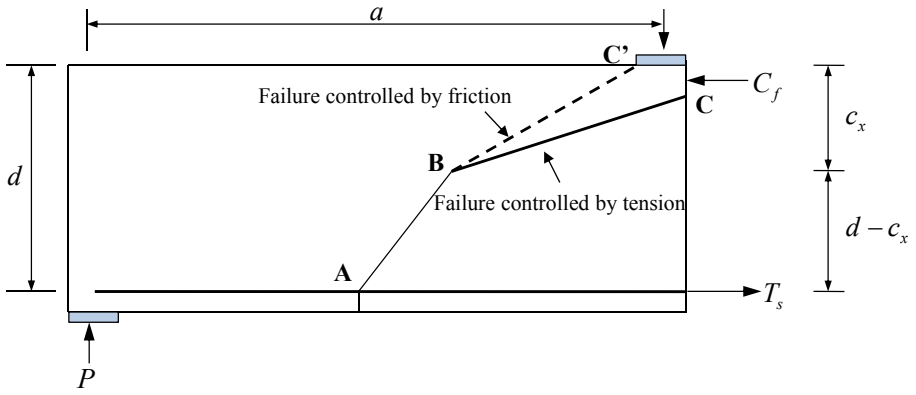

Figure 6.3 Critical crack path dependent failure mechanism

Diagonal tension failure occurs when *a/d*>2.5. Fig. (6.4) illustrates the diagonal tension failure. The diagonal crack starts from the last flexural crack and propagates to the neural axis with further increase in load. Diagonal cracks must exist before a shear failure can occur. The corresponding diagonal cracking shear can be calculated as the shear necessary to cause a principal tensile stress equal to the tensile strength of the concrete. In most reinforced concrete beams, however, flexural cracks occur first and extend more or less vertically into the beam. These

alter the state of stress in the beam, causing a stress concentration near the head of the crack.

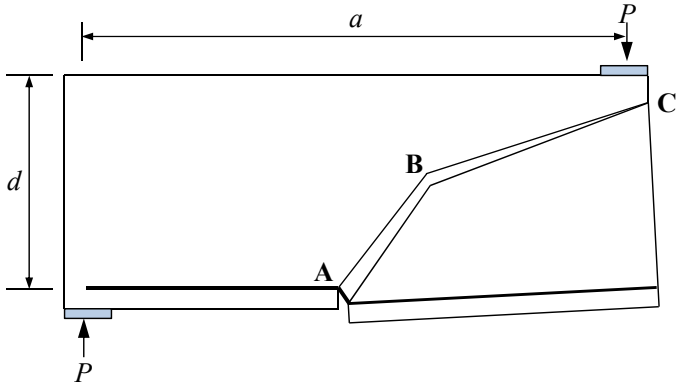

Figure 6.4 Diagonal tension failure

Diagonal compression failure is mainly caused by the crushing of concrete in the compression zone at the top of the critical diagonal crack. Other types of failure include the crushing of concrete in the web, crushing of concrete underneath the supports. Experiments have shown that in simply supported deep beams with a shear span-to-depth ratio *a/d* between 1.0 and 2.5 approximately.

Sliding failure occurs due to shear friction caused by the resultant compressive strength as shown in Fig. (6.5).

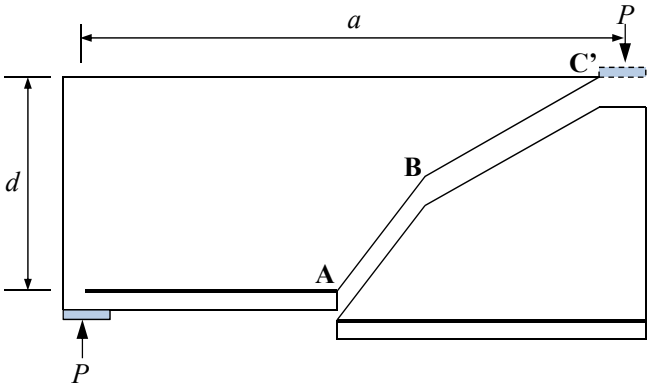

Figure 6.5 Sliding failure

True shear failure occurs when shear span is too short $a/d < 1$. In this case shear is carried by concrete strut and the final failure is splitting or it may fail in compression at the support.

6.3 Diagonal Cracking Strength

6.3.1 General

To calculate the shear strength of reinforced concrete beams without web reinforcement, it is very important to know the stress states at the crack tip. In LEFM, for these purposes, a stress intensity factor has been used to estimate the normal stress or shear stress at the tip of diagonal crack.

ACI 318-08 estimate the shear contribution of concrete in reinforced concrete beams when the critical diagonal crack initiates. This code provision assumes that the beams cannot carry an additional load after that.

In this section, diagonal cracking strength is proposed by using the linear elastic fracture mechanics considering the crack propagation.

6.3.2 Effective Stress Intensity Factor

Jenq and Shah (1989) assumed that the stress intensity factor can be approximated by the stress intensity factor of a pure bend beam with a symmetric edge notch subjected to bending moment. It is noted that the Jenq and Shah model is based on a single crack located at center of the beam length. As shown in Fig. (6.6), stress states are very different between a central crack and a inclined crack tip. Only the normal stress acts on the single central crack tip. On the other hand, both normal stress and shear stress act on the diagonal crack tip simultaneously.

Since stress intensity factor is defined as the stress state at the crack although the Jenq and Shah model can be predict diagonal shear failure of concrete beams their model seems to underestimate the diagonal shear strength of concrete beams.

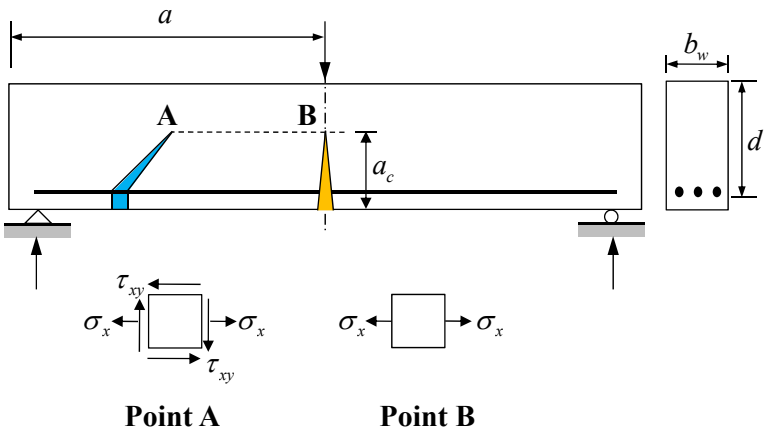

Figure 6.6 Stress states at the center and inclined cracks

After propagation of flexural cracks in the concrete cover zone the inclined crack occurs due to combined stresses with horizontal normal stress and shear stress. This crack propagates from the reinforcement steel to the end of the concrete tensile zone. Because the variation of principal stresses depends on the depth of the beam, thus stress intensity factor will vary throughout the beam depth.

In flexural tension zone, the crack tip is subjected to combined stresses, horizontal normal stress and shear stress, both mode-I (opening) and mode-II (sliding) components exist in this zone.

Thus, the stress intensity factors for mode-I and mode-II fracture can be expressed in terms of principal stress and crack length as follows.

$$K_I = \sigma_{x1}\sqrt{\pi a_c}, \qquad K_{II} = \tau_{x1y1}\sqrt{\pi a_c} \tag{6.2}$$

where σ_{x1} means the principal tensile stress, τ_{x1y1} represents the shear stress acting on the cracked plane, and a_c is the length of the newly inclined crack developed from initial crack tip which assumes the flexural crack in pure bending zone.

Combining K_I and K_{II} and organizing yields

$$K_{eff} = \tau_{xy}\sqrt{1+\left(\frac{\sigma_x}{\tau_{xy}}\right)^2}\sqrt{\pi a_{eff}} \tag{6.3}$$

where a_{eff} means the effective crack length as shown in Fig. (6.7). Thus, effective crack length a_{ceff} can be expressed as

$$a_{eff} = h - c \tag{6.4}$$

where c means the depth of neutral axis represented by as follows.

$$\frac{c}{d} = \sqrt{(n\rho)^2 + 2n\rho} - n\rho \tag{6.5}$$

It is noted that the effective crack length is defined as the vertical component of diagonal crack in this study.

As you can see Eq. (6.3), the effective stress intensity factor in flexural tension zone depends on the ratio of shear stress to normal stress and the angle of initial crack.

In this zone a diagonal crack will propagate when a principal tensile stress reaches the maximum value. Therefore, the effective stress intensity factor in flexural tension zone should be equal to K_{Ic} as follows.

$$K_{eff} = K_{Ic} \tag{6.6}$$

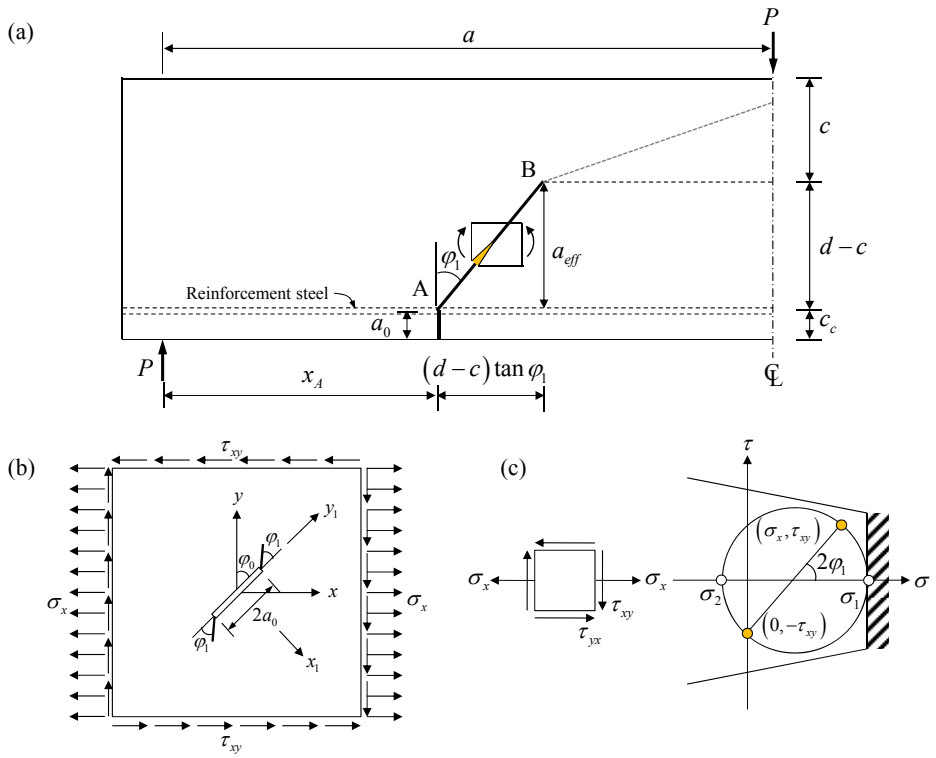

Figure 6.7 Mode-I fracture in flexural tension zone: (a) mode-I fracture; (b) inclined crack and (c) stress states and Mohr's circle

6.3.3 Critical Stress Intensity Factor

Based on the linear elastic fracture mechanics, it is assumed that flexural tension zone fails when the principal tensile stress reaches the ultimate state. Thus, the failure mechanism of this zone assumes to be governed by mode-I fracture (opening).

The critical stress intensity factor is obtained by

$$K_{Ic} = \sigma_u \sqrt{\pi a_0} \tag{6.7}$$

where σ_u is the ultimate principal tensile stress and a_0 represents initial crack length. In this study, ultimate tensile stress is equal to tensile strength of concrete and initial crack length is same as the concrete cover as shown in Fig.(6.7). Thus,

$$\sigma_u = f_{ct} \tag{6.8}$$

$$a_0 = c_c \tag{6.9}$$

where f_{ct} is tensile stress of concrete and c_c means the length of concrete cover. It should be noted that critical stress intensity factor is expressed in terms of tensile strength of concrete and initial crack length. Generally a critical stress intensity factor have been expressed in terms of elastic modulus of concrete (E_c) and fracture energy (G_f) by energy approach. However, in this study, critical stress intensity factor is obtained by applying the maximum stress at the crack tip considering failure condition of concrete and initial crack length directly.

The critical intensity factor K_{Ic} in the LEFM is defined as $\sqrt{EG_f}$. Therefore, to find the critical intensity factor fracture energy G_f should be known. Bazant and Oh (1983) have proposed that energy release rate G_f is calculated by following empirical formula by analyzing numerous test data.

$$G_f = \left(2.72 + 3.10 f_{ct}\right) f_{ct}^2 \frac{d_a}{E_c} \quad \text{[N/mm]} \tag{6.10}$$

where d_a is the maximum aggregate size. Here, an energy release rate G_f is expressed in terms of the tensile strength of concrete, elastic modulus and maximum aggregate size in crack band theory.

Fig. (6.8) shows the comparisons of the proposed critical stress intensity factor with the formula proposed by Bazant and Oh (1983).

Proposed critical stress intensity factor shows the different values for effective depth. On the other hand, Eq. (6.10) shows almost constant values regardless of size of specimens.

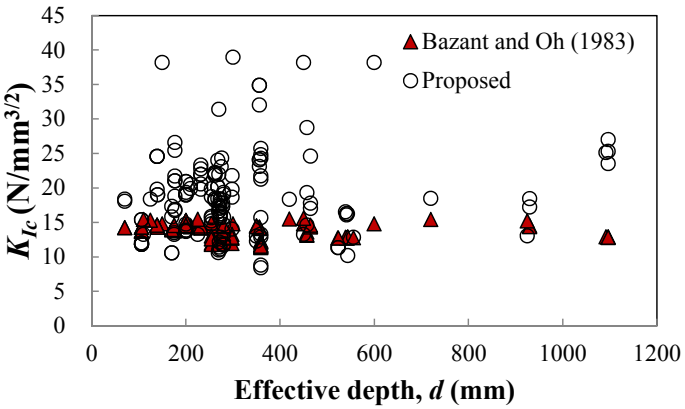

Figure 6.8 Comparison of prediction with critical stress intensity factor proposed by Bazant and Oh (1983)

Fig (6.9) and Table (6-1) show the proposed critical stress intensity factor calculated from Eq. (6.7) with the selected test results (Chana, 1981) . As the effective depth increases proposed critical stress intensity factor for mode-I fracture increases. This means that the proposed critical stress intensity factor depends on the size.

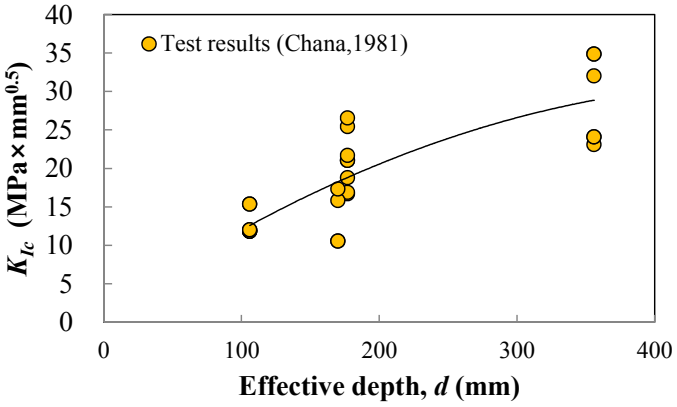

Figure 6.9 Critical stress intensity factor for mode-I fracture

Table 6-1 Experimental results by Chana (1981)

Beam	f_c' [MPa]	b_w [mm]	d [mm]	h [mm]	c_c [mm]	a/d	ρ [%]	V_t [kN]	v_t [MPa]	K_{Ic} [N/mm$^{3/2}$]
2.1a	39.5	203	356	406	50	3.00	1.73	96.0	0.21	34.9
2.1b	39.5	203	356	406	50	3.00	1.73	97.1	0.21	34.9
2.2a	33.3	203	356	406	50	3.00	1.73	87.4	0.21	32.0
2.2b	33.3	203	356	406	50	3.00	1.73	94.4	0.23	23.1
2.3a	36.2	203	356	406	50	3.00	1.73	99.4	0.23	24.1
2.3b	36.2	203	356	406	50	3.00	1.73	96.4	0.22	24.1
3.1a	27.6	100	177	202	25	3.00	1.77	23.8	0.26	21.0
3.1b	27.6	100	177	202	25	3.00	1.77	23.9	0.26	21.0
3.2a	29.4	100	177	202	25	3.00	1.77	24.5	0.26	21.7
3.2b	29.4	100	177	202	25	3.00	1.77	25.5	0.27	25.4
3.3a	32.1	100	177	202	25	3.00	1.77	26.5	0.26	26.6
3.3b	32.1	100	177	202	25	3.00	1.77	23.2	0.23	18.8
D1	25.3	100	177	202	25	3.00	1.77	22.1	0.25	16.7
D2	25.9	100	177	202	25	3.00	1.77	23.4	0.26	16.9
4.1a	24.7	60	106	121	15	3.00	1.78	9.8	0.31	11.8
4.1b	24.7	60	106	121	15	3.00	1.78	8.7	0.28	11.8

4.2a	24.7	60	106	121	15	3.00	1.78	9.0	0.28	11.8
4.2b	24.7	60	106	121	15	3.00	1.78	9.7	0.31	11.8
4.3a	41.7	60	106	121	15	3.00	1.78	11.7	0.28	15.4
4.3b	41.7	60	106	121	15	3.00	1.78	12.3	0.30	15.4
4.4a	41.7	60	106	121	15	3.00	1.78	9.6	0.23	12.0
4.4b	41.7	60	106	121	15	3.00	1.78	10.5	0.26	12.0
5.1a	32.2	200	170	200	30	3.00	1.84	47.8	0.25	10.5
5.1b	32.2	200	170	200	30	3.00	1.84	47.8	0.25	10.5
5.2a	31.8	200	170	200	30	3.00	1.84	55.0	0.29	15.8
5.2b	31.8	200	170	200	30	3.00	1.84	56.0	0.29	17.3

Diagonal cracking angle can be calculated by using the Mohr's circle as shown in Fig. (6.7-c). Therefore, the orientation of section of principal stress with respect to the vertical face of the member, denoted as φ_1 is given by

$$\tan\left(2\varphi_1\right)=\frac{2\tau_{xy}}{\sigma_x} \tag{6.11}$$

Because the diagonal crack in flexural tension zone occurs when the principal tensile stress reaches the tensile strength of concrete, a following equation must be satisfied.

$$\sigma_1=\frac{\sigma_x}{2}+\sqrt{\left(\frac{\sigma_x}{2}\right)^2+\tau_{xy}^2}=f_{ct} \tag{6.12}$$

By using Eq. (6.12), the ratio of shear stress to normal stress can be expressed as follows.

$$\frac{\tau_{xy}}{\sigma_x}=\sqrt{\left(\frac{f_{ct}}{\sigma_x}\right)^2-\left(\frac{f_{ct}}{\sigma_x}\right)} \tag{6.13}$$

As a result, the ratio of shear stress to normal stress depends on the normal stress at cracked section in flexural tension zone. Fig. (6.10) shows the variation of diagonal crack angle in flexural tension zone for normal stress and the ratio of shear stress to normal stress. The angle decreases with increasing the normal stress. However, the angle increases as the ratio of shear stress to normal stress increases. As a result, the angle will converge to the 45 degrees.

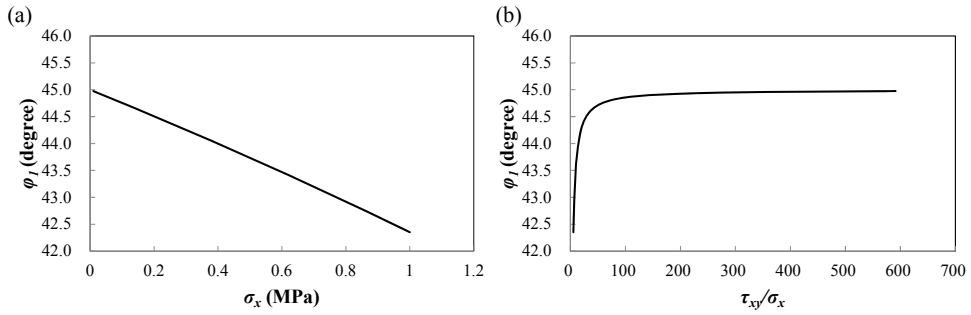

Figure 6.10 Variation of diagonal crack angle in flexural tension zone: (a) for normal stress and (b) for the ratio of shear stress to normal stress

6.3.4 Shear Strength of Flexural Tension Zone

As mentioned in Section 6.3.2, an effective stress intensity factor at the flexural tension zone is given by following relationship between normal stress and shear stress.

$$K_{eff} = \tau_{xy}\sqrt{1+\left(\frac{\sigma_x}{\tau_{xy}}\right)^2}\sqrt{\pi a_{eff}} \tag{6.14}$$

Because the mode-I fracture occurs when the effective stress intensity factor is equal to critical stress intensity factor for mode-I fracture $K_{Ic} = \sigma_u\sqrt{\pi a_0}$, by using the Eqs (6.7) and (6.14), the shear stress is obtained as follows.

$$\tau_{xy} = \frac{f_{ct}}{\sqrt{1+\left(\frac{\sigma_x}{\tau_{xy}}\right)^2}}\sqrt{\frac{a_0}{h-c}} \tag{6.15}$$

where a_0 means the initial crack length. If the concrete strain reaches the $\varepsilon_{ct} = f_{ct} / E_c$ at any point where the diagonal crack initiates, the crack propagates to near the neutral axis rapidly without additional load. Therefore, it can be assumed that the initial crack length can be considered as the crack which occurs at concrete cover zone.

As a result, the shear strength can be written as follows.

$$V_{fi} = \frac{0.84 f_{ct} bh}{\sqrt{1+\left(\frac{\sigma_x}{\tau_{xy}}\right)^2}}\sqrt{\frac{c_c}{h-c}} \tag{6.16}$$

where c_c is the concrete cover length

According to ACI 318-08 usually estimate the shear contribution in reinforced concrete beams at the time of the initiation of critical diagonal crack. To predict the diagonal cracking strength it is assumed that critical diagonal crack starts at the end of the flexural crack. The ACI code provision has recommended the diagonal cracking strength as follows.

$$v_{cr} = \frac{1}{6}\sqrt{f_c'} \text{ [MPa]} \tag{6.17}$$

Hong and Ha (2012) proposed the diagonal cracking strength by using the stress conditions at the flexural bond cracks and the equilibrium condition of the whole system of the infinitesimal element of concrete and steel bars in the horizontal direction as follows.

$$v_{cr} = 0.2\sqrt{f_c^{'}} \text{ [MPa]} \tag{6.18}$$

It is seen that Eq. (6.15) contains the ratio of shear stress to normal stress. As a result, the proposed diagonal cracking strength depends on this value because this value represents the stress state at the tip of critical diagonal crack.

To compare the diagonal cracking strength, the ratio of shear stress to normal stress was obtained from Eq. (6.19).

$$\frac{\tau_{xy}}{\sigma_x} = \sqrt{\left(\frac{f_{ct}}{\sigma_x}\right)^2 - \left(\frac{f_{ct}}{\sigma_x}\right)} \tag{6.19}$$

where σ_x and τ_{xy} are normal stress and shear stress at the crack tip, respectively. Because a critical diagonal crack propagates to the neutral axis, normal stress can be considered as modulus of rupture f_r specified in ACI 318-08.

$$f_r = 0.625\sqrt{f_c^{'}} \text{ [MPa]} \tag{6.20}$$

Therefore the ratio of shear stress to normal stress is obtained as follows.

$$\frac{\tau_{xy}}{\sigma_x} = \sqrt{\left(\frac{f_{ct}}{f_r}\right)^2 - \left(\frac{f_{ct}}{f_r}\right)} \tag{6.21}$$

As a result, the ratio of shear stress to normal stress depends on the concrete strength because f_{ct} and f_r are function of concrete strength. Fig. (6.11) shows the ratio of shear stress to normal stress for concrete strength $f_c^{'}$. This value increases with increasing the concrete strength.

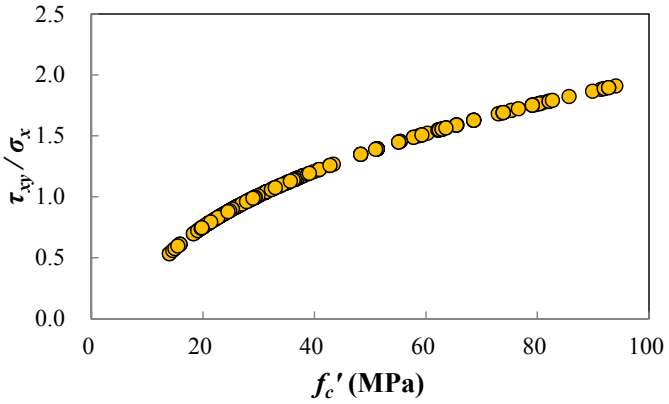

Figure 6.11 Variation of the ratio of shear stress to normal stress for concrete strength

Fig. (6.12) shows the comparison of proposed diagonal cracking strength with ACI code provision and previous researches. Therefore, equation (6.15) indicates that the proposed diagonal cracking strength is more conservative than those of recommended strength obtained by ACI 318-08 and Hong and Ha (2012) (See Fig. (6.13~6.15)). However, for high-strength concrete, $f_c' > 50\text{MPa}$, those values are not conservative with respect to strength recommended by ACI 318-08.

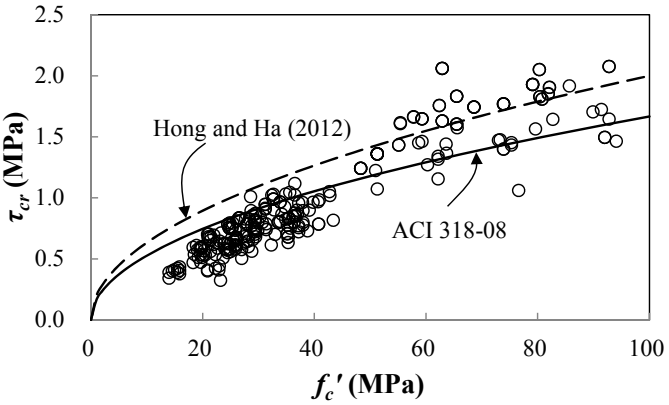

Figure 6.12 Cracking strength for concrete strength

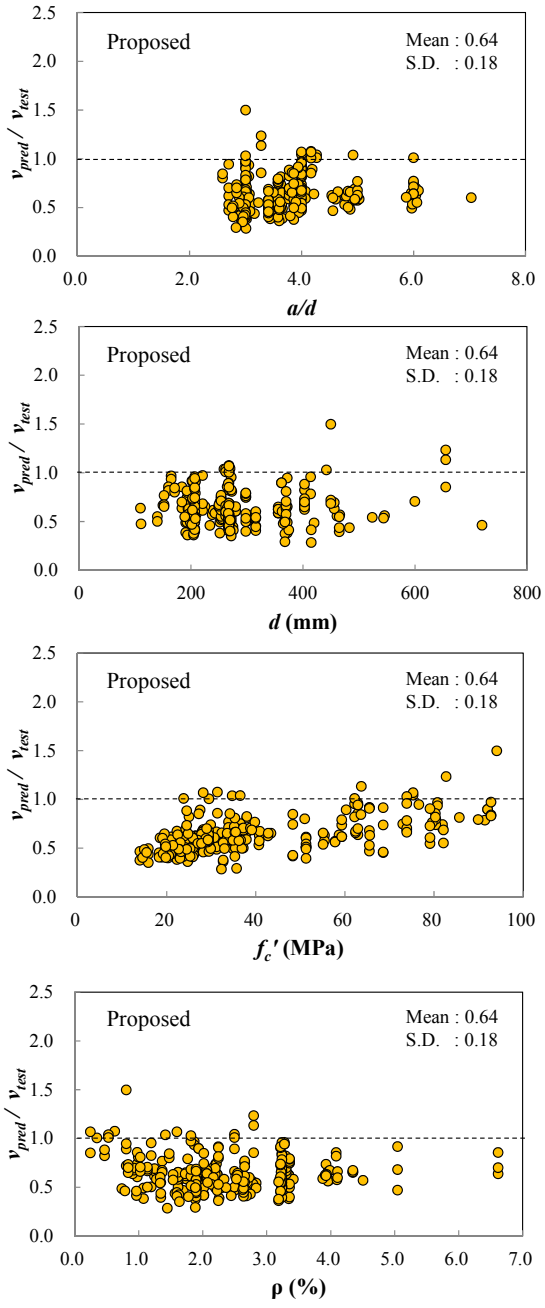

Figure 6.13 Comparison of prediction with experimental results

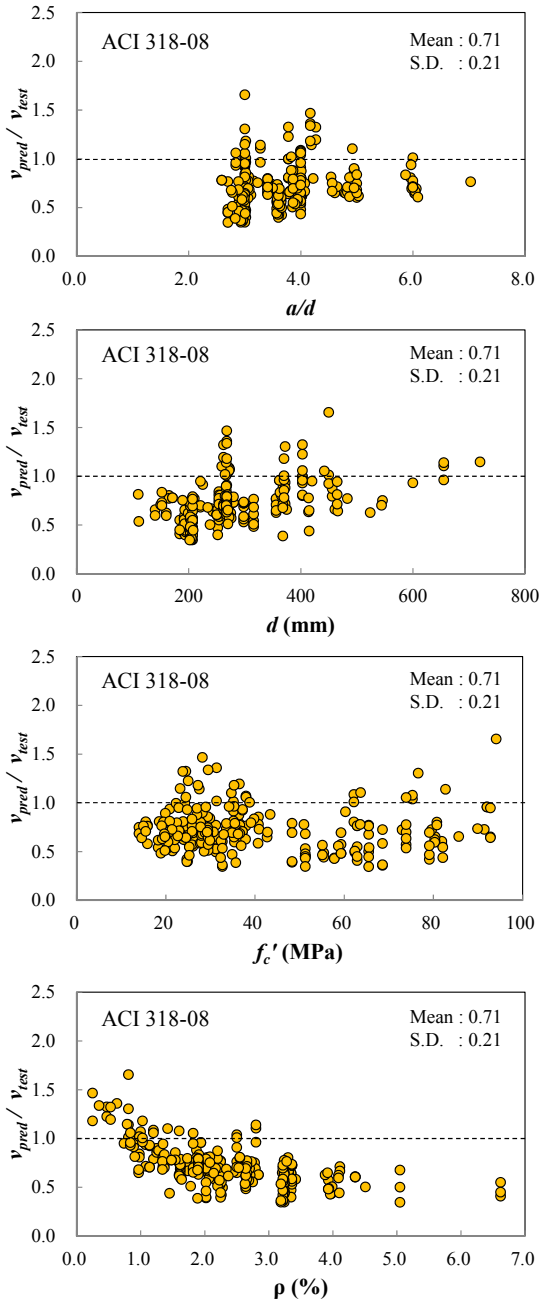

Figure 6.14 Comparison of prediction of ACI 318-08 with experimental results

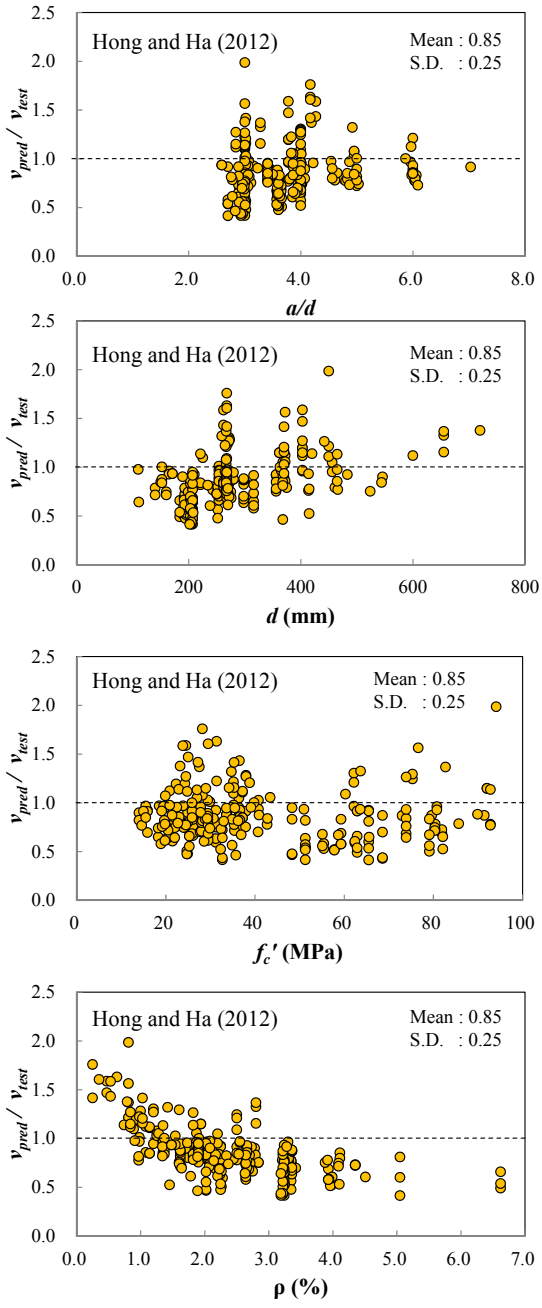

Figure 6.15 Comparison of prediction of Hong et al. with experimental results

6.4 Shear Strength for Diagonal Tension Failure

6.4.1 General

The results of experiments show that the shear failure of reinforced concrete slender beams without web reinforcement is always governed by tension failure rather that compression failure in compression zone. During the many years, researchers have made a lot of attempts to predict the shear strength reinforced concrete beams based on mainly experimental and statistical studies although the design formulas for diagonal tension failure have been improved. Especially, the current formulas which contain the size effect are based on the statistical analysis only.

Thus, it is necessary to evaluate the shear strength based on theoretical background. In this section, by using the failure criteria and effective stress intensity factor, a newly strength model is proposed on the basis of crack propagation and crack path.

6.4.2 Failure Criteria

Diagonal tension failure occurs when a principal tensile stress reaches a tensile stress of concrete in compression zone. As shown in Fig. (6.16) the principal tensile stress is obtained by combining normal stress and shear stress at the crack tip. Thus, a following equation is fulfilled.

$$\sigma_1 = -\frac{\sigma_x}{2} + \sqrt{\left(\frac{\sigma_x}{2}\right)^2 + \tau_{xy}^2} = f_{ct} \tag{6.22}$$

where σ_x and τ_{xy} are normal stress and shear stress at the crack tip and f_{ct} means the tensile stress of concrete.

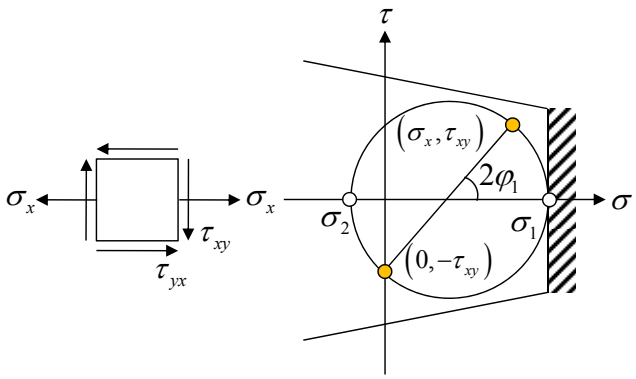

Figure 6.16 Stress state of compression zone and Mohr's circle

In this study, following tensile strength of concrete was used

$$f_{ct} = 0.3 f_c^{'2/3} \tag{6.23}$$

This is an average value evaluated from the relatively few shear tests where the tensile strength of concrete was actually determined by means of control specimen. (Reineck, 1991)

Thus, the shear stress is obtained as follows.

$$\tau_{xy} = \sqrt{f_{ct}^2 + \sigma_x f_{ct}} \tag{6.24}$$

Fig. (6.17) shows the variation of shear stress for normal stress. The shear stress increases with increasing the normal stress. Since the tensile stress is function of compressive stress of concrete, the shear stress increases with increasing the compressive stress of concrete.

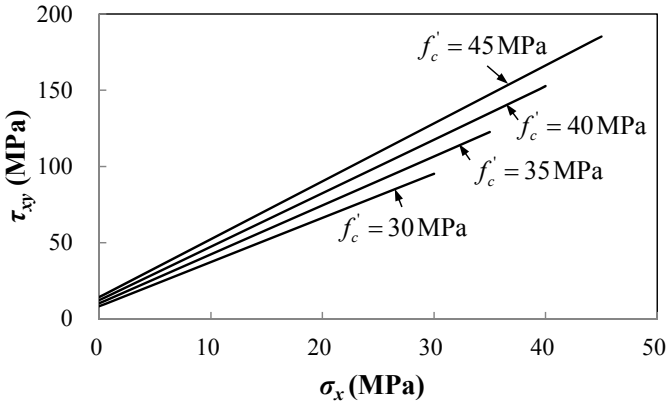

Figure 6.17 Variation of shear stress for normal stress at the crack tip

6.4.3 Effective Stress Intensity Factor

To apply the linear elastic fracture mechanics, it is assumed that softening of concrete occurs in compression zone. Fig. (6.18) shows the critical diagonal crack at compression zone. In this region, both compressive stress and shear stress act on the plane simultaneously. The inclined crack propagated already as a_0 and then the new crack grows from the initial crack tip.

Thus, the stress intensity factors for mode-I and mode-II fracture can be expressed as follows.

$$K_I = \sigma_{x1}\sqrt{\pi a_c} \tag{6.25}$$

$$K_{II} = \tau_{x1y1}\sqrt{\pi a_c} \tag{6.26}$$

From Fig. (6.18-c), principal tensile stress and shear stress are as follows.

$$\sigma_{x1} = -\sigma_x \cos^2 \varphi_1 + 2\tau_{xy} \sin\varphi_1 \cos\varphi_1 \tag{6.27}$$

$$\tau_{x1y1} = \sigma_x \sin\varphi_1 \cos\varphi_1 + \tau_{xy}\left(2\cos^2\varphi_1 - 1\right) \tag{6.28}$$

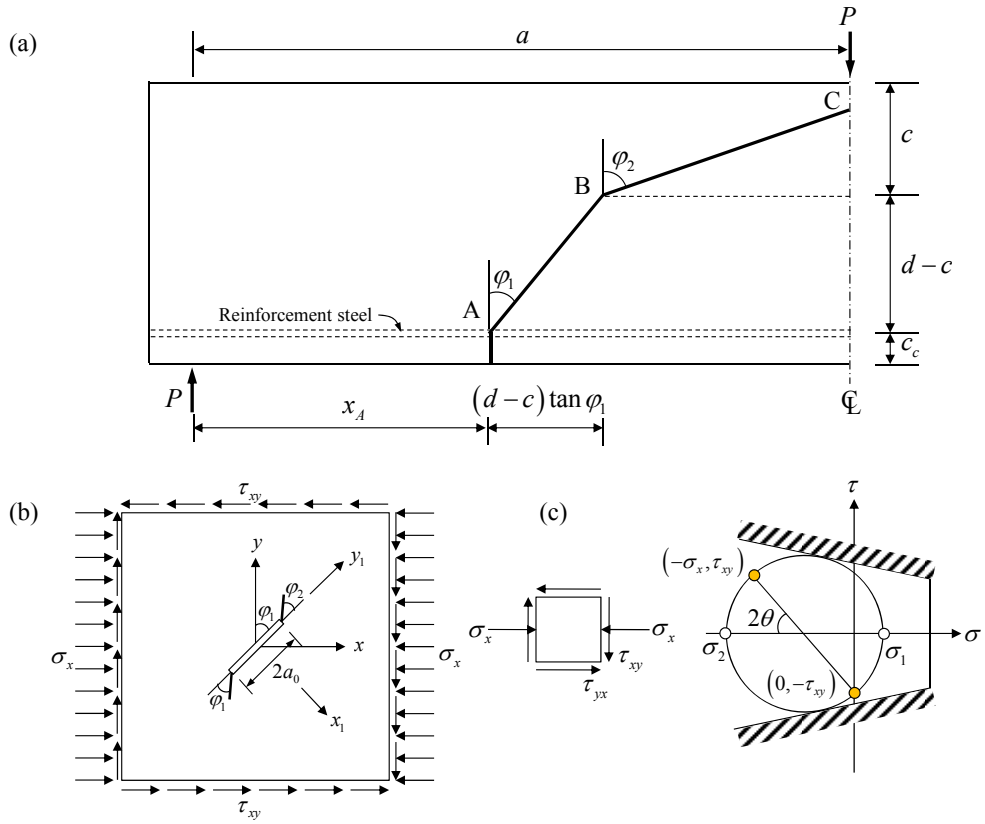

Figure 6.18 Mode-I fracture in compression zone: (a) mode-I fracture; (b) inclined crack and (c) stress states and Mohr's circle

where φ_1 means the angle of inclined crack in pure shear zone as illustrated in Fig. (6.18).

Inserting the principal stress σ_{x1} and shear stress τ_{x1y1} into Eqs.(6.27) and (6.28) yields.

$$K_I = \tau_{xy}\sqrt{\pi a_c}\left(2\sin\varphi_1\cos\varphi_1 - \frac{\sigma_x}{\tau_{xy}}\cos^2\varphi_1\right) \tag{6.29}$$

$$K_{II} = \tau_{xy}\sqrt{\pi a_c}\left[\left(2\cos^2\varphi_1 - 1\right) + \frac{\sigma_x}{\tau_{xy}}\sin\varphi_1\cos\varphi_1\right] \tag{6.30}$$

where σ_x and τ_{xy} are normal stress and shear stress at the crack tip, respectively. An effective stress intensity factor for mixed mode fracture is

$$K_{eff} = \sqrt{\left(K_I\right)^2 + K_{II}^2} \tag{6.31}$$

Substituting Eq.(6.29) and Eq. (6.30) into Eq. (6.31) and organizing yields

$$K_{eff} = \tau_{xy}\sqrt{\pi a_{eff}}\sqrt{\left(\frac{\sigma_x}{\tau_{xy}}\right)^2\cos^2\varphi_1 - 2\left(\frac{\sigma_x}{\tau_{xy}}\right)\sin\varphi_1\cos\varphi_1 + 1} \tag{6.32}$$

where φ_1 is initial crack angle which has 45 degrees and a_{eff} means the diagonal crack length from the longitudinal reinforcement to the crack tip developed in compression zone as shown in Fig. (6.19). Since the initial crack a_0 was developed in concrete cover zone already, an effective crack propagates from point **B** to the loading point as illustrated in Fig. (6.19-b).

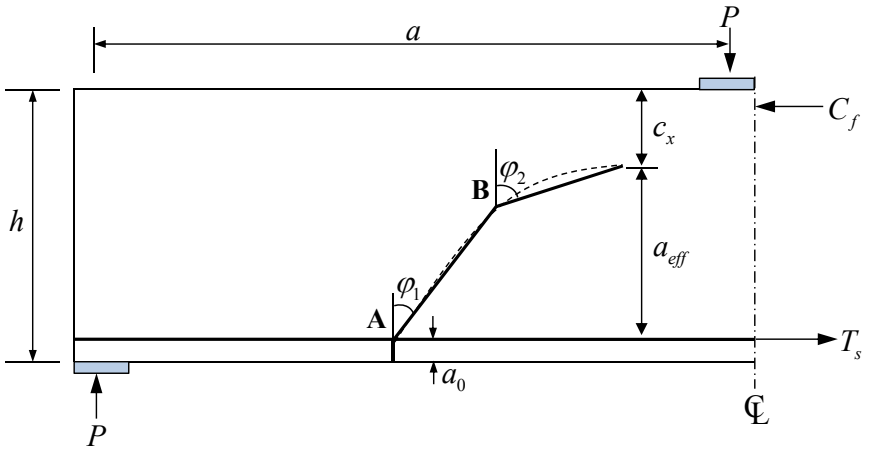

Figure 6.19 Initial and effective crack length

Thus, the initial crack length and effective crack length are obtained as follows.

$$a_0 = c_c \tag{6.33}$$

$$a_{eff} = d - c_x \tag{6.34}$$

where c_x represents the depth of neutral axis at cracked section. Because it is assumed that the softening occurs in compression zone, if critical diagonal crack is developed at any point, crack will propagate to the loading plate very rapidly.

In this study, effective crack length is defined as the vertical component to the diagonal crack. However, this may be wrong. Jenq and Shah (1989) is applied this method in his research to determine the shear strength of reinforced concrete beams without web reinforcement by using linear elastic fracture mechanics. Although this method does not have any logical basis, there are not significant problems to apply.

From Eq. (6.32), an effective stress intensity factor is obtained as follows.

$$K_{eff} = \tau_{xy}\sqrt{\pi a_{eff}}\sqrt{0.5\left(\frac{\sigma_x}{\tau_{xy}}\right)^2 - \left(\frac{\sigma_x}{\tau_{xy}}\right) + 1} \tag{6.35}$$

According to the LEFM, a diagonal crack will propagate when the effective stress intensity factor is equal to critical stress intensity factor for mode-I or mode-II fracture. If the failure of the compression zone is governed by the mode-I fracture, a diagonal tension failure will occur.

6.4.4 Shear Strength

To determine the shear strength by using effective stress intensity factor for mixed mode, it is assumed that the principal tensile stress reaches the tensile stress at the crack tip in compression zone as shown in Fig. (6.20).

Once the crack occurs at any location fracture process zone is formed. In case of concrete, this zone is very large as described in Section. Thus, it is assumed that the critical diagonal crack occurs at point B fracture process zone is formed throughout the compression zone. Although the stresses exist at the fracture process zone, in this study, these stresses are ignored.

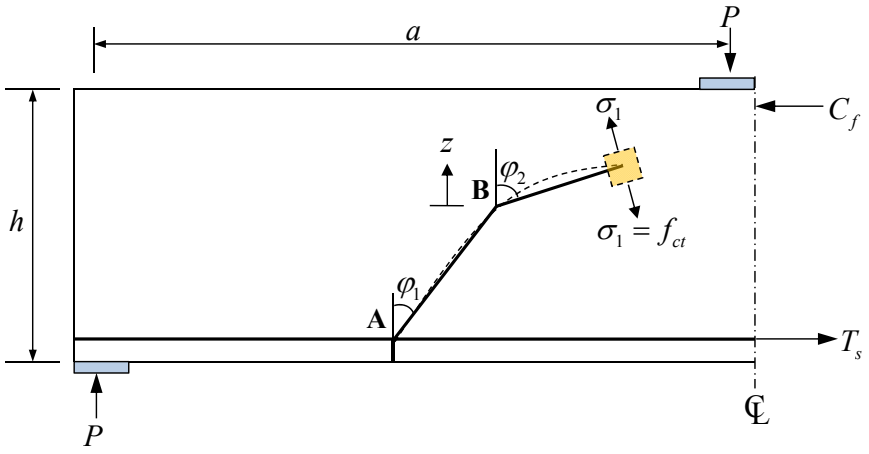

Figure 6.20 Failure condition of diagonal tension failure

As mentioned in Section, a diagonal tension failure will occur when the effective stress intensity factor is equal to the critical stress intensity factor for mode-I fracture as following relationship in linear elastic fracture mechanics approaches.

$$K_{eff} = \sigma_1 \sqrt{\pi a_{eff}} = K_{Ic} \tag{6.36}$$

where $\sigma_1 = \dfrac{K_{Ic}}{\sqrt{\pi a_{eff}}} = \dfrac{K_{Ic}}{\sqrt{D}\sqrt{\pi a_{eff} / D}} = \dfrac{K_{Ic}}{\sqrt{D} k\left(\alpha_{eff}\right)}$

where D is the size of member.

According to Bazant the critical stress intensity factor depends on the beam size, shape, or notch depth. This means that this value varies with testing condition. Thus, Bazant proposed the nominal stress intensity factor K_{IN} as the stress intensity

factor computed for the actual load and the initial crack length. Then, the apparent fracture toughness K_{INu} is defined as the value of K_{IN} at peak load. Thus,

$$K_{INu} = K_{Ic} \tag{6.37}$$

In this study, the critical stress intensity factor for mode-I K_{Ic} can be represented as

$$K_{Ic} = \sigma_{1u}\sqrt{\pi a_0} \tag{6.38}$$

where σ_{1u} means the ultimate principal tensile stress at the crack tip, a_0 is the initial crack length. Because diagonal tension failure occurs when σ_{1u} is equal to tensile stress f_{ct}, the critical stress intensity factor K_{Ic} is expressed as follows.

$$K_{Ic} = f_{ct}\sqrt{\pi a_0} \tag{6.39}$$

From Eq. (6.35), the critical stress intensity factor can be obtained as follows.

$$K_{Ic} = \tau_{xy}\sqrt{\pi a_{eff}}\sqrt{0.5\left(\frac{\sigma_x}{\tau_{xy}}\right)^2 - \left(\frac{\sigma_x}{\tau_{xy}}\right) + 1} \tag{6.40}$$

By using the Eq. (6.39) the shear stress at the crack tip can be written as

$$\tau_{xy} = \frac{K_{Ic}}{\sqrt{\pi a_{eff}}\sqrt{0.5\left(\frac{\sigma_x}{\tau_{xy}}\right)^2 - \left(\frac{\sigma_x}{\tau_{xy}}\right) + 1}} \tag{6.41}$$

Inserting the critical stress intensity factor for mode-I fracture into the Eq. ( ) yields

$$\tau_{xy} = \frac{f_{ct}}{\sqrt{0.5\left(\frac{\sigma_x}{\tau_{xy}}\right)^2 - \left(\frac{\sigma_x}{\tau_{xy}}\right) + 1}} \sqrt{\frac{a_0}{a_{eff}}} \tag{6.42}$$

where a_{eff} is the effective crack length in compression zone. The ratio of normal stress to shear stress can be calculated from following equation.

$$\frac{\tau_{xy}}{\sigma_x} = \sqrt{\left(\frac{f_{ct}}{\sigma_x}\right)^2 + \frac{f_{ct}}{\sigma_x}} \tag{6.43}$$

As a result, shear stress is function of tensile stress of concrete and initial and effective crack length. If the initial crack length is constant, shear stress decreases as the crack propagates more. Besides, the shear stress is reduced with increasing the ratio of normal stress to shear stress at the crack tip.

As a result, the shear strength can be expressed as follows.

$$V = \tau_{xy} bh = \frac{f_{ct} bh}{\sqrt{0.5\left(\frac{\sigma_x}{\tau_{xy}}\right)^2 - \left(\frac{\sigma_x}{\tau_{xy}}\right) + 1}} \sqrt{\frac{a_0}{a_{eff}}} \tag{6.44}$$

where b is the width and h means the total height.

Diagonal tension failure is caused by the combing normal compressive stress and shear stress at the tip of critical diagonal crack in compression zone of simply supported reinforced concrete beams subjected to concentrated load.

The process to calculate the shear strength of reinforced concrete beams subjected to concentrated load is summarized as following.

1) Assume the compressive strain of the loading point ε_{ca}.

2) Calculate the depth of neutral axis c_a and moment arm jd_a

3) Determine the moment M_a and shear demand V_a

4) Calculate the x_0 and x_1

5) Calculate the ε_x, c_x, jd_x, and M_A, V_A

6) Determine the a_0 and a_{eff}

8) Determine the shear strength τ_{xy}

A slender beam generally appears the flexural behavior. When the shear force developed by flexure of a beam reaches the shear capacity, the failure is governed by shear behavior. Fig. (6.21) shows the proposed flexural-shear behavior of reinforced concrete beams without web reinforcement. As the concrete strain at loading point increases the moment the shear demand increases. At that time, the shear capacity at the compression zone decreases due to softening of concrete in compression zone. The predicted shear strength is determined the intersection of the shear demand curve and shear capacity curve.

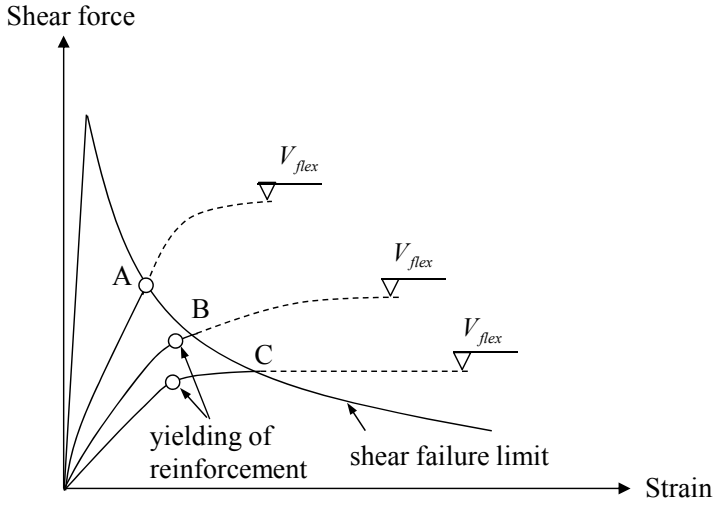

Figure 6.21 Proposed flexural-shear behavior

Fig. (6.22) shows the flexural-shear behavior of the test specimens AO-3-3b and AO-3-7b with rectangular cross section subjected to concentrated load by Mphonde et al. (1984). Primary parameter is concrete strength. Except the concrete strength, all parameters are same. The width of specimen, shear span-to-depth ratio, and longitudinal reinforcement ratio is 152 mm, 3.58, and 3.36%, respectively. As the concrete strength increases the shear strength increases. In case of AO-3-3b specimen, shear strength is determined after yielding of longitudinal reinforcement. On the other hand, shear strength of AO-3-7b specimen is obtained before the yielding. As a result, the predicted shear strength depends on the compressive strength of concrete.

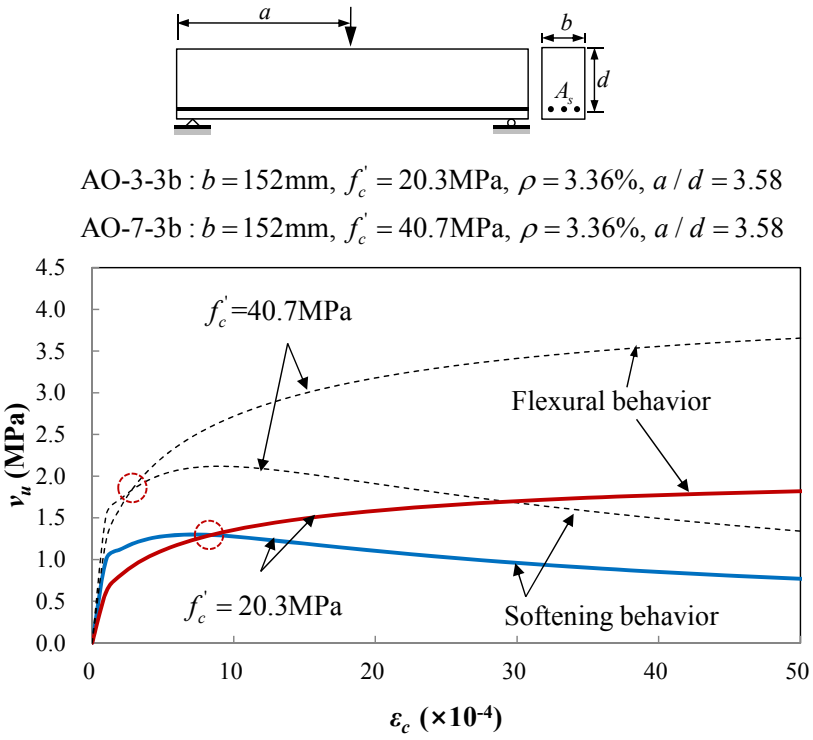

Figure 6.22 Analysis results for diagonal tension failure

6.4.5 Verification and Effect of Primary Parameters

The proposed model is applied as follows for the prediction of the ultimate shear strength of reinforced concrete slender beams without web reinforcement.

In order to investigate the influence of shear span-depth ratio and effective depth on shear stress, total 214 test results from the literature are selected. This test data list includes the test results of Ahmad et al. (1986), Bresler et al. (1963), Chana (1981), Cossio et al. (1960), Elzanaty et al. (1986), Feldman et al. (1955), Hallgren (1994), Harnadi et al. (1980), Hanson (1961), Kani (1967), Krefeld et al. (1966), Podgorniak (1998), Laupa et al. (1953), Leonhardt et al. (1962), Mathey et al. (1963), Morrow et al. (1957), Mphonde et al. (1984), Rajagopalan et al. (1968), Remmel (1991), Ruesch et al. (1962), Schcolz (1994), Taylor (1986, 1972), Thorenfeld et al. (1990), Walraven (1978), Thorenfeldt (1990), Islam et al. (1998), Lambolle et al. (1990), Kulkami et al. (1998), Coderwail et al. (1974), Moody et al. (1954), Ferguson (1956) for slender beams with various strength of concrete $14.0 \le f_c^{'} \le 59.3$[MPa] , beam width $90 \le b \le 400$ [mm] , effective depth $110 \le d \le 930$ [mm] , shear span-to-depth ratio $2.76 \le a/d \le 8.04$, total height $125 \le h \le 1000$ [mm], and longitudinal reinforcement ratio $0.25 \le \rho \le 4.51$ [%].

The cross section of all specimens is rectangular and failed by diagonal shear failure. And they are simply supported and subjected to one or two symmetric concentrated loads. Table and Fig. shows the comparisons of the proposed model with code provisions, ACI 318-08 for shear span-to-depth ratio a/d, compressive strength of concrete $f_c^{'}$, effective depth d and longitudinal reinforcement ratio ρ.

Fig. (6.23~6.26) presents the comparison of the predicted shear strength with test results for primary design parameters, shear span-to-depth ratio, concrete strength, effective depth, and longitudinal reinforcement ratio. It can be shown that the

theoretical results are in good agreement with the experiment results compared to other code provisions. The average of prediction to experiment ratio is 1.06 and the standard deviation is 0.17. On the other hand, for ACI 318-08, 0.72 in mean value and 0.20 in standard deviation, respectively.

Fig. (6.23) shows the ultimate shear strength for effective depth. The proposed model represents the size effect very reasonably, on the other hand, shear strength predicted by ACI 318-08 is size independent.

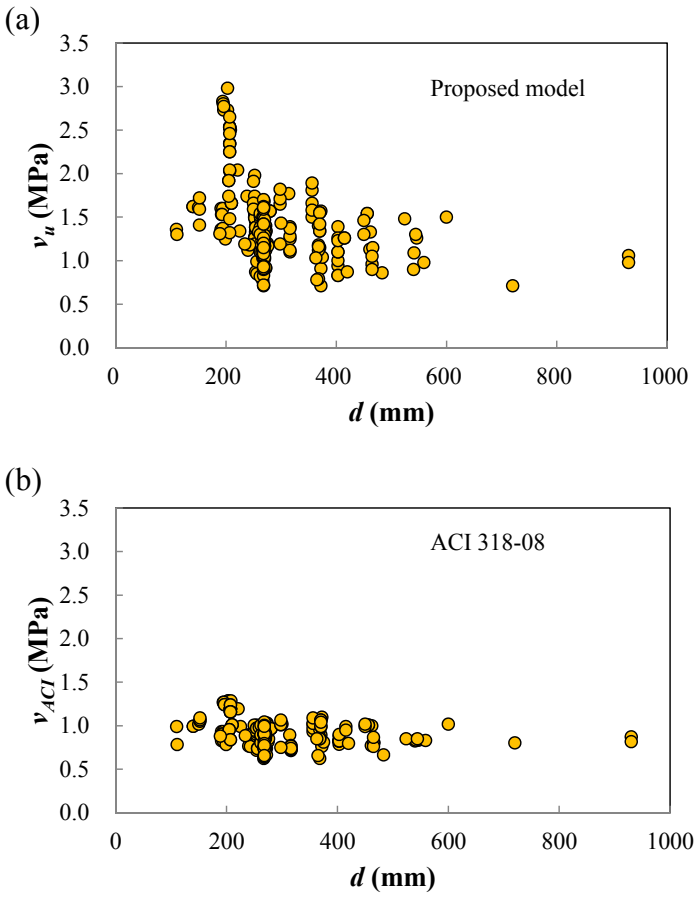

Figure 6.23 Ultimate shear strength for effective depth: (a) proposed model and (b) ACI 318-08

Table 6-2 Dimensions and properties of test specimen

Authors	Numbers of specimens	f_c' [MPa]	b [mm]	d [mm]	a/d	h [mm]	ρ [%]
Ahmad et al. (1986)	3	59.3	127	203 ~208	3.00 ~4.00	254	1.77 ~3.93
Bresler et al. (1963)	3	21.4 ~35.9	305 ~307	461 ~466	3.97 ~6.93	556 ~561	1.81 ~2.73
Chana (1981)	3	31.2 ~37.0	203	356	3.00	406	1.74
Cossio et al. (1960)	9	18.5 ~34.9	152	252	3.00 ~6.03	305	0.98 ~3.35
Elzanaty et al. (1986)	5	19.7 ~38.0	178	269 ~273	4.00	305	1.00 ~2.50
Feldman et al. (1955)	4	24.5 ~26.6	152	252	3.02 ~6.04	305	3.35
Hallgren (1994)	10	24.7 ~57.8	150 ~157	191 ~196	3.57 ~3.66	232 ~249	2.25 ~4.10
Harnadi et al. (1980)	3	20.9 ~28.8	100	370 ~372	3.44 ~5.97	400	1.08 ~1.70
Hanson (1961)	5	19.9 ~29.4	152	267	4.95	305	1.25 ~2.53
Kani (1967)	13	24.0 ~26.1	151 ~156	269 ~546	2.95 ~8.04	305 ~610	2.66 ~2.84
Krefeld et al. (1966)	28	15.9 ~36.5	152 ~254	238 ~483	2.89 ~6.09	305 ~533	1.34 ~4.51
Podgorniak et al. (1998)	3	35.2	300	110 ~450	3.00 ~3.07	125 ~500	0.81 ~0.91
Laupa et al. (1953)	6	14.0 ~30.7	152	262 ~269	4.54 ~4.65	305	1.90 ~4.11
Leonhardt et al. (1962)	22	19.8 ~37.2	100 ~225	140 ~600	2.78 ~6.00	160 ~670	1.14 ~2.07
Mathey et al. (1963)	9	22.3 ~27.8	203	403	2.84 ~3.78	457	0.47 ~2.55
Morrow et al. (1957)	11	14.0 ~43.4	305 ~308	356 ~375	2.76 ~5.87	406	1.87 ~3.92
Mphonde et al. (1984)	4	20.3 ~40.7	152	298	3.58	337	2.34 ~3.36
Rajagopalan et al. (1968)	10	22.5 ~36.5	151 ~154	259 ~268	3.83 ~4.92	311	0.25 ~1.73
Ruesch et al. (1962)	3	22.0 ~23.1	90 ~180	111 ~262	3.60 ~3.62	134 ~302	2.63 ~2.64

Authors	Numbers of specimens	f_c' [MPa]	b [mm]	d [mm]	a/d	h [mm]	ρ [%]
Taylor (1986)	10	23.0 ~40.8	200 ~400	370 ~930	3.00 ~3.02	406 ~1000	1.03 ~1.54
Thorenfeld et al. (1990)	8	51.3	150	207	3.00 ~4.00	250	1.82 ~3.24
Walraven (1978)	2	22.9 ~23.2	200	420 ~720	3.00	450 ~750	0.74 ~0.79
Thorenfeldt (1990)	2	55.1	150	207	3.00 ~4.00	250	3.23.
Islam et al. (1998)	9	25.3 ~48.3	150	205 ~207	2.90 ~3.86	250	2.02 ~3.19
Lambolle et al. (1998)	2	32.3 ~35.3	200	415	3.01	450	0.97 ~1.45
Kulkami et al. (1998)	3	39.8 ~42.8	102	152	3.50 ~5.00	178	1.37
Coderwail et al. (1974)	1	28.2	135	234	3.08	260	0.97
Moody et al. (1954)	22	14.6 ~39.1	152 ~178	262 ~272	2.95 ~3.41	305	1.60 ~2.37
Ferguson (1956)	1	27.8	101	189	3.23	210	2.08
Total	214	14.0 ~59.3	90 ~400	110 ~930	2.76 ~8.04	125 ~1000	0.25 ~4.51

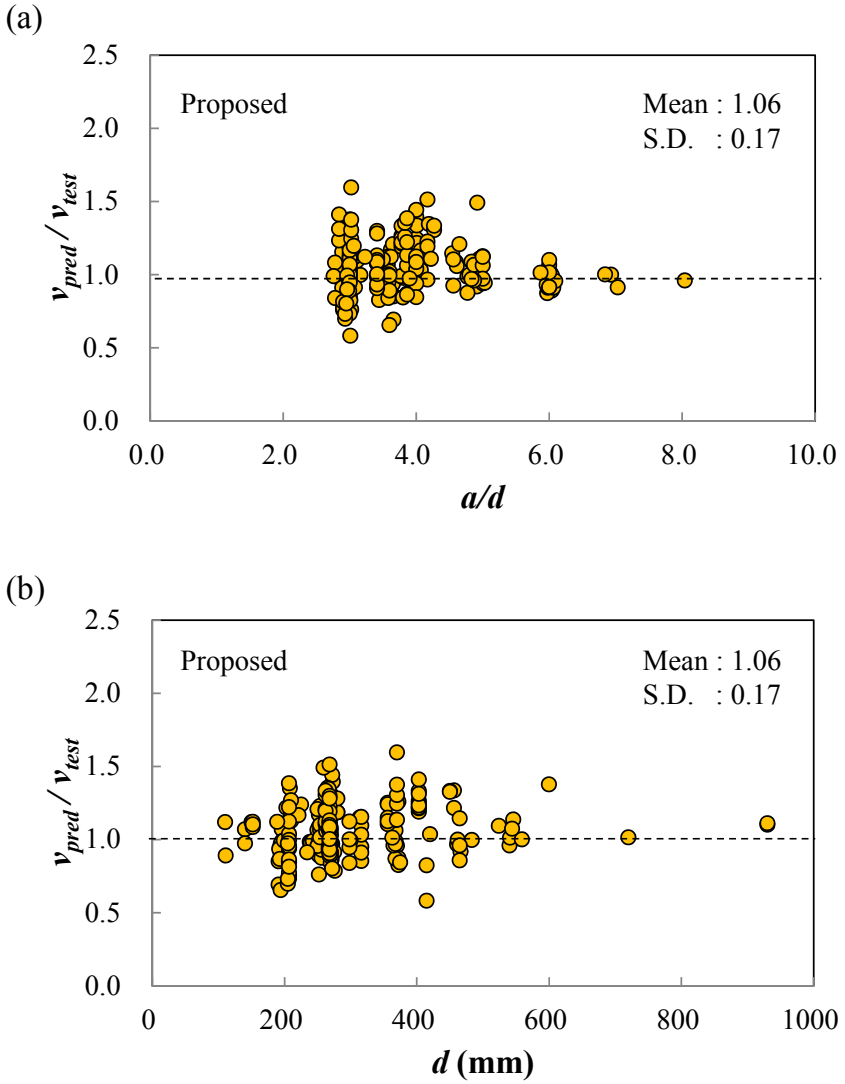

Figure 6.24 Comparison of predictions with experimental results: (a) for shear span-to-depth ratio, (b) effective depth

(c)

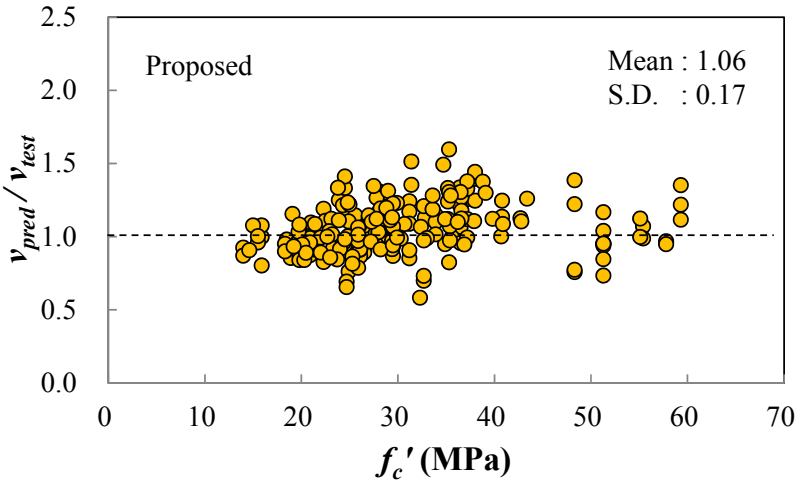

(d)

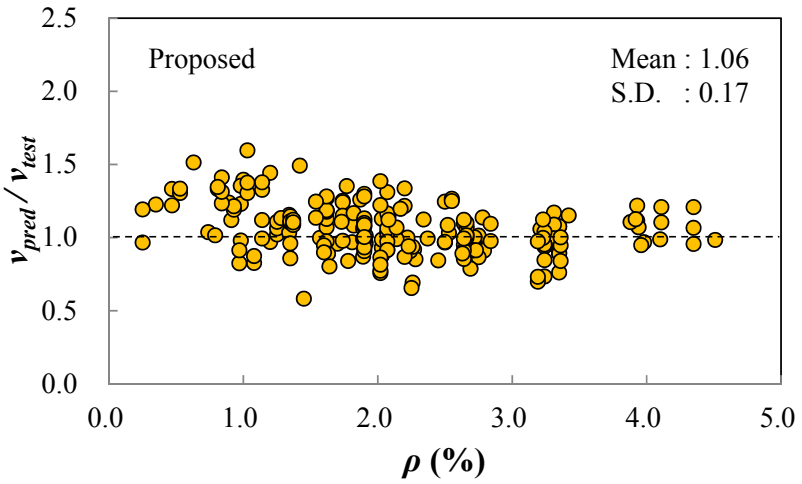

Figure 6.25 Comparison of predictions with experimental results: (c) for concrete strength, (b) longitudinal reinforcement ratio

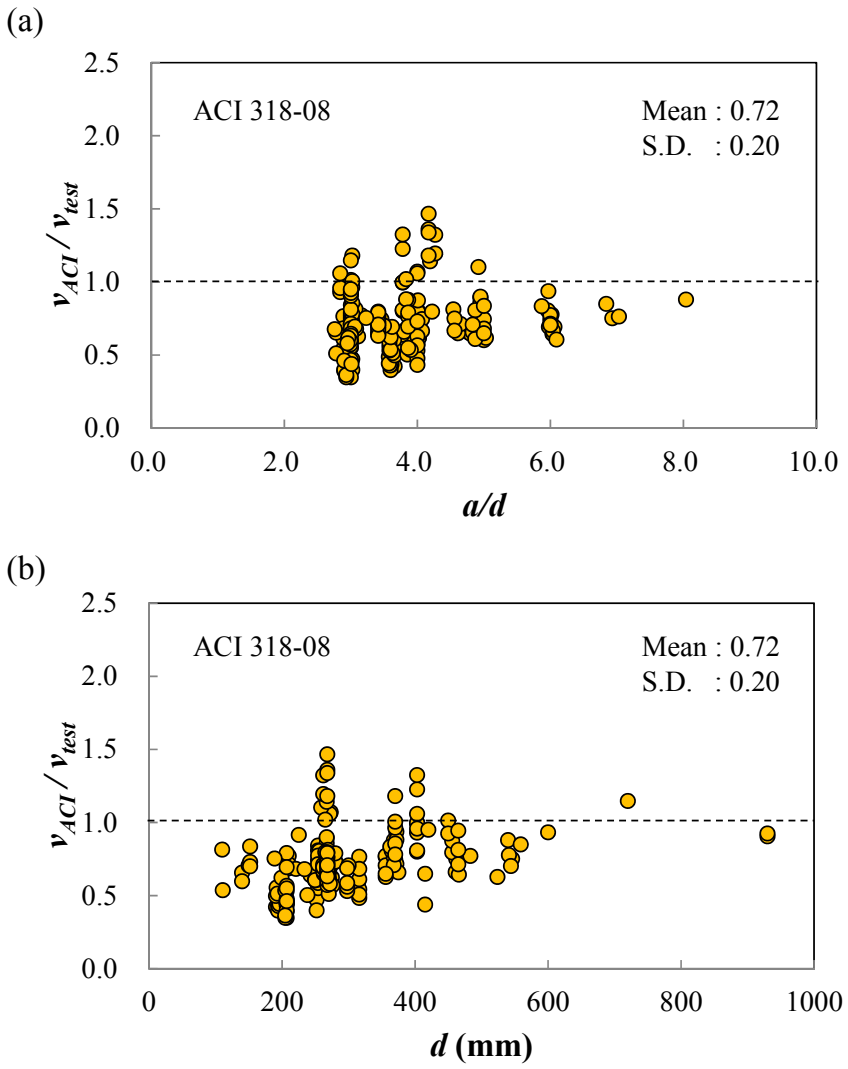

Figure 6.26 Comparison of ACI 318-08 with experimental results: (a) for shear span-to-depth ratio, (b) effective depth

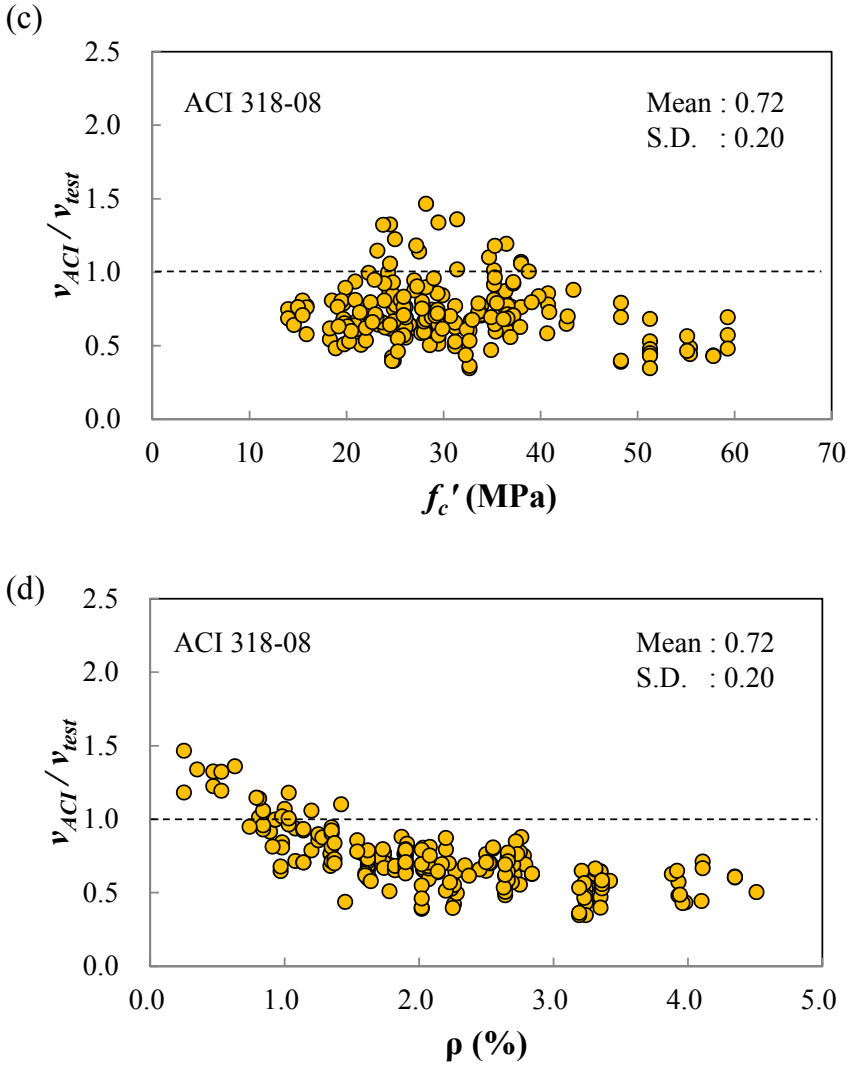

Figure 6.27 Comparison of ACI 318-08 with experimental results: (a) for shear span-to-depth ratio, (b) effective depth

6.5 Shear Strength for Sliding Failure

6.5.1 Introduction

In reinforced concrete design, there are situations where transfer of shear across a specific plane needs to be considered. Generally, shear friction is the term used to describe the mechanism of shear transfer along a concrete-to-concrete interface. Generally, the sliding failure occurs due to shear friction capacity.

In the theory of plasticity, concrete is assumed as a rigid plastic material. When the combined stresses exceed the modified Mohr-Coulomb failure criteria, a sliding failure takes place along a surface in the space or along a line in the plane. To determine the shear capacity of reinforced concrete beams without web reinforcement, Zhang (1994) proposed the crack sliding model. This model is based on the upper bound theorem of the plasticity. According to the crack sliding model, the cracking of concrete introduces potential yield line due to a reduced sliding resistance. As a result, shear failure occurs as sliding in cracks.

Shear friction capacity caused by sliding failure can be obtained by using the modified Mohr-Coulomb failure criteria. Design codes such as Eurocode 2 and ACI 318-08 define the maximum shear stress that can be transferred through aggregated interlock in terms of the Coulomb failure criteria as following equation.

$$\tau = c + \mu\sigma \tag{6.45}$$

where σ is normal stress, c is cohesion and μ represents the coefficient related to the roughness of the interface. The cohesion factor c is usually defined in terms of the concrete tensile strength.

In fracture mechanics approaches, the sliding failure can be explained by mixed mode fracture containing mode-I and mode-II fracture because the diagonal cracks

propagates due to combination of normal stress and shear stress. When a stress intensity factor, which is function of shear stress at the diagonal crack tip and crack length for mixed mode fracture, is equal to the critical stress intensity factor for mode-II fracture, the diagonal crack will propagate.

6.5.2 Shear Transfer across a crack

The forces transferring shear across an inclined crack in a beam without web reinforcement are illustrated in Fig. (6.27).

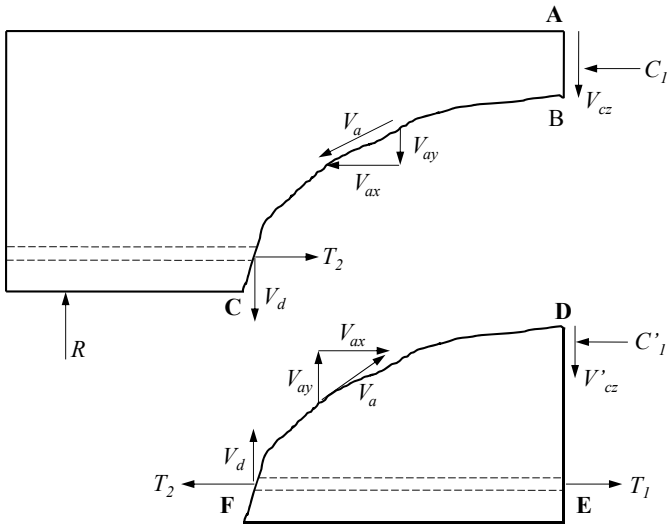

Figure 6.28 Forces transferring shear across an inclined crack

Shear is transferred across line A-B-C by V_{cz}, the shear in compression zone, by V_{ay}, the vertical component of the shear transferred across the crack by interlock of the aggregate particles on the two faces of the crack, and by V_d, the dowel action of the longitudinal reinforcement.

Especially, according to Fenwick and Paulay's experiments about 70% of the contribution of shear strength is caused by aggregate interlock approximately, while the remaining 30% was carried by the compression zone and dowel action. After that, Taylor estimated that the contribution of aggregate interlock was predominant. As a result, the magnitudes of contribution of aggregate interlock is 35~50%, dowel force and compression zone represent 15~25%, 20~40%, respectively.

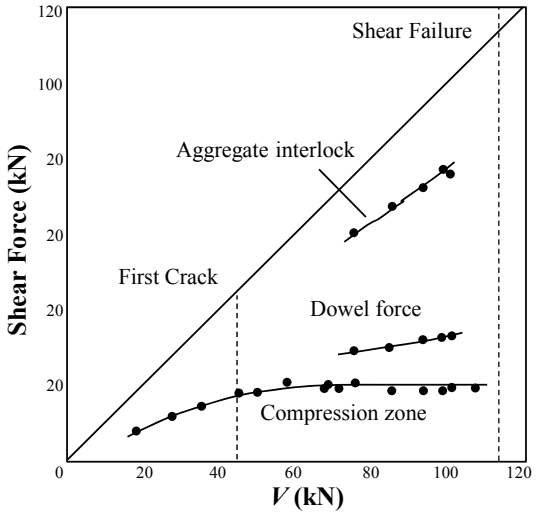

Figure 6.29 Components of shear resistance obtained by Taylor (1970)

Shear transfer in the interface was due primarily to aggregate interlock and hence caused by those aggregates that protruded from the crack surface. However, as cracks go through the aggregate in lightweight and high-strength concrete yet still have the ability to transfer shear, the term friction is more appropriate. The four basic parameters involved are the crack interface shear stress, normal stress, crack width, and crack slip. Walraven (1981) made numerous tests and developed a model that considered the probability that aggregate particles, idealized as spheres, would project from the crack interface. As slip develops, the matrix phase deforms

plastically, coming into contact with projecting aggregates. The stresses in the contact zones are comprised of a constant pressure, and a constant shear.

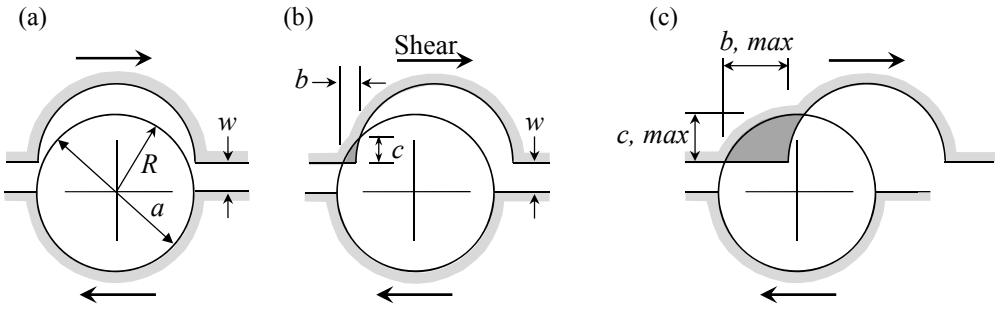

Figure 6.30 Walraven's crack model: (a) no contact; (b) growing contact and (c) maximum contact

Walraven tested 88 push-off shear transfer specimens. The major difference between these tests and those by Mattock and others was that Walraven kept the crack widths, w, constant throughout each test. Vecchio and Collins proposed the relationships between the shear across the crack v_{ci}, the crack width w, and the required compressive stress on the crack f_{ci} have been experimentally studied by a number of investigators, including Walraven. Based on Walraven's work the following relationship was derived.

$$v_{ci} = 0.18 v_{ci\max} + 1.64 f_{ci} - 0.82 \frac{f_{ci}^2}{v_{ci\max}} \tag{6.46}$$

where

$$v_{ci\max} = \frac{\sqrt{-f_c'}}{0.31 + 24w/(a+16)} \tag{6.47}$$

And where a is the maximum aggregate size in millimeters and the stress stress are in MPa. The crack width w is computed from the spacing, s_θ, of the inclined crack as

$$w = \varepsilon_1 s_\theta \tag{6.48}$$

where ε_1 is the principal tensile strain, which is assumed to act perpendicular to the crack, and s_θ is the spacing of the cracks, measured perpendicular to the cracks

$$s_\theta = \frac{1}{\frac{\sin\theta}{s_{mx}} + \frac{\cos\theta}{s_{my}}} \tag{6.49}$$

Collins and Kuchma (1999) proposed the following simple equation using the parameters identified by the MCFT.

$$v_c = \frac{V_c}{bd} = \frac{245}{1275 + 35\frac{0.9d}{d_a + 16}}\sqrt{f_c'} \tag{6.50}$$

Collins and Kuchma assumed a uniform crack opening displacement along the shear crack, equal to the average crack width, that corresponds to a strong stress singularity with a power of -1 around the crack tip. This means that the size effect on the shear strength with a power of -1 for very large sizes.

CEB-FIP Model code provides design equations (6.51) and (6.52) for rough interfaces. This model assumes a linear relationship up to a crack slip of 0.1mm.

Where less than s_u shear slip occurs along the interface, the mobilized shear stress corresponding to the actual shear slip value may be calculated as follows.

$$\text{For } s < 0.1\text{mm} \quad \tau = 5\tau_{ult} s \tag{6.51}$$

$$\text{For } s \geq 0.1\text{mm} \quad \left[\frac{\tau}{\tau_u}\right]^4 - 0.5\left[\frac{\tau}{\tau_u}\right]^3 = 0.3s - 0.03 \tag{6.52}$$

where $\tau_u = 0.4 f_c'^{2/3} \sigma^{1/3}$ and s in mm.

The shear slip along a rough interface is accompanied by a crack opening, which may be calculated as follows

$$w = 0.6 s^{2/3} \text{ [mm]} \tag{6.53}$$

Reineck (1991) used the following constitutive equations for the friction of crack faces without normal stress σ on the crack face. Shear stress decreases as the crack width increases linearly.

$$\tau_{fr} = 0.45 f_t' \left(1 - \frac{w}{0.9}\right) \tag{6.54}$$

where f_t' is the concrete tensile strength

6.5.3 Failure Criteria

To define the failure mechanism of the compression zone, modified Mohr-Coulomb failure criteria was used. It is based on the observation that failure often occurs along certain sliding planes or yield planes, the resistance of which is determined by a parameter termed the cohesion and an internal friction, the magnitude of which depends on the normal stress in the sliding failure. Sliding failure is assumed to occur in a section when the Coulomb frictional hypothesis is fulfilled. In other words, if the shear stress τ in the section exceeds the sliding resistance, sliding failure will occur.

Shear friction failure occurs when a following condition is satisfied.

$$\frac{1}{2}(\sigma_1 - \sigma_2) = c\cos\varphi - \frac{1}{2}(\sigma_1 + \sigma_2)\sin\varphi \tag{6.55}$$

where σ_1 and σ_2 mean principal tensile and compressive stress and φ represents the internal angle.

Inserting $\mu = \tan\varphi$, we have

$$\left(\mu + \sqrt{1+\mu^2}\right)^2 \sigma_1 - \sigma_2 = 2c\left(\mu + \sqrt{1+\mu^2}\right) \tag{6.56}$$

If a parameter k is defined by

$$k = \left(\mu + \sqrt{1+\mu^2}\right)^2 \tag{6.57}$$

Therefore, the conditions for sliding failure can be written as follows.

$$k\sigma_1 - \sigma_2 = 2c\sqrt{k} \tag{6.58}$$

Since the compression test will always involve sliding failure, following equation is fulfilled.

$$f_c^{'} = 2c\sqrt{k} \tag{6.59}$$

If concrete is identified with a modified Coulomb material, the parameter k has a value of around 4 for low strength concrete. If this value is selected as $\mu = 0.75$ and corresponding to an angle of friction is $\varphi = 37^\circ$, From Eq. ( ), cohesion c is obtained as follows.

$$c = \frac{1}{4} f_c^{'} \tag{6.60}$$

Since the sliding failure due to shear friction occurs at compression zone of beams, principal tensile and compressive stresses can be represented as follows.

$$\sigma_1 = -\frac{\sigma_x}{2} + \sqrt{\left(\frac{\sigma_x}{2}\right)^2 + \tau_{xy}^2} \tag{6.61}$$

$$\sigma_2 = -\frac{\sigma_x}{2} - \sqrt{\left(\frac{\sigma_x}{2}\right)^2 + \tau_{xy}^2} \tag{6.62}$$

where σ_x is normal stress and τ_{xy} means the shear stress at the tip of critical diagonal crack.

Substituting Eqs.(6.61) and (6.62) into Eq. (6.55) and organizing yields

$$\tau_{xy} = 0.2\sqrt{f_c'^2 + 3f_c'\sigma_x - 4\sigma_x^2} \tag{6.63}$$

As you can see that if the normal stress is zero the shear stress is equal to $0.2f_c'$. ACI 318-08 have proposed the upper limit on shear friction strength. According to this code provision for normal-weight concrete either placed monolithically or placed against hardened concrete with surface intentionally roughened, shear strength shall not exceed the smallest of $0.2f_c'A_c$, $\left(3.3+0.08f_c'\right)A_c$ and $11A_c$. However, as shown in Fig. (6.30), because the shear stress obtained from Eq. (6.63) depends on normal stress, the shear stress increases with increasing the normal stress at first time. After peak point, the shear stress is reduced as the normal stress increases.

The ratio of shear stress to normal stress can be obtained from Eq. (6.63) by dividing into the normal stress.

$$\frac{\tau_{xy}}{\sigma_x} = 0.2\sqrt{\left(\frac{f_c'}{\sigma_x}\right)^2 + 3\left(\frac{f_c'}{\sigma_x}\right) - 4} \tag{6.64}$$

Fig. (6.31) shows that the variation of the ratio of shear stress to normal stress with increasing the ratio of compressive strength to normal stress. The ratio of shear

stress to normal stress increases with increasing the ratio of compressive strength to normal stress.

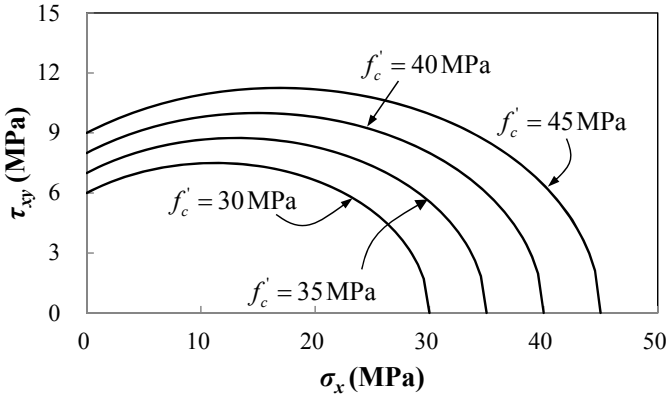

Figure 6.31 Variation of shear stress for normal stress in case of sliding failure

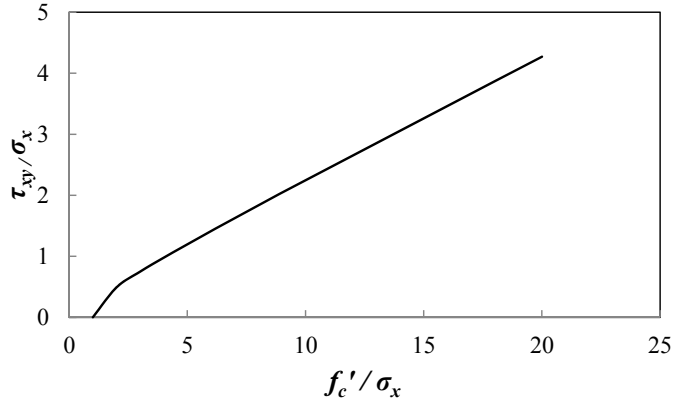

Figure 6.32 Variation of the ratio of shear stress to normal stress for concrete strength

6.5.4 Shear Strength

In LEFM, if the effective stress intensity factor for mixed mode is equal to the critical stress intensity factor for mode-II fracture K_{IIc}, sliding failure will occur.

$$K_{eff} = K_{IIc} \tag{6.32}$$

In this case, the shear stress at the crack tip is obtained as follows.

$$\tau_{xy} = \frac{K_{IIc}}{\sqrt{\pi a_{eff}}\sqrt{0.5\left(\frac{\sigma_x}{\tau_{xy}}\right)^2 - \left(\frac{\sigma_x}{\tau_{xy}}\right) + 1}} \tag{6.33}$$

where σ_x is the normal compressive stress and τ_{xy} is the shear stress at the diagonal crack tip.

The critical stress intensity factor for mode-II fracture K_{IIc} can be written as function of ultimate shear stress τ_u and initial crack length a_0.

$$K_{IIc} = \tau_u \sqrt{\pi a_0} \tag{6.34}$$

As described in Fig. (6.32), generally the shear stress is the maximum at the neutral axis. Thus, the ultimate shear stress can be calculated by using the stress states at near the neutral axis. The ultimate shear stress for sliding failure τ_u is obtained by using modified Mohr-Coulomb criterion.

Inserting the principal stresses $\sigma_1 = \tau_{xy}$, $\sigma_2 = -\tau_{xy}$ and internal angle $\varphi = 37^\circ$, cohesion $c = 1/4 f_c^{'}$ into Eq. ( ), the ultimate shear stress can be expressed as

$$\tau_u = 0.2 f_c^{'} \tag{6.35}$$

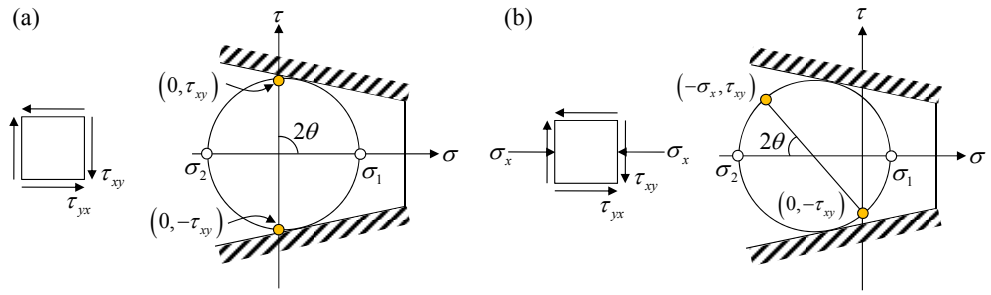

Figure 6.33 Stress states and Mohr's circle: (a) pure shear and (b) biaxial stress

Substituting Eq. (6.35) into Eq. (6.34) yields

$$K_{IIc} = 0.2 f_c^{'} \sqrt{\pi a_0} \tag{6.36}$$

As a result, the critical stress intensity factor for mode-II fracture is defined as the function of concrete strength $f_c^{'}$ and initial crack length a_0. This equation can also be expressed as follows.

$$K_{IIc} = 0.2 f_c^{'} \sqrt{h} \sqrt{\pi \frac{a_0}{h}} = 0.2 f_c^{'} \sqrt{h} k(\alpha_c) \tag{6.37}$$

where h means the total height of beams.

If the dimensionless function $k(\alpha_c)$ is constant, K_{IIc} increases proportional to $\sqrt{h}$. Fig.(6.33) shows the critical stress intensity factor for mode-II fracture for effective depth. Experimental results by Chana (1981) were selected. As the effective depth increases the critical stress intensity factor mode-II fracture increases. This means that critical stress intensity factor for mode-II fracture is dependent on the size.

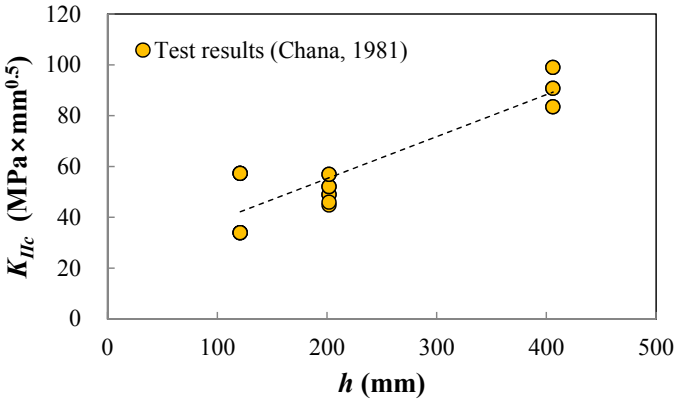

Figure 6.34 Critical stress intensity factor K_{IIc} for mode-II fracture

Inserting Eq.(6.36) into Eq. (6.33), the shear stress at the crack tip can be obtained as follows.

$$\tau_{xy} = \frac{0.2 f_c^{'}}{\sqrt{0.5\left(\frac{\sigma_x}{\tau_{xy}}\right)^2 - \left(\frac{\sigma_x}{\tau_{xy}}\right) + 1}} \sqrt{\frac{a_0}{a_{eff}}} \tag{6.38}$$

where $\frac{\tau_{xy}}{\sigma_x} = 0.2\sqrt{\left(\frac{f_c^{'}}{\sigma_x}\right)^2 + 3\left(\frac{f_c^{'}}{\sigma_x}\right) - 4}$

The shear stress depends on the initial crack length a_0 and effective crack length a_{eff}. Fig. (6.34) illustrates the initial and effective crack length for diagonal tension failure. In this study, initial crack length is defined as the concrete cover length. And the effective crack length is determined the length increased from the neutral axis.

$$a_0 = c_c \tag{6.39}$$

$$a_{eff} = d - c_x \tag{6.40}$$

where c_x represents the depth of neutral axis at cracked section as shown in Fig. (6.34).

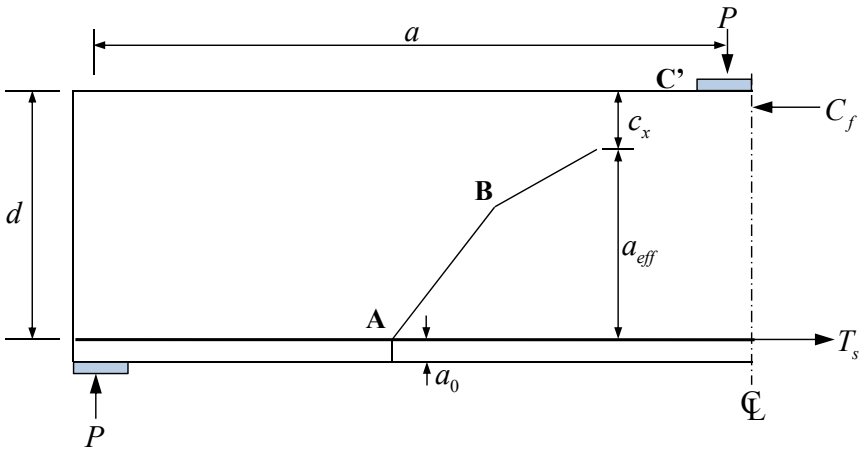

Figure 6.35 Initial and effective crack length for sliding failure mode

Finally, the proposed shear strength for sliding failure is obtained as follows.

$$V_{fr} = \frac{0.2 f_c' bh}{\sqrt{0.5\left(\frac{\sigma_x}{\tau_{xy}}\right)^2 - \left(\frac{\sigma_x}{\tau_{xy}}\right) + 1}} \sqrt{\frac{a_0}{a_{eff}}} \tag{6.41}$$

Fig. (6.35) shows the analysis results for specimen 8-1 tested by Leonhardt et al. (1962). Material properties of this specimen are shown in Fig. (6.35) also. As a result, the ultimate shear stress v_u is obtained from the intersection between flexural behavior curve and sliding failure limit curve after yielding of reinforcement.

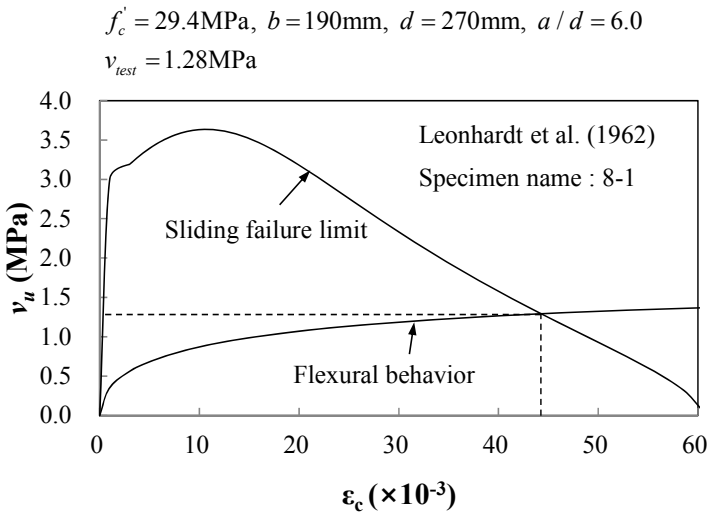

Figure 6.36 Proposed flexural-shear behavior for sliding failure

6.5.5 Verification

The proposed sliding crack model is applied as follows for the prediction of the ultimate shear strength of reinforced concrete slender beams without web reinforcement.

In order to investigate the influence of shear span-depth ratio and effective depth on shear stress, total 77 test results from the literature are selected. This test data list includes the test results of Cossio et al. (1960), Elzanaty et al. (1986), Feldman et al. (1955), Hallgren (1994), Harnadi et al. (1980), Hanson (1961), Kani (1967), Krefeld et al. (1966) for slender beams with various strength of concrete $18.3 \le f_c' \le 52.8$[MPa] , beam width $100 \le b \le 254$ [mm] , effective depth $191 \le d \le 559$ [mm] , shear span-to-depth ratio $2.89 \le a/d \le 8.04$, total height $232 \le h \le 640$ [mm], and longitudinal reinforcement ratio $0.98 \le \rho \le 4.51$ [%].

The cross section of all specimens is rectangular and failed by diagonal shear failure. And they are simply supported and subjected to one or two symmetric concentrated loads. Table 6-3 shows the comparisons of the proposed sliding model with ACI 318-08 for shear span-to-depth ratio a/d, compressive strength of concrete $f_c^{'}$, effective depth d and longitudinal reinforcement ratio ρ.

Fig. (6.36) presents the comparisons of predicted value for sliding failure with for diagonal tension failure. The average of prediction for sliding failure to experiment ratio is 1.26 and the standard deviation is 0.26. On the other hand, for diagonal tension failure, 1.00 in mean value and 0.14 in standard deviation, respectively.

As a result, the proposed theory for sliding failure accurately predicts the experimental observation for the ultimate shear force of extensive well-grounded test series of slender beams in case of $a/d > 4$. However, in case of $a/d \leq 4$, the predictions of proposed model tends to overestimate.

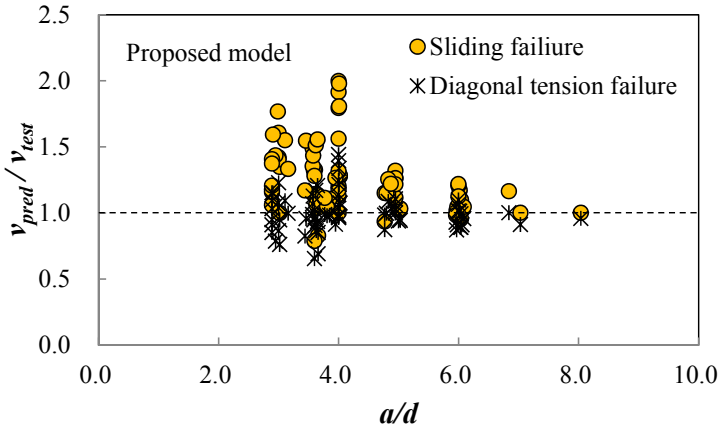

Figure 6.37 Comparison of predictions with experimental results for *a/d*

Table 6-3 Dimensions and material properties of test specimens

Authors	Specimen name	f_c' [MPa]	b [mm]	d [mm]	a/d	h [mm]	ρ [%]	v_{test} [MPa]	v_{dt} [MPa]	v_{fr} [MPa]	(2)/(1)†	(3)/(1)†
Cossio et al. (1960)	L-2a	34.9	152	252	3.02	305	3.35	2.09	1.98	2.82	0.95	1.35
	L-3	26.6	152	252	4.02	305	3.35	1.39	1.50	1.78	1.08	1.28
	L-4	24.5	152	252	5.02	305	3.35	1.34	1.27	1.38	0.95	1.03
	L-5	26.5	152	252	6.03	305	3.35	1.33	1.19	1.27	0.89	0.95
	A2	29.9	152	254	3.00	305	0.98	1.08	1.33	1.74	1.23	1.61
	A3	18.5	152	254	4.00	305	0.98	0.89	0.87	0.89	0.98	1.00
	A-12	25.4	152	254	3.00	305	3.33	1.53	1.59	2.17	1.04	1.42
	A-13	21.0	152	254	4.00	305	3.33	1.21	1.26	1.46	1.04	1.20
	A-14	26.1	152	254	5.00	305	3.33	1.42	1.33	1.46	0.94	1.03
Elzanaty et al. (1986)	F11	19.7	178	272	4.00	305	1.20	0.94	0.91	1.06	0.97	1.13
	F12	19.7	178	269	4.00	305	2.50	1.14	1.10	1.34	0.96	1.18
	F8	38.0	178	273	4.00	305	1.00	0.96	1.34	1.84	1.39	1.91
	F13	38.0	178	272	4.00	305	1.20	0.97	1.40	1.94	1.44	2.00
	F14	38.0	178	269	4.00	305	2.50	1.35	1.68	2.42	1.25	1.79
Feldman (1955)	L-2A	24.9	152	252	3.02	305	3.35	2.09	1.59	2.09	0.76	1.00
	L-3	26.6	152	252	4.02	305	3.35	1.39	1.50	1.79	1.08	1.28
	L-4	24.5	152	252	5.03	305	3.35	1.34	1.26	1.38	0.94	1.03
	L-5	26.5	152	252	6.04	305	3.35	1.34	1.19	1.28	0.89	0.96
Hallgren (1994)	B90SB 17-2-45	24.7	157	191	3.66	232	2.26	1.97	1.36	1.63	0.69	0.83
	B90SB 18-2-45	24.7	155	194	3.60	235	2.25	2.10	1.37	1.65	0.65	0.79
	B91SD 1-4-61	57.8	156	194	3.61	247	3.98	2.92	2.83	3.88	0.97	1.33
	B91SD 2-4-61	57.8	156	195	3.59	248	3.96	2.96	2.80	3.91	0.95	1.32
	B91SD 5-4-58	55.4	156	196	3.57	249	3.94	2.55	2.73	3.80	1.07	1.49
	B91SD 6-4-58	55.4	150	196	3.57	249	4.10	2.81	2.77	3.80	0.99	1.35
	B90SB 5-2-33	31.2	156	191	3.66	232	2.28	1.88	1.60	1.95	0.85	1.04
	B90SB 6-2-33	31.2	156	194	3.61	235	2.24	1.77	1.60	2.02	0.91	1.14
	B90SB 9-2-31	29.5	156	192	3.65	233	2.26	1.64	1.53	1.86	0.94	1.14
	B90SB 10-2-31	29.5	157	193	3.63	234	2.20	1.77	1.53	1.88	0.87	1.06
Harnadi et al. (1980)	G1	28.8	100	370	3.46	400	1.70	1.20	1.15	1.86	0.96	1.55

Authors	Specimen name	f_c' [MPa]	b [mm]	d [mm]	a/d	h [mm]	ρ [%]	v_{test} [MPa]	v_{dt} [MPa]	v_{fr} [MPa]	(2)/(1)†	(3)/(1)†
Harnadi et al. (1980)	G2	22.3	100	372	3.44	400	1.08	1.10	0.91	1.29	0.83	1.17
	G3	20.9	100	372	5.97	400	1.08	0.81	0.71	0.83	0.87	1.02
Hanson (1961)	A4	19.9	152	267	4.95	305	1.25	0.83	0.85	0.93	1.02	1.12
	B4	29.4	152	267	4.95	305	1.25	1.05	1.12	1.33	1.06	1.26
	BW4	28.2	152	267	4.95	305	1.25	0.99	1.09	1.30	1.11	1.32
	8B2	29.3	152	267	4.95	305	2.53	1.29	1.33	1.63	1.03	1.26
	B2	29.3	152	267	4.95	305	2.22	1.29	1.29	1.57	1.00	1.22
Kani (1967)	63	24.9	154	546	4.00	610	2.78	1.11	1.26	1.73	1.14	1.56
	64	24.4	156	540	8.04	610	2.76	0.94	0.90	0.94	0.96	1.00
	66	25.1	156	541	6.02	610	2.75	1.08	1.09	1.26	1.01	1.17
	79	24.8	153	559	6.84	610	2.72	0.98	0.98	1.14	1.00	1.16
	74/75	25.9	152	524	3.11	610	2.84	1.35	1.48	2.10	1.09	1.55
	71	26.0	155	544	2.99	610	2.66	1.21	1.30	2.14	1.07	1.77
	81	26.1	153	272	5.98	305	2.79	1.23	1.12	1.29	0.91	1.05
	84	26.1	151	271	4.00	305	2.84	1.35	1.32	1.78	0.98	1.31
	96	24.0	156	275	3.95	305	2.71	1.31	1.20	1.66	0.91	1.26
	83	26.1	156	271	3.00	305	2.75	1.54	1.33	2.16	0.87	1.40
	97	25.9	152	276	2.95	305	2.69	1.49	1.17	2.14	0.79	1.44
	91	26.1	154	269	6.06	305	2.70	1.23	1.12	1.26	0.91	1.02
	92	26.1	152	270	7.03	305	2.73	1.12	1.02	1.12	0.91	1.00
Krefeld et al. (1966)	11A2	28.7	152	314	2.91	381	3.42	1.54	1.77	2.45	1.15	1.59
	12A2	28.6	152	238	3.85	305	4.51	1.77	1.74	1.96	0.98	1.11
	18A2	18.3	152	316	2.89	381	2.64	1.32	1.25	1.55	0.95	1.18
	18B2	18.9	152	316	2.89	381	2.64	1.50	1.28	1.59	0.85	1.06
	18C2	21.5	152	316	2.89	381	2.64	1.53	1.39	1.77	0.91	1.16
	18D2	21.0	152	316	2.89	381	2.64	1.25	1.37	1.76	1.09	1.41
	16A2	21.1	152	240	3.81	305	1.74	1.15	1.12	1.20	0.98	1.05
	17A2	20.9	152	243	3.77	305	2.14	1.19	1.18	1.33	0.99	1.11
	3AC	19.8	152	256	4.77	305	2.03	1.13	0.99	1.06	0.87	0.94
	3CC	19.5	152	256	5.96	305	2.03	0.91	0.85	0.90	0.93	0.98
	3AAC	32.8	152	256	3.58	305	2.03	1.43	1.61	2.05	1.13	1.43
	4AAC	27.7	152	254	3.60	305	2.66	1.50	1.53	1.92	1.02	1.28
	5AAC	31.2	152	252	3.62	305	3.31	1.49	1.74	2.25	1.17	1.51
	6AAC	32.7	152	250	3.65	305	4.35	1.58	1.91	2.46	1.21	1.56
	3AC	30.3	152	256	4.77	305	2.03	1.37	1.35	1.58	0.98	1.15
	4AC	29.0	152	254	4.80	305	2.66	1.39	1.39	1.60	1.00	1.15
	5AC	31.2	152	252	4.83	305	3.31	1.42	1.54	1.78	1.09	1.26
	6AC	32.4	152	250	4.87	305	4.35	1.56	1.66	1.90	1.07	1.22

Authors	Specimen name	f_c' [MPa]	b [mm]	d [mm]	a/d	h [mm]	ρ [%]	v_{test} [MPa]	v_{dt} [MPa]	v_{fr} [MPa]	(2)/(1)†	(3)/(1)†
Krefeld et al. (1966)	4CC	36.5	152	254	6.00	305	2.66	1.36	1.45	1.64	1.07	1.21
	5CC	35.6	152	252	6.04	305	3.31	1.50	1.49	1.65	0.99	1.10
	6CC	36.5	152	250	6.09	305	4.35	1.66	1.59	1.74	0.96	1.05
	C	15.9	203	483	3.16	533	1.57	0.86	0.86	1.15	1.00	1.33
	OCA	33.9	152	254	6.00	305	2.66	1.26	1.38	1.53	1.10	1.22
	OCB	33.9	152	254	6.00	305	2.66	1.36	1.38	1.53	1.01	1.13
	OCA	36.4	254	456	4.01	508	2.20	1.27	1.54	2.29	1.21	1.81
	OCB	36.4	254	456	4.01	508	2.20	1.15	1.54	2.28	1.34	1.98
	15A2	19.1	152	316	2.89	381	1.34	0.95	1.10	1.31	1.15	1.37
	15B2	19.7	152	316	2.89	381	1.34	1.08	1.12	1.31	1.03	1.21
										Avg.	1.00	1.26
										S.D	0.14	0.26

† (1) v_{test} : experimental results

† (2) v_{dt} : proposed shear strength for diagonal tension failure

† (3) v_{fr} : proposed shear strength for sliding failure

6.5.6 Summary

This section has presented the critical crack path dependent shear strength of reinforced concrete slender beams without reinforcement. By using location of inclined crack tip, stress intensity factor, and failure criteria of concrete, shear strength based on crack path was determined. The main points are given as follows:

(1) To evaluate the critical crack path dependent shear strength of RC slender beams without web reinforcement, newly failure mechanism based on critical inclined crack propagation was proposed.

(2) The ratio of shear stress to normal stress was determined by considering the location of critical inclined crack tip. The vertical distance y and horizontal distance x are calculated from the neural axis and a support, respectively. Consequentially, the ratio depends on the location of crack tip.

(3) The stress intensity factors for mode-I (opening) and mode-II (sliding) fracture were obtained from principal tensile stress and shear stress acting on cracked plane under the given stress states.

(4) The critical stress intensity factor for mode-I and mode-II fracture were determined from the ultimate normal stress and shear stress in mode-I and mode-II fracture, respectively. Additionally, initial crack length is also considered.

(5) The angle of critical inclined crack was obtained by using the failure criterion of concrete, modified Mohr-Coulomb criteria. As a result, this angle depends on the ratio of shear stress to normal stress at the crack tip.

6.6 Shear Strength of Reinforced Concrete Short Beams without Web Reinforcement

6.6.1 Introduction

In this chapter, we will derive the shear strength of reinforced concrete short beams proposed model based on crack growth. During the last 50 years, numerous studies on the shear strength of reinforced concrete short beams have been carried out. Many experimental results have been showed that the reinforced concrete short beams with shear span-to-depth ratio between 1.0 and 2.5 fail because of crushing of concrete in the diagonal strut. However, despite these developments, a rational and fundamental theory explaining the shear failure of short beams is still missing.

In case of short beams, an important question is whether size effects also occur in the case of short beams. Walraven et al. (1994) proposed that in the short beams without web reinforcement, a significant size effect occurs. And size effect in short beams is very similar to that in slender beams in spite of the different types of failure. Crack propagation which is dependent beam depth is the key to explanation of size effect.

The failure mechanism in a deep beam ($a/d<2.5$) differs significantly from that of a slender beam ($a/d>2.5$). Short shear spans with a/d form 1 to 2.5 develop inclined cracks and, after redistribution of internal forces, are able to carry additional load, in part by arch action. The final failure of such beams will be causes by a bond failure, a splitting failure, or a dowel failure along the tension reinforcement or by crushing of the compression zone over the crack. The latter is referred to as a shear compression failure. Because the inclined crack generally extends higher into the beam than does a flexural crack, failure occurs at less than the flexural moment capacity.

However, if the reinforced concrete deep beams have a very small amount of longitudinal reinforcement, flexural-shear failure occurs even though shear span-to-depth ratio is small. In this case, flexural crack develop on the bottom of the beam or near the midspan of the beam at first. As applied load is increased, more flexural cracks follow accompanied by diagonal cracking. The longitudinal reinforcement will yield and critical diagonal crack will develop along the diagonal strut.

6.6.2 Failure Mode of Diagonal Strut

Concrete single strut subjected to uniaxial compressive stress has two different failure mechanisms. One is general compression failure induced by longitudinal cracks and the other is sliding failure by inclined crack as shown in Fig. (6.37) Main difference between two failure mechanisms is the causes of cracks. The Longitudinal cracks occur when principal tensile stress reaches the tensile stress of concrete, in this case principal tensile stress is same as the horizontal normal stress.
On the other hand, diagonal crack occurs principal tensile stress combining normal stress and shear stress reaches the tensile stress of concrete as follows

$$\sigma_h = f_{ct} \tag{6.42}$$

$$\sigma_1 = f_{ct} \tag{6.43}$$

where σ_h means horizontal normal stress and σ_1 represents principal tensile stress combining normal stress and shear stress.
In both of two cases, it is identical that concrete failure occurs when compressive stress reaches f_c'.

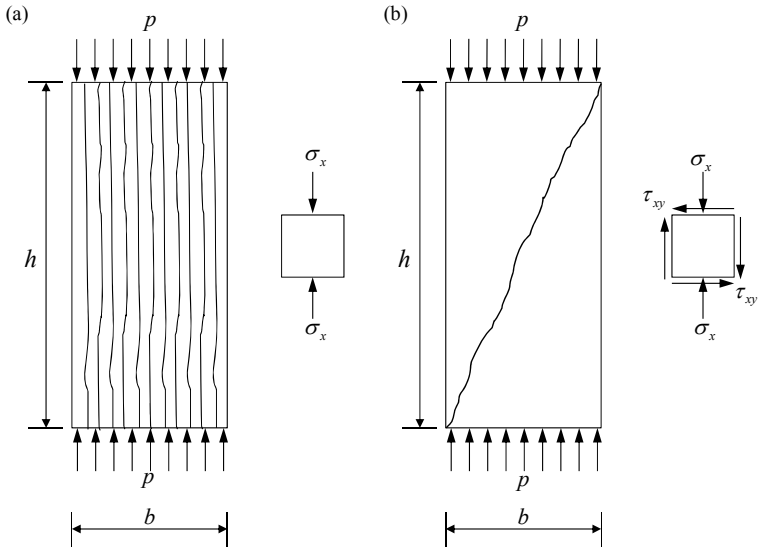

Figure 6.38 Two different failure mechanism of concrete strut: (a) General compressive failure mechanism; (b) Compressive sliding failure mechanism

In plasticity theory and general fracture mechanics approaches, general a failure mechanism of uniaxial compression assumes as shown in Fig. (6.37-a). To determine the compressive strength, let's consider the single strut as shown in Fig. (6.37-b). It is assumed that the strut carries the uniaxial compression stress $f_c^{'}$.

6.6.3 Uniaxial Compression

When concrete is subjected to uniaxial compression, the structural behavior of concrete is governed by localization of failure. Especially, the post-peak region of load-deformation curve greatly affected. It has been reported that the failure mechanism of uniaxial compression depends on such test conditions as specimen size, compressive strength friction between the loading plate and the specimen.

Particularly, the compressive failure is observed in reinforced concrete deep beams. In the previous researches, the size effect was found on the shear strength of RC deep beams without web reinforcement. This is because the localized failure of compression.

Therefore, it is necessary to study the behavior of concrete under compression by considering the localization of cracks in order to analyze the post-peak behavior of concrete more accurately.

6.6.4 Stress Concentrations

Consider the stresses in a bar of rectangular cross section (width b, thickness t) subjected to uniaxial compressive load P as shown in Fig.(6.38). The peak stress directly under the load may be several times the average stress P/bt, depending upon the area over which the load is applied. However, the maximum stress diminishes rapidly as we move away from the point of load application, as shown by the stress diagram in the figure. At a distance from the end of the bar equal to the width b of the bar, the stress distribution is nearly uniform, and the maximum stress is only a few percent larger than the average stress.

It should be noted that when the prismatic bar is subjected to uniaxial compressive force internal stress depends on the height of prismatic bar.

6.6.5 Concentrated Load at a Point of a Straight Boundary

As above mentioned, the stresses in the prismatic bar depend on the height. To explain this phenomenon, let us consider a concentrated vertical force P acting on a horizontal straight boundary *AB* of an infinitely large plate as shown in Fig. The distribution of the load along the thickness of the plate is uniform. And it is

assumed that the thickness of the plate is taken as unity, so that P is the load per unit thickness. a is the distance from the horizontal straight boundary AB and d represents the diameter of circle shown in Fig. (6.39-a).

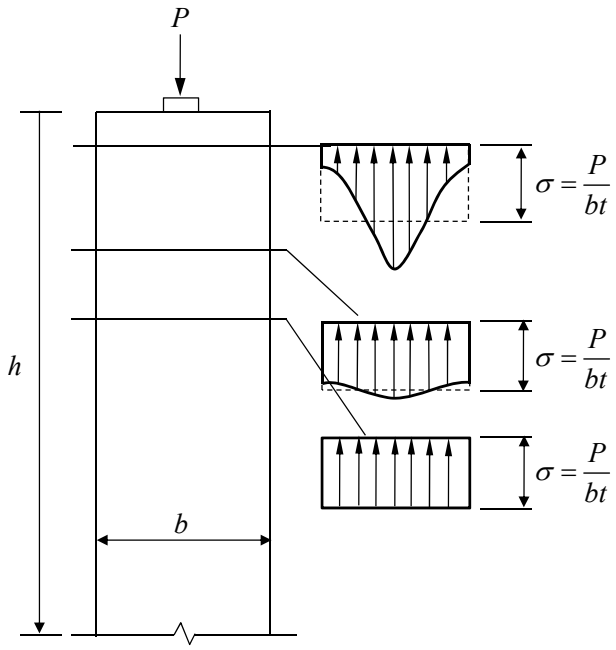

Figure 6.39 Stress distributions near the end of a bar of rectangular cross section subjected to a concentrated load P acting over a small area (Gere, 2001)

There is a basic solution called the simple radial distribution. Any element C at a distance r from the point of application of load is subjected to a simple compression in the radial direction. Thus, the stress components are

$$\sigma_{rr} = -\frac{2P}{\pi}\frac{\cos\theta}{r}, \quad \sigma_{\theta\theta} = \tau_{r\theta} = 0 \tag{6.44}$$

These values of the stress component should satisfy the equilibrium condition in polar coordinates as follows.

$$\sigma_r = \frac{1}{r}\frac{\partial \phi}{\partial r} + \frac{1}{r^2}\frac{\partial^2 \phi}{\partial \theta^2} = -\frac{2P}{\pi}\frac{\cos\theta}{r} \tag{6.45}$$

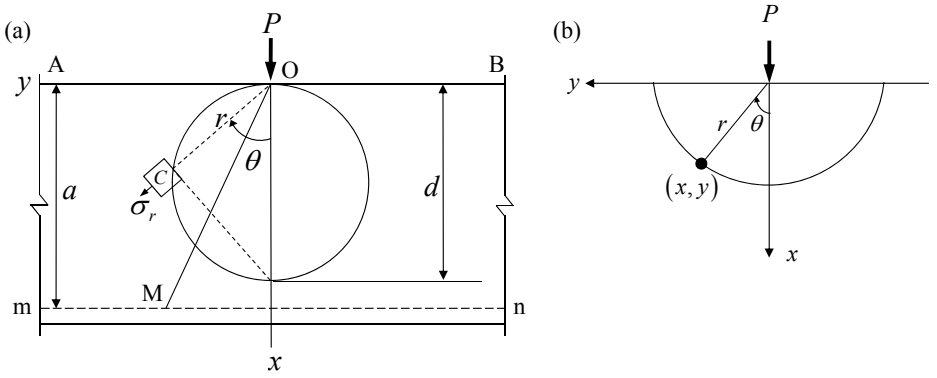

Figure 6.40 Concentrated force at a point a straight boundary: (a) Concentrated vertical force P acting on a horizontal straight boundary AB of an infinitely large plate; (b) Distribution of the load along the thickness of the plate (Timoshenko, 1970)

$$\sigma_\theta = \frac{\partial^2 \phi}{\partial r^2} = 0 \tag{6.46}$$

$$\tau_{r\theta} = -\frac{\partial}{\partial r}\left(\frac{1}{r}\frac{\partial \phi}{\partial \theta}\right) = 0 \tag{6.47}$$

where ϕ represents the stress function and is expressed as

$$\phi = -\frac{P}{\pi} r\theta \sin\theta \tag{6.48}$$

Taking a horizontal plane *mn* at a distance a from the straight edge of the plate, the normal and shear components of the stress on this plane at any point M are calculated from the simple compression in the radial direction as follows.

$$\sigma_{xx} = \sigma_{rr}\cos^2\theta = -\frac{2P}{\pi}\frac{\cos^3\theta}{r} = -\frac{2P}{\pi a}\cos^4\theta \tag{6.49}$$

$$\sigma_{yy} = \sigma_{rr}\sin^2\theta = -\frac{2P}{\pi}\frac{\cos\theta\sin^2\theta}{r} = -\frac{2P}{\pi a}\sin^2\theta\cos^2\theta \tag{6.50}$$

$$\tau_{xy} = \sigma_{rr}\sin\theta\cos\theta = -\frac{2P}{\pi}\frac{\sin\theta\cos^2\theta}{r} = -\frac{2P}{\pi a}\sin\theta\cos^3\theta \tag{6.51}$$

As a result, the normal stresses σ_x, σ_y and shear stress τ_{xy} can be expressed in terms of the distance a. In other words, the stresses are inversely proportional to the distance a.

Fig. (5.10) shows the distribution of stresses σ_x (vertical axis, compressive stress) and τ_{xy} along the horizontal plane *mn* is represented graphically.

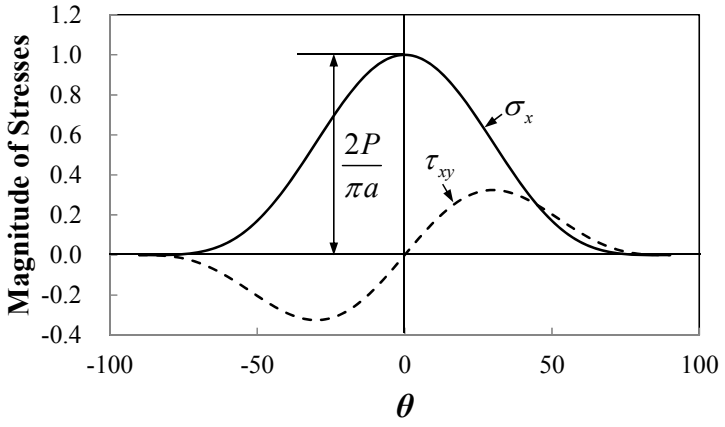

Figure 6.41 Distribution of normal and shear stresses

6.6.6 Sliding Failure of Prismatic Body

As mentioned already, there are three stress components in prismatic body in pure compression.

We consider a rectangular disk of modified Coulomb material with compressive and shear stresses as shown in Fig. (5.11). The disk has thickness B and width D and loaded with the pure compression. In this study, since it is very difficult to explain the sliding failure in case of only compressive stresses act, it is assumed that the normal stress and shear stress act in the prismatic body and the sliding failure occurs due to shear stress.

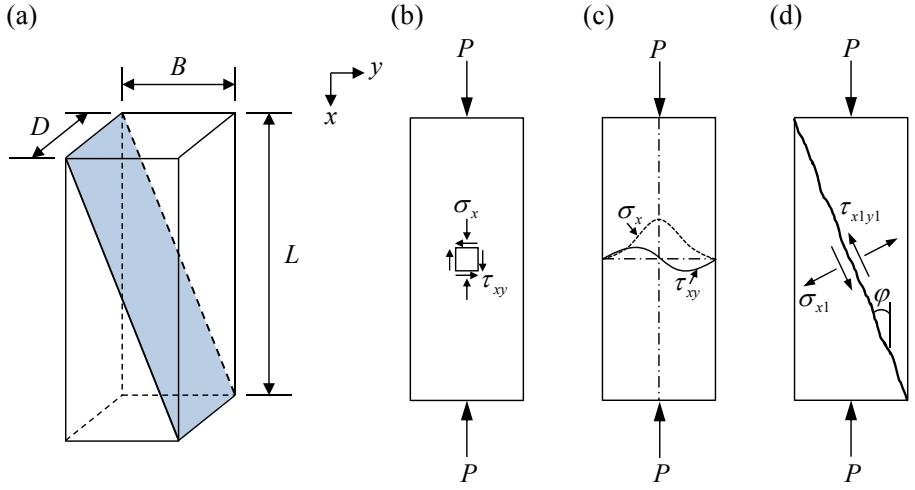

Figure 6.42 Sliding failure of a prismatic body: (a) Dimensions; (b) Normal and shear stresses; (c) Distribution of stresses; (d) Inclined crack

Normal and shear stress can be expressed as follows

$$\sigma_{xx} = \sigma_{rr} \cos^2 \theta \tag{6.52}$$

$$\sigma_{xy} = \sigma_{rr} \sin\theta \cos\theta \tag{6.53}$$

where σ_{rr} means the normal stress component in the radial direction and given by

$$\sigma_{rr} = -\frac{2P}{\pi}\frac{\cos\theta}{r} \tag{6.54}$$

The principal tensile stress σ_{x1} and the shear stress acting on the cracked plane τ_{x1y1} are obtained as follows

$$\sigma_{x1} = \sigma_x \cos^2\theta + 2\tau_{xy}\sin\theta\cos\theta \tag{6.55}$$

$$\tau_{x1y1} = -\sigma_x \sin\theta\cos\theta + \tau_{xy}\left(2\cos^2\theta - 1\right) \tag{6.56}$$

Substituting Eq. (6.54) into Eq. (6.52) and organizing yields

$$\sigma_{x1} = -\frac{2P}{\pi a}\cos^4\theta\left(1+\sin^2\theta\right) \tag{6.57}$$

$$\tau_{x1y1} = \frac{2P}{\pi a}\sin^3\theta\cos^3\theta \tag{6.58}$$

It should be noted that the principal tensile stress and shear stress expressed by Eqs. (6.57) and (6.58) depends on the distance a. These values decrease with increasing the distance a.

Stress intensity factors for mode-I and mode-II fracture can be written as follows

$$K_I = \sigma_{x1}\sqrt{\pi a_c} = -\frac{2P}{\pi a}\cos^4\theta\left(1+\sin^2\theta\right)\sqrt{\pi a_c} \tag{6.59}$$

$$K_{II} = \tau_{x1y1}\sqrt{\pi a_c} = \frac{2P}{\pi a}\sin^3\theta\cos^3\theta\sqrt{\pi a_c} \tag{6.60}$$

Thus, the effective stress intensity factor for mixed mode fracture is

$$K_{eff} = \sqrt{K_I^2 + K_{II}^2} = \frac{2P}{\pi a}\cos^4\theta\sin\theta\sqrt{\pi a_{eff}} \tag{6.61}$$

where a_{eff} represents the effective crack length.

Since the prismatic body fails due to sliding failure, effective stress intensity factor is equal to the critical stress intensity factor for mode-II fracture as following equation.

$$K_{IIc} = \tau_u \sqrt{\pi a_0} \tag{6.62}$$

where a_0 means the initial crack length.

As a result, the compressive force P is obtained as follows

$$P = \frac{\tau_{xy} \pi a}{2\cos^4 \theta \sin\theta} \sqrt{\frac{a_0}{a_{eff}}} \tag{6.63}$$

Since the shear stress is equal to $0.2 f_c^{'}$ by failure criterion of concrete, modified Mohr-Coulomb criteria, Eq. (6.63) is modified as follows

$$P = \frac{0.31 f_c^{'} a}{\cos^4 \theta \sin\theta} \sqrt{\frac{a_0}{a_{eff}}} \tag{6.64}$$

Since the initial crack length a_0 is constant, the compressive force per unit thickness decreases as the ratio of total crack length to initial crack length increases. To determine the ultimate compressive force the angle of inclined crack should be determined. As mentioned above, sliding failure occurs due to shear stress. So, it is assumed that when shear stress reaches the maximum sliding failure occurs as shown in Fig. (6.43).

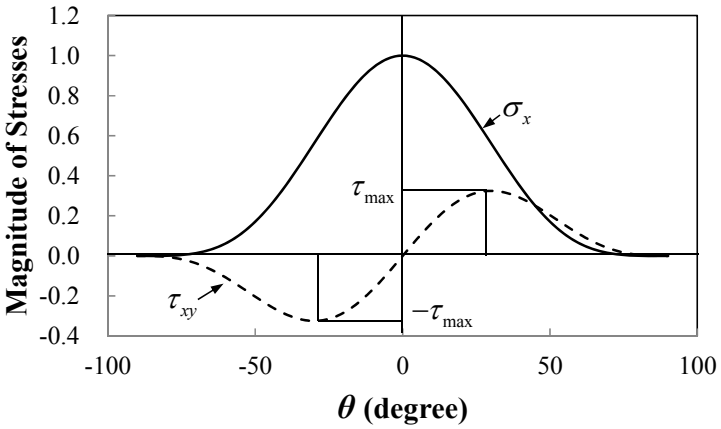

Figure 6.43 Maximum shear stresses

The angle corresponding to maximum shear stress can be obtained as follows.

$$\frac{d\sigma_{xy}}{d\theta} = -\frac{2P}{\pi a}\left(\cos^4\theta - 3\sin^2\theta\cos^2\theta\right) = 0 \tag{6.65}$$

Solving the above equation the angle in the equation which satisfies is $\theta = 30^\circ$.

If the distance a is equal to the height of prismatic body h, Eq. (6.65) can be modified as follows.

$$P = 1.1 f_c' h \sqrt{\frac{a_0}{a_{eff}}} \tag{6.66}$$

As mentioned in Section, the compressive force is the load per unit thickness. Thus, the ultimate compressive force corresponding to the area of cross-section is obtained as follows.

$$P_u = 1.1 f_c' b_w h \sqrt{\frac{a_0}{a_{eff}}} \tag{6.67}$$

If initial crack length is constant the compressive force inversely proportional to effective crack length. This means that the compressive force depends on the strength of concrete and crack length. Since the effective crack length is always larger than initial crack length, the compressive force decreases as the effective crack length increases.

Table (6-4) and Fig. (6.44) show the variation of compressive force for size of specimen and angel. To estimate the size effect, some examples are used. It is assumed that effective crack propagates from the initial crack tip at the bottom of the specimen with rectangular cross section toward the loading point diagonally. The parameters and properties are represented Table (6-4). Initial crack length a_0 10mm, θ is 30 degrees, and height h varies 100~500mm.

As a result, compressive stress decreases as the size of specimen increases. And additionally, As the θ increases the compressive stress also decreases as shown in Fig. (6.44-b). The angle of inclined crack is important parameter.

It should be noted that the size effect shows in pure compression.

Table 6-4 Examples for estimation of size effect

a_o [mm]	h [mm]	θ [degree]	a_{eff} [mm]	$k(\alpha_0)$	$\frac{P_u}{hf_c'}$
10	100	30	103.9	0.316	0.341
10	200	30	219.4	0.224	0.235
10	300	30	334.9	0.183	0.190
10	400	30	450.3	0.158	0.164
10	500	30	565.8	0.141	0.146

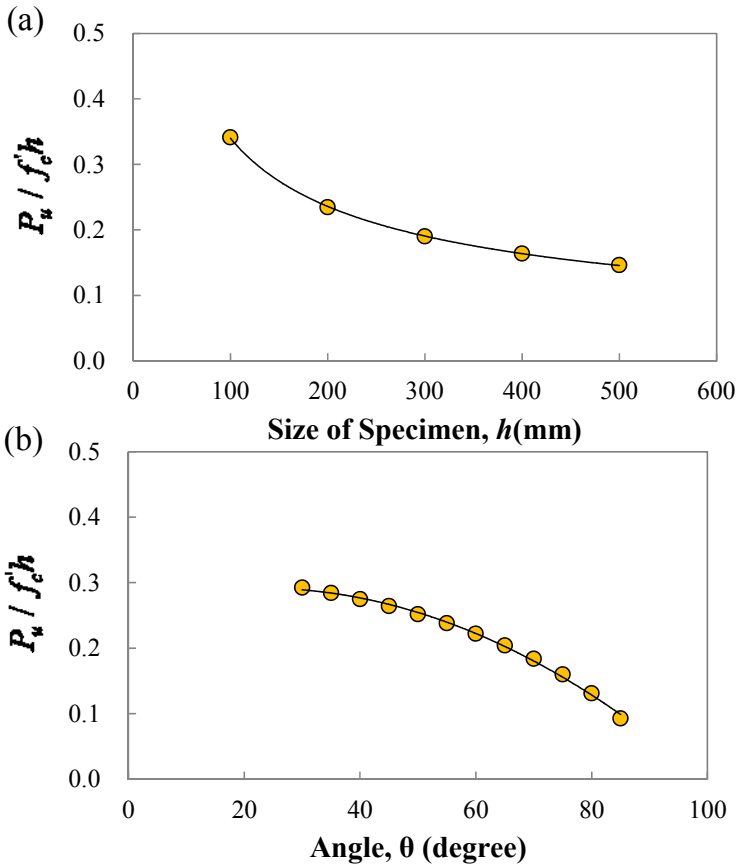

Figure 6.44 Normalized compressive force: (a) Size effect of compressive force; (b) Degradation of compressive force for angle

To predict the ultimate shear strength, a simple strut and tie model based on the theory of plasticity can be used. Let us consider the single strut and tie model as shown in Fig. (6.45). The strut carries the uniaxial compressive stress. And it is assumed that when this stress reaches the ultimate stress shear failure occurs.

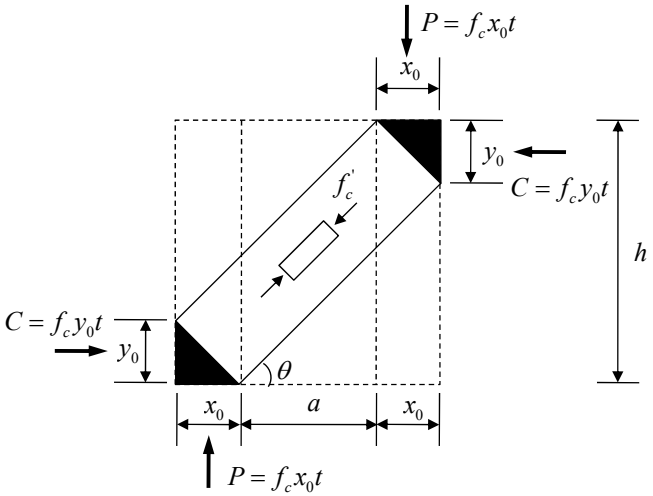

Figure 6.45 Single strut

If the strut inclination with a horizontal axis is θ

$$\tan\theta = \frac{x_0}{y_0} = \frac{h - y_0}{a + x_0} \tag{6.68}$$

If the strut has to carry the vertical load P,

$$P = x_0 t f_c' \tag{6.69}$$

where t means the thickness.

To maintain equilibrium the horizontal resultant of compressive forces C is

$$C = y_0 t f_c' \tag{6.70}$$

From Eq. (6.69) size of nodal zone can be obtained as follows

$$x_0 = \frac{P}{t f_c'} \tag{6.71}$$

If Eq. (6.71) is divided by height h we can obtain the ratio of shear stress to strength of concrete

$$\frac{x_0}{h} = \frac{P}{thf_c'} = \frac{\tau}{f_c'} \tag{6.72}$$

τ represents the average shear stress along the overall depth h.

Then, the size of y_0 is determined as

$$\frac{y_0}{h} = \frac{1}{2} - \sqrt{\frac{1}{4} - \frac{x_0}{h}\left(\frac{a}{h} + \frac{x_0}{h}\right)} \tag{6.73}$$

Since this equation must have positive value, that is, when square root reaches zero the requirement of y_0 / h reaches the maximum. Therefore, the maximum values of y_0 / h is 1/2.

Substituting this results into Eq. (6.73) and organizing yields

$$\frac{x_0}{h} = \frac{1}{2}\left[\sqrt{1 + \left(\frac{a}{h}\right)^2} - \frac{a}{h}\right] \tag{6.74}$$

This means that the maximum value of the average stress is

$$\frac{\tau}{f_c'} = \frac{1}{2}\left[\sqrt{1 + \left(\frac{a}{h}\right)^2} - \frac{a}{h}\right] \tag{6.75}$$

The formula determines the highest load which can be carried by a strut of depth h and shear span a.

In compressive sliding failure mechanism, it is assumed that vertical normal stress and shear stress are existed in the concrete.

Stress intensity factors for mode-I and mode-II fracture expressed by principal tensile stress and shear stress acting on cracked plane are represented as follows

$$K_I = \tau_{xy}\sqrt{\pi a_c}\cos\varphi\left(2\sin\varphi - n\cos\varphi\right) \tag{6.76}$$

$$K_{II} = \tau_{xy}\sqrt{\pi a_c}\left[\left(2\cos^2\varphi - 1\right) + n\sin\varphi\cos\varphi\right] \tag{6.77}$$

where a_c is length of crack and φ means the angle of inclined crack respect to vertical axis and n represents the ratio of normal stress to shear stress.

By using these stress intensity factors, effective stress intensity factor for inclined crack can be obtained as follows.

$$K_{eff} = \sqrt{K_I^2 + K_{II}^2} = \tau_{xy}\sqrt{\pi a_{eff}}\sqrt{n^2\cos^2\varphi - 2n\sin\varphi\cos\varphi + 1} \tag{6.78}$$

Angle of inclined crack is calculated from Mohr's circle as follows

$$\tan\left(2\varphi\right) = \frac{2\tau_{xy}}{\sigma_x} \tag{6.79}$$

where σ_x represents the compressive stress of concrete.

When sliding failure occurs in diagonal strut the ratio of shear stress to normal stress is $\tau_{xy} / \sigma_x = -5.22$

Thus, the angle of inclined crack with respect to vertical axis as shown in Fig.(6.42) is

$$\varphi = -42.26^{\circ} \tag{6.80}$$

This means that the angle of inclined crack is constant when sliding failure occurs at diagonal strut.

In sliding failure, effective stress intensity factor is equal to critical stress intensity factor for mode-II fracture.

$$K_{eff} = K_{IIc} = \tau_u \sqrt{\pi a_0} \tag{6.81}$$

where a_0 represents length of initial crack.

Shear stress for sliding failure is

$$\tau_u = 0.2 f_c^{'} \tag{6.82}$$

Thus, shear stress is given by

$$\tau_{xy} = \frac{0.2 f_c^{'}}{\sqrt{n^2 \cos^2 \varphi - 2n \sin \varphi \cos \varphi + 1}} \sqrt{\frac{a_0}{a_{eff}}} \tag{6.83}$$

Inserting Eq. (6.80) into Eq. (6.83), ultimate shear stress is obtained as follows.

$$\tau_{xy} = 0.24 f_c^{'} \sqrt{\frac{a_0}{a_{eff}}} \tag{6.84}$$

Finally, ultimate shear stress is expressed as function of compressive strength of concrete and length of initial crack and effective crack.

6.6.7 Shear Strength of Short Beams

To calculate the shear strength of deep beams, a simple strut-and-tie model for reinforced concrete deep beams without web reinforcement is presented as shown in Fig. (6.46). The shear failure of the beam is assumed the crushing of the concrete strut after flexural crack shown in concrete cover zone has fully developed. And it is assumed that longitudinal reinforcement is yielded in advance before the crushing

of the concrete. Therefore, the depth of neutral axis can be considered as size of nodal zone.

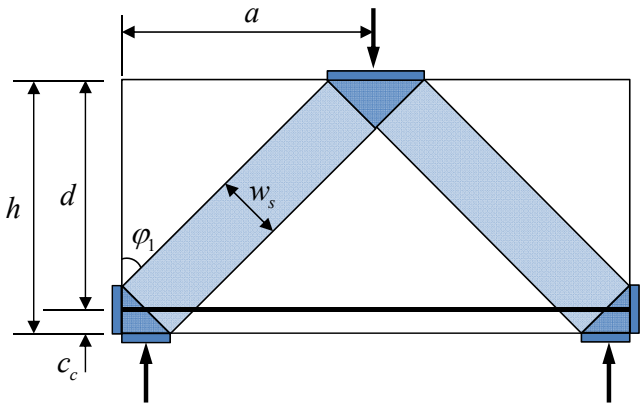

Figure 6.46 Strut-and-tie model for deep beam

Shear stress can be derived from Eq. (6.85) expressed in terms of compressive strength of concrete and initial crack length and effective crack length as follows.

$$\tau_{xy} = 0.24 f_c^{'} \sqrt{\frac{a_0}{a_{eff}}} \tag{6.85}$$

where a_0 represents the initial crack length and a_{eff} means the effective crack length.

Thus, the shear strength of deep beams is given by

$$V_u = 0.24 f_c^{'} \sqrt{\frac{a_0}{a_{eff}}} BD \tag{6.86}$$

where B is thickness of diagonal strut and D means depth of diagonal strut as shown in Fig. (6.42-a).

In this study, initial crack length assumes the same as concrete cover length c_c, therefore, effective crack length can be written as follows

$$a_{eff} = \frac{d}{\cos\varphi} \tag{6.90}$$

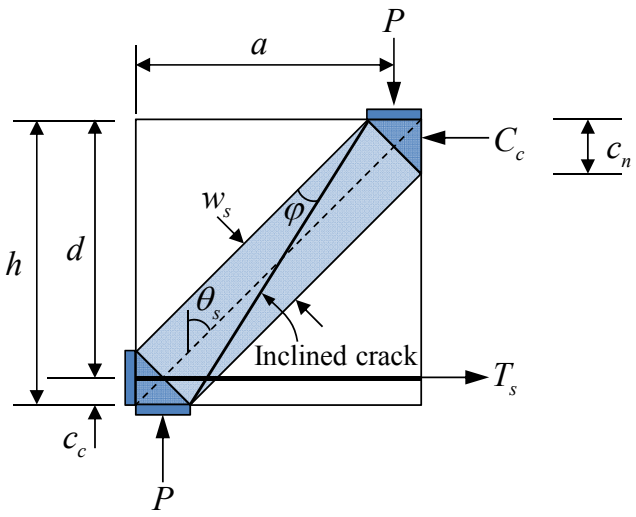

Figure 6.47 Diagonal single strut of deep beams

Substituting Eq.(6.90) into Eq.(6.86) yields

$$V_u = 0.24 f_c^{'} \sqrt{\frac{c_c \cos\varphi}{d}} \frac{c_n}{\sin\theta_s} \frac{h}{\cos\theta_s} \tag{6.91}$$

where c_n is depth of neutral axis expressed by $c_n = d\left[\sqrt{[n\rho]^2 + 2n\rho} - n\rho\right]$, and θ_s means angle of diagonal strut and assumed to be $\tan\theta_s = a/d$.

6.6.8 Verification

The proposed model is applied as follows for the prediction of the ultimate shear strength of reinforced concrete deep beams without web reinforcement tested by Walraven et al. (1994). They investigated the size effect of short beams in shear-

loaded. Table (6-5) shows the information of test data. The material properties were kept constant and the specimen size was varied. The depth of the member was varied between 200 and 1000mm, whereas all other variables remained constant. In all the tests, the slenderness ratio was *a/d*=1. The reinforcement ratio of the specimens was generally 1.1 percent, so that failure by yielding of the longitudinal steel was excluded in advance.

In Fig. (6.48), normalized shear stress $v_u = V_u / \left(b_w d \sqrt{f_c^{'}} \right)$ at inclined shear cracking are represented as a function of the effective depth d . It is shown that shear stress at shear failure decreases as increases the effective depth. This means shear stress of deep beams is size dependent.

Table 6-5 Information of test data obtained by Walraven et al.(1994)

Authors	Speci-men	$f_c^{'}$ [MPa]	b_w [mm]	d [mm]	a/d	h [mm]	c_c [mm]	ρ (%)	V_u [kN]	v_u [MPa]
Walraven (1994)	V711	18.1	250	160	1.0	200	40	1.1	165	0.97
	V022	19.9	250	360	1.0	400	40	1.1	270	0.67
	V511	19.8	250	560	1.0	600	40	1.1	350	0.56
	V411	19.4	250	740	1.0	800	60	1.1	365	0.45
	V211	20.4	250	930	1.0	1000	70	1.1	505	0.48

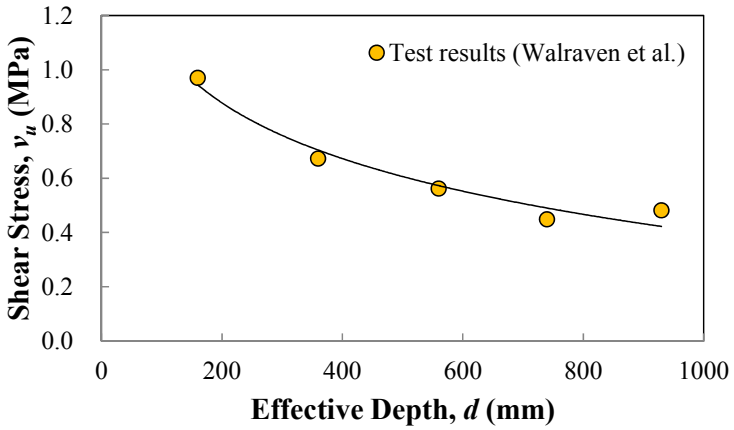

Figure 6.48 Test results and size effect obtained by Walraven et al.(1994)

For comparison of experimental results and predictions, five specimens tested by Walraven et al. (1994) compared with the theoretical predictions from Eq. (7.70) with a varying effective depth. Table (6-6) and Fig. (6.49) show the comparison of ultimate shear strength or stress between test results and predictions. It is assumed that the angle of diagonal strut is constant and longitudinal reinforcement is yielded in advance as mentioned in Section. Both the test results and predictions show a tendency in which ultimate shear strength decreases as the effective depth increases. The ratio of experimental results to prediction was 1.02 in mean value and 0.12 in standard deviation, respectively.

Table 6-6 Comparison of ultimate shear strength between test results and predictions

Authors	Speci-men	c_n [mm]	φ_1 (degree)	$V_{u,test}$ [kN]	$v_{u,test}$ [MPa]	$V_{u,pred.}$ [kN]	$v_{u,pred.}$ [MPa]	$\frac{V_{u,test}}{V_{u,pred.}}$
Walraven et al. (1994)	V711	59.5	42.26	165	0.97	149.5	0.88	1.10
	V022	131.4	42.26	270	0.67	246.5	0.62	1.10
	V511	204.6	42.26	350	0.56	305.9	0.49	1.14
	V411	271.5	42.26	365	0.45	422.0	0.52	0.86
	V211	337.9	42.26	505	0.48	537.3	0.51	0.94
Mean								1.03
Standard Deviation								0.12

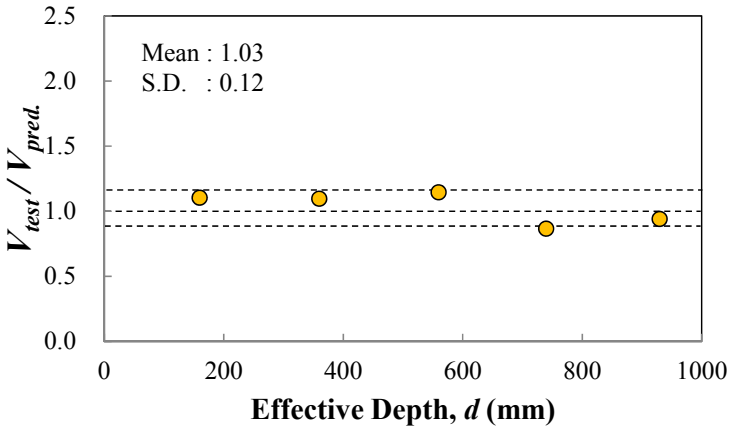

Figure 6.49 Comparison of shear stress between test data and predictions

Fig. (6.50) shows the comparisons of size effect between the proposed model based on concrete softening and theory of plasticity proposed by using the strut-and-tie model as illustrated in Fig. (6.42). To compare the predictions with experimental results, 5 test specimens by Walraven et al. (1994) were selected. As a result, shear strength decreases as the effective depth increases mostly. However, the proposed

model based on diagonal crack growth and concrete softening appears the size effect better than the theory of plasticity. On the other hand, shear strength base on strut-and-tie model does not indicate the size effect precisely.

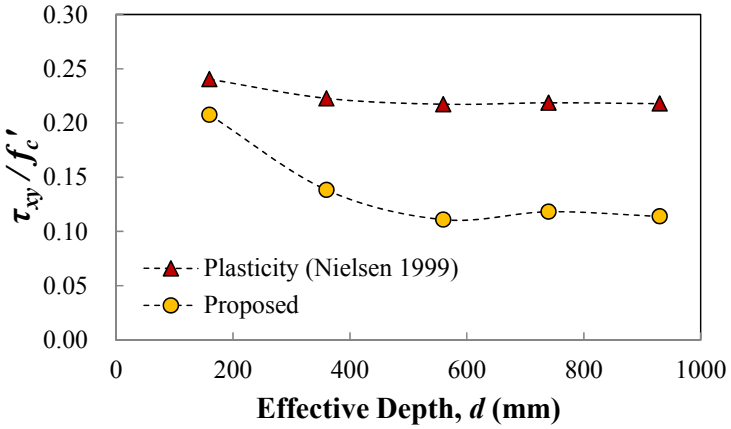

Figure 6.50 Comparisons of size effect between proposed model based on concrete softening and theory of plasticity

6.6.9 Summary

In this section, based on failure mode of diagonal single strut and crack propagation, shear strength of reinforced concrete deep beams without web reinforcement was investigated. It is assumed that there are two stress components, that is, normal and shear stress, in diagonal single strut based on theory of elasticity. The main points can be summarized in following.

(1) Based on theory of elasticity, normal and shear stress distributions were investigated. Unlike general solutions by the strut-and-tie model, in this

study, it is assumed that both normal and shear stresses exist in the diagonal single strut.

(2) To obtain the shear strength of deep beams, it is assumed that diagonal single strut fails when the combined stress reaches the ultimate shear stress.

(3) Diagonal strut fails when effective stress intensity factor K_{eff} is equal to critical stress intensity factor mode-II fracture K_{IIc}.

(4) Shear strength decreases as the length of effective crack increases. Because how long the length of crack eventually means that the large the size of specimen, size effect also shows in deep beams without web reinforcement.

(5) The proposed shear strength based on the softening of concrete and crack propagation appear the size effect clearly than theory of plasticity by using the strut-and-tie model.

(6) As a result of comparisons of predictions with experimental results, it can be shown that predicted strength by the proposed equation agree well with the experimental results.

7. Summary and Conclusions

7.1 Summary

This dissertation aims at contributing a better understanding the size effect and focus on theoretical prediction of the shear strength of reinforced concrete beams without web reinforcement based on critical crack path and crack length.

Numerous experiments and analysis for shear strength of reinforced concrete slender beams and deep beams have been studied for many years. Currently design code provisions present the empirical design equations based on the tremendous experimental results. Even though they consider the primary parameters, especially size effect, which are affected the shear strength, current design codes and the equations proposed by many researchers are based on the empirical and statistical consideration.

To determine the shear strength and investigate the size effect of reinforced concrete beams, critical crack path dependent failure mechanism was proposed. This study assumes biaxial stress fields at the diagonal critical crack tip in both diagonal tension failure and sliding failure modes. The transition area which is located from uniaxial stress states below the neutral axis of beams to biaxial stress states above the neutral axis requires the change of primary fracture mode. This failure is defined as material failure such as separation and sliding. To provide the deformation dependent strength model, failure mechanism was investigated by using the modified Mohr-Coulomb criteria. For investigating the stress states at critical diagonal crack tip, size dependent critical stress intensity factors for mode-I and mode-II fracture were proposed. From the relationship between the stress

intensity factor and critical stress intensity factor, it is known that size effect is related to the crack length for both mode-I and mode-II fracture.

Since the proposed model based on the crack propagation is function of initial crack length and effective crack length, it can properly explain the degradation of shear strength as the crack length increases precisely and can estimate shear strength of reinforced concrete slender and deep beams considering the size effect. Due to these advantages, the proposed strength model can more accurately estimate the strength of existing experimental results compared to other theoretical strength model.

7.2 Conclusions

For estimating shear strength of RC slender and deep beams without web reinforcement and explaining size effect, theoretical studies had been performed in linear elastic fracture mechanics approach. The conclusions of this dissertation can be summarized as follows:

(1) Critical stress intensity factors for mode-I and mode-II fracture can be defined as function of ultimate stress at a crack tip and crack length and they are dependent on the size.

(2) The Ultimate stress is determined by the material failure criteria. From modified Mohr-Coulomb criteria ultimate shear stress is obtained as $\tau_u = 0.2 f_c^{'}$ (MPa) slender beams and as $\tau_u = 0.24 f_c^{'}$ (MPa) for deep beams.

(3) The proposed strength model based on crack propagation is more reasonable to explain the sliding failure mode of prismatic body of concrete than theory of plasticity since both normal stress and shear stress exist in the concrete diagonal strut under uniaxial compression.

(4) The relationship between initial and effective crack length affects the size effect of reinforced concrete beams.

(5) As a result of comparison of shear strength due to the diagonal tension failure with the strength due to the sliding failure, it is recognized that shear strength depends on the critical crack path.

(6) The proposed theory accurately predicts the experimental results for the ultimate shear stress of slender and deep beams with various strengths of concrete, steel ratio, shear span-to-depth ratio and effective depth.

References

1. ACI Committee 318, "Building Code Requirements for structural Concrete (ACI 318-08) and Commentary (318R-08),"American Concrete Institute, Farmington Hilles, Michigan, 2008, 473 pp.

2. ACI Committee 446, "Fracture Mechanics of Concrete: Concept, Models and Determination of Material Properties," In Fracture Mechanics of Concrete Structures, edited by Bazant, Z. P., Elservier Applied Science, Londeon, pp. 1~140.

3. BS 8110, "Structural Use of Concrete, Part 1, Code of Practice for design and Construction," British Strandards Institution, London, 1997, 172pp.

4. Bazant, Z. P., and Sun, H.-H., "Size Effect in Diagonal Shear Failure: Influence of Aggregate Size and Stirrups." ACI Material Journal, V. 84, No. 4, July-Aug. 1987, pp. 259~272.

5. Bresler, B., and Scordelis, A. C., "Shear Strength of Reinforced Concrete Beams," ACI Journal, Proceedings Vol. 60, No. 1, Jan. 1963, pp. 51~74.

6. Bresler, B., and Pister, K. S., "Strength of Concrete Under Combined Stresses," ACI Journal, Vol. 55, No. 3, September. 1958, pp. 321~345.

7. Bazant, Z. P., and Kim, J.-K, "Size Effect in Shear Failure of Longitudinally Reinforced Beams," ACI Journal, vo. 81, 1984, pp. 456~468.

8. Bazant, Z. P., and Plans, J., "Fracture and Size Effect in Concrete and Other Quasibrittle Materials," CRC Press, Boca Raton, Florida, 1998, 616 pp.

9. Bazant, Z. P., and Oh, B.-H., "Crack Band Theory for Fracture of Concrete," Materials and Structures, 16, 1983, pp. 155~177.

10. Bentz, E. C., Vecchio, F. J., and Collins, M. P., "Simplified Modified Compression Field Theory for Calculating Shear Strength of Reinforced Concrete Elements," ACI Structural Journal, V. 103, No. 4, July-August, 2006, pp. 614~624.

11. Chana, P. S., "Some Aspects of Modelling the Behaviour of Reinforced Concrete under Shear Loading," Technical Report No. 543, Cement and Concrete Association, Wexham Springs, 1981. 22 pp.

12. Collins, M. P., and Kuchma, D., "How Safe are our Large, Slightly Reinforced Concrete Beams, Slabs, and Footings?" ACI Structural Journal, V. 96, No. 4, July-Aug. 1999, pp. 482~490.

13. Comite Euro-International du Beton, "CEB-FIP Model Code 1990 : Design Code," Thomas Telford, London, 437 pp.

14. Collins, M. P., and Mitchell, D., Adebar, P. and Vecchio, F. J., "General Shear Design Method," ACI Structural Journal, Vol. 93, No. 1, January-Febrary 1996, pp. 36~45.

15. Collins, M. P., and Mitchell, D., "Prestressed Concrete Structures", Prentice-Hall Inc, Englewood Cliffs, N.J., 1991. 766 pp.

16. Collins, M. P., and Mitchell, D., "A Rational Approach to Shear Design : The 1984 Canadian Code Provisions," ACI Structural Journal, November-December 1986, pp. 925~933.

17. CSA (Canadian Strandards Assocition), "Design of Concrete Structures," CSA A23.3-94, December 1994, 200 pp.

18. Elfgren. L., "Fracture Mechanics of Concrete Structures From Theory to Applications," Report of the Technical Committee 90-FMA Fracture Mechanics to Concrete - Applications RILEM, Chapman and Hall, NY. USA, 407 pp.

19. Elzanaty, A. H.., Nilson, A. H., and Slate, F. O., "Shear Capacity of Reinforced Concrete Beams using High-Strength Concrete," ACI Journal Proceedings, V. 83, No. 2, 1986, pp. 290~296.

20. Erdogan, F., and Sih, G. C., "On the Crack Extension in Plates under Plane Loading and Transverse Shear," Journal of Basic Engineering, Vol. 85, 1963, pp. 519~527.

21. Gustafsson, P. J., and Hillerborg, A., "Sensitivity in the Shear Strength of Longitudinally Reinforced Beams to Fracture Energy of Concrete," ACI Structural Journal, Vol. 85, No. 3, May-June 1988, pp. 286~294.

22. Griffith, A. A., "The Phenomena of Rupture and Flow in Solids," Philosophical Transactions of the Royal Society of London A221, pp. 163~198.

23. Griffith, A. A., "The Theory of Rupture," Proceedings of First International Congress of Applied Mechanics, Delft, 1921, pp. 55~63.

24. Gere, J. M, "Mechanics of Materials," 5th Edition, Brooks/Cole Thomson Learning, CA., USA, 2001, 926 pp.

25. Hasegawa, T., Shioya, T., and Okada, T., "Size Effect on Splitting Tensile Strength of Concrete," Proceedings, Japan Concrete Institute 7th Conference, June 1985, pp. 309~312.

26. Ha, T. H., "Effective Strength of Compressive Strut in Reinforced Concrete Members," Ph.D Dissertation, Department of Architecture and Architecture Engineering, Seoul Natonal University, Seoul, Korea, 2004.

27. Higgins, D. D., and Bailey, J. E., "Fracture Measurements on Cement Paste," Journal of Material Science, Vol. 11, No. 11, 1976, pp. 1995~2003.

28. Hillerborg. A., Modeer, M., and Petersson, P. -E., "Analysis of Crack Formation and Crack Growth in Concrete by Means of Fracture Mechanics and Finite Elements," Cement and Concrete Research, Vol. 6, No. 6, 1976, pp. 773~782.

29. Hillerborg, A., "Additional Concrete Fracture Energy Tests Performed by 6 Laboratories According to a Draft RILEM Recommendation. Report No. TVBM-3017, Division of Building Materials, Lund Institute of Technology, Lund, Sweden, 1984.

30. Hong, S. G., and Ha, T. H, "Effective Capacity of Diagonal Strut for Shear Strength of Reinforced Concrete Beams without Shear Reinforcement," ACI Structural Journal, Vol. 109, No. 2, March-April 2012, pp. 139~148.

31. Hsu, T. T. C., and Slate, F. O., "Tensile Bond Strength Between Aggregate and Cement Paste or Mortar," ACI Journal, V. 60, No. 4, March 1 1963, pp. 465~486.

32. Irwin, G. R., "Plastic Zone Near a Crack and Fracture Toughness, " in Proceedings of the Seventh Sagamore Ordnance Materials Conference, Syracuse University, 1960, pp.IV-63.

33. Irwin, G. R., "Linear Fracture Mechanics, Fracture Transition, and Fracture Control," Engineering Fracture Mechanics, Vol. 1, No. 2, 1968, pp. 241~257.

34. Irwin, G. R., "Analysis of Stresses and Strains Near the End of a Crack Traversing a Plate," J. Appl. Mech, -T. ASME, 24, 1957, pp. 361~364.

35. Irwin, G. R., "Fracture," In Handbuch der Physik, Vol. 6, Flugge, ed., Springer-Verlag, Berlin, pp. 551~590.

36. Inglis, C. E., "Stresses in a Plate due to the Presence of Cracks and Sharp Corners," T. Inst. Naval Archtects, 44, 1913, pp. 219~241.

37. Ingraffea, A. R., and Gerstle, W. H., "Applications of Fracture Mechanics to Cementitious Composites," Edited by Shah, S. P., Martinus Nijhoff, Dordrecht/Boston/Lancaster, 1985, pp. 247.

38. Jin-Ping Zhang, "Strength of Cracked Concrete: Part-1," Danmarks Tekniske Universitet, 1994, pp. 106.

39. JSCE Guidelines for Concrete, "Stadard Specifications for Concrete Structures - 2002 Structural Performance Verification," Japan Society of Civil Engineers, JSCE, Tokyo, Japan, January 2005, pp.76~82.

40. Jenq, Y.-S., and Shah, S. P., "Shear Resistance of Reinforced Concrete Beams-A Fracture Mechanics Apporach," in Fracture Mechanics: Application to Concrete, edited by Li, V. C., and Bazant, Z. P., SP118, American Concrete Institute, Detroit, MI, 1989, pp. 237~258.

41. Jensen, J. F., "Plastic Solutions for Reinforced Concrete Beams in Shear," IABSE Colloquium, Plasticity in Reinforced Concrete, Copenhagen, 1979.

42. Kani, G. N. J., "How Safe are Our Large Reinforced Concrete Beams," ACI Journal, Proceedeings V. 61, No. 2, Feb. 1964, pp. 441~467.

43. Reineck, K. H., Kuchma, D. A., Kim, K. S. and Marx, S., “Shear Database for Reinforced Concrete Members without Shear Reinforcement,” ACI Structural Journal, V. 100, No. 2, March-April, 2003, pp. 240~249.

44. Karayiannis, C. G., and Chalioris, C. E., "Experimental Investigation of the Influence of Stirrups on the Shear Failure Mechanism of Reinforced Concrete Beams," Proceedings of the 13th Hellenic Conference on Concrete, Rethymnon, Greece, V. 1, 1999, pp. 133~141. (in Greek)

45. Kotsovos, M. D., "Effect of Testing Techniques on the Post-Ultimate Behavior of Concrete in Compression," Materiaux et Constructions, Vol. 16, No. 1, 1983, pp. 3~12.

46. Leonhardt, F., and Walther, R., "Schubversuche an Einfeldrigen Stahlbetonbalken mit und ohne SchubbeWehrung zur Ermittlung der Schubtragfahigkeit und der Obersen Schubspannungsgrenze," DAfStb, Heft 151, W. Ernst u. Sohn, Berlin, 1962, 84 pp. (in German)

47. McGregor, J. G., Sozen, M. A., and Siess, C. P., "Strength and Behavior of Prestressed Concrete Beams with Web Reinforcement," University of Illinois Civil Engineering Studies, Structural Research Series 210, Urbana, I11., Aug. 1960.

48. Mattock, A. H., "Diagonal Tension Cracking in Concrete Beams with Axial Forces," Journal of the Structural Division, ASCE, V. 95, No. 9, 1969, pp. 1887~1900.

49. Markeset. G., and Hillerborg. A., "Softening of Concrete in Compression - Localization and Size Effects," Cement and Concrete Research, Vol. 25, No. 4, 1995, pp. 702~708.

50. Moody, J. G.; Viest, I. M,; Elstner, R. C.; and Hognestad, E., "Shear Strength of Reinforced Concrete Beams, Part 1-Tests of Simple Beams," ACI Journal, Proceedings V. 51, No. 12, Dec. 1954, pp. 317-332.

51. Mphonde, A. G., and Fracntz, G. C, "Shear Tests of High- and low-Strength Concrete Beams without Stirrups," ACI Journal, V. 81, No. 4, 1984, pp. 350~357.

52. Muttoni, A., and Ruiz, M. F., "Shear Strength of Members without Transverse Reinforcement as Function of Critical Shear Crack Width," ACI Structural Journal, Vol. 105, No. 2, March-April 2008, pp. 163~172.

53. Muttoni, A., and Ruiz, M. F., "Shear and Punching Strength of Slabs without Shear Reinforcement," Beton-und Stahlbetonbau, V. 98, 2003, pp. 74~84.

54. Nielsen, M. P., "Limit Analysis and Concrete Plasticity", 2th Edition, CRC press, Boca Raton, Fla., 1999, 908 pp.

55. Okamura, H., and Watanabe, J., and Takano, T., "Application of the Compliance Concept in Fracture Mechanics," ASTM STP 536, American Society for Testing and Materials, Philadelphia, PA, 1073, pp. 423~438.

56. Okamura, H., and Watanabe, J., and Takano, T., "Deformation and Strength of Cracked Members under Bending Moment and Axial Force," Engineering Fracture Mechanics, Vol. 7, 1975, pp. 531~539.

57. Ohgishi, S., Ono, H., Takatsu, M. and Tanahashi, I., "Influence of Test Conditions of Fracture Toughness of Cement Paste and Mortar," In Fracture Toughness and Fracture Energy of Concrete, F. H. Wittmann, ed., Elsevier Science, Amsterdam, the Netherlands, pp. 281~290.

58. Park, H. G., Choi, K. K, and Wight, J. K., "Strain-Based Shear Strength Model for Slender Beams without Web Reinforcement," ACI Structural Journal, V. 103, No. 6, November-December 2006, pp. 783~793.

59. Reineck, K. H., "Ultimate Shear Force of Structural Concrete Members without Transverse Reinforcement Derived from a Mechanical Model," ACI Structural Journal, V. 88, No, 5, September-Octorber, 1991, pp. 592~602.

60. Rice, J. R., "A Path Independent Integral and the Approximate Analysis of Strain Concentrations by Notches and Cracks," Journal of Applied Mechanics, Vol. 35, 1968, pp. 379~386.

61. Shah et al., "Fracture Mechanics of Concrete: Applications of Fracture Mechanics to Concrete, Rock, And Other Quasi-Brittle Materials," John Wiley & Sons, NY, USA, pp. 552.

62. Taylor, H. P. J., "Investigation of the forces carried across cracks in reinforced concrete beams in shear by interlock of aggregate," Technical report 42.447, CCA, 1970, London.

63. Taylor, H. P. J., "Shear Strength of Large Beams, "Journal of the Structural Deivision, ASCE, Vol. 98, No. 11, Nov. 1972, pp. 2473~2490.

64. Timoshenko, S. P., and Goodier, J. N., "Theory of Elasticity," 3rd Edition, MacGraw-Hill International Editions, Singarpore, 1970, 551 pp.

65. Taylor, H. P. J., "The Fundamental Behavior of Reinforced Concrete Beams with Bending and Shear," ACI-ASCE Publication, SP42, 1974, pp. 43~77.

66. Vecchio, F. J., and Collins, M. P., "The Modified Compression Field Theory for Reinforced Concrete Elements Subjected to Shear," ACI Journal, Vol. 83, No. 2, March-April 1986, pp. 219~231

67. Van Mier, J. G. M., "Strain Stofteing of Concrete under Multiaxial Loading Condtitions," Ph.D Thesis, Eindhoven University of Technology, Eindhoven, The Netherlands, 1984.

68. Van Mier, J. G. M., "Mode II Fracture Localization in Concrete Loaded in Compression," Journal of Structural Engineering, ASCE, Vol. 135, No. 1, January 2009, pp. 1~8.

69. Van Geel, E., "Behavior of Concrete in Multiaxial Compression," Ph.D. Thesis, Eindhoven University of Technology, Eindhoven, The Netherlands.

70. Vonk, R. A., "Softening of Concrete Loaded in Compression," Ph.D. thesis, Eindhoven University of Technology, Eindhoven, The Netherlands, 1992.

71. Walraven, J. C., "The Influence of Depth on the Shear Strength of Lightweight Concrete Beams without Shear Reinforcement," Stevin Laboratory Report No. 5-78-4, Delft University of Technology, Delft, The Netherlands, 1978.

72. Walraven, J., and Lehwalter, N., "Size Effect in Short Beams Loaded in Shear," ACI Structural Journal, V. 91, No. 5, September-October, 1994, pp. 585~593.

73. Y.S. Jenq and S.P. Shah, "Mixed-mode fracture of concrete", International Journal of Fracture, 38, 1998, pp. 123~142.

74. Zsutty, T. C., "Shear Strength Prediction for Separate Categories of Simple Beam Tests," ACI Journal, Proceedings V. 68, No. 2, Feb. 1971, pp. 138~143.

75. Zararis, P. D,, and Papadakis, G. C., "Diagonal Shear Failure and Size Effect in RC Beams without Web Reinforcement," Journal of Structural Engineering, ASCE, V. 127, No. 7, 2001, pp. 733~742.

76. Zararis, P. D., "Shear Strength and Minimum Shear Reinforcement of Reinforced Concrete Slender Beams," ACI Structural Journal, V. 100, No. 2, March-April 2003, pp. 203~214.

Appendix : Details of Beams without Web Reinforcement

Authors	Specimen name	$f_c^{'}$ [MPa]	b [mm]	d [mm]	a/d	h [mm]	ρ [%]	f_y [MPa]	V_{test} [kN]
Ahmad et al. (1986)	A1	59.3	127	203	4.00	254	3.93	414	57.8
	A2	59.3	127	203	3.00	254	3.93	414	68.9
	A8	59.3	127	208	3.00	254	1.77	414	48.9
Bresler (1963)	0A-1	21.4	310	461	3.97	556	1.81	555	166.9
	0A-2	23.3	305	466	4.91	561	2.27	555	178.0
	0A-3	35.9	307	462	6.93	556	2.73	552	189.0
Chana (1981)	2.1	37	203	356	3.00	406	1.74	478	96.0
	2.2	31.2	203	356	3.00	406	1.74	478	87.4
	2.3	33.9	203	356	3.00	406	1.74	478	99.4
Cossio et al. (1960)	L-2a	34.9	152	252	3.02	305	3.35	282	80.1
	L-3	26.6	152	252	4.02	305	3.35	310	53.4
	L-4	24.5	152	252	5.02	305	3.35	303	51.2
	L-5	26.5	152	252	6.03	305	3.35	330	51.0
	A2	29.9	152	254	3.00	305	0.98	469	41.8
	A3	18.5	152	254	4.00	305	0.98	452	34.3
	A-12	25.4	152	254	3.00	305	3.33	314	59.0
	A-13	21	152	254	4.00	305	3.33	393	46.9
	A-14	26.1	152	254	5.00	305	3.33	364	54.7
Elzanaty et al. (1986)	F11	19.7	178	272	4.00	305	1.20	434	45.5
	F12	19.7	178	269	4.00	305	2.50	434	54.6
	F8	38	178	273	4.00	305	1.00	434	46.7
	F13	38	178	272	4.00	305	1.20	434	47.0
	F14	38	178	269	4.00	305	2.50	434	64.6
Feldman et al. (1955)	L-2A	24.9	152	252	3.02	305	3.35	283	80.1
	L-3	26.6	152	252	4.02	305	3.35	310	53.4
	L-4	24.5	152	252	5.03	305	3.35	303	51.2

Authors	Specimen name	$f_c^{'}$ [MPa]	b [mm]	d [mm]	a/d	h [mm]	ρ [%]	f_y [MPa]	V_{test} [kN]
	L-5	26.5	152	252	6.04	305	3.35	331	51.2
Hallgren (1994)	B90SB 17-2-45	24.7	157	191	3.66	232	2.26	630	59.0
	B90SB 18-2-45	24.7	155	194	3.60	235	2.25	630	63.0
	B91SD 1-4-61	57.8	156	194	3.61	247	3.98	494	88.5
	B91SD 2-4-61	57.8	156	195	3.59	248	3.96	494	90.0
	B91SD 5-4-58	55.4	156	196	3.57	249	3.94	494	78.0
	B91SD 6-4-58	55.4	150	196	3.57	249	4.10	494	82.5
	B90SB 5-2-33	31.2	156	191	3.66	232	2.28	651	56.0
	B90SB 6-2-33	31.2	156	194	3.61	235	2.24	651	53.5
	B90SB 9-2-31	29.5	156	192	3.65	233	2.26	651	49.0
	B90SB 10-2-31	29.5	157	193	3.63	234	2.20	651	53.5
Harnadi et al. (1980)	G1	28.8	100	370	3.46	400	1.70	400	44.5
	G2	22.3	100	372	3.44	400	1.08	460	41.0
	G3	20.9	100	372	5.97	400	1.08	800	30.3
Hanson (1961)	A4	19.9	152	267	4.95	305	1.25	611	33.8
	B4	29.4	152	267	4.95	305	1.25	611	42.8
	BW4	28.2	152	267	4.95	305	1.25	611	40.0
	8B2	29.3	152	267	4.95	305	2.53	637	52.4
	B2	29.3	152	267	4.95	305	2.22	637	52.4
Kani (1967)	63	24.9	154	546	4.00	610	2.78	352	93.2
	64	24.4	156	540	8.04	610	2.76	352	79.0
	66	25.1	156	541	6.02	610	2.75	352	90.8
	79	24.8	153	559	6.84	610	2.72	381	83.7

Authors	Specimen name	$f_c^{'}$ [MPa]	b [mm]	d [mm]	a/d	h [mm]	ρ [%]	f_y [MPa]	V_{test} [kN]
Kani (1967)	74/75	25.9	152	524	3.11	610	2.84	365	107.9
	71	26	155	544	2.99	610	2.66	374	102.1
Kani (1967)	81	26.1	153	272	5.98	305	2.79	343	51.2
	84	26.1	151	271	4.00	305	2.84	342	55.4
	96	24	156	275	3.95	305	2.71	335	56.3
	83	26.1	156	271	3.00	305	2.75	343	65.0
	97	25.9	152	276	2.95	305	2.69	366	62.5
	91	26.1	154	269	6.06	305	2.70	364	51.0
	92	26.1	152	270	7.03	305	2.73	369	45.9
Krefeld et al. (1966)	11A2	28.7	152	314	2.91	381	3.42	401	73.4
	12A2	28.6	152	238	3.85	305	4.51	401	64.1
	18A2	18.3	152	316	2.89	381	2.64	478	63.2
	18B2	18.9	152	316	2.89	381	2.64	487	72.1
	18C2	21.5	152	316	2.89	381	2.64	487	73.4
	18D2	21	152	316	2.89	381	2.64	487	60.1
	16A2	21.1	152	240	3.81	305	1.74	487	41.8
	17A2	20.9	152	243	3.77	305	2.14	408	44.1
	3AC	19.8	152	256	4.77	305	2.03	386	44.1
	3CC	19.5	152	256	5.96	305	2.03	386	35.6
	3AAC	32.8	152	256	3.58	305	2.03	386	55.6
	4AAC	27.7	152	254	3.60	305	2.66	401	57.9
	5AAC	31.2	152	252	3.62	305	3.31	378	57.0
	6AAC	32.7	152	250	3.65	305	4.35	368	60.1
	3AC	30.3	152	256	4.77	305	2.03	386	53.4
	4AC	29	152	254	4.80	305	2.66	401	53.8
	5AC	31.2	152	252	4.83	305	3.31	378	54.3
	6AC	32.4	152	250	4.87	305	4.35	368	59.2
	4CC	36.5	152	254	6.00	305	2.66	401	52.5

Authors	Specimen name	$f_c^{'}$ [MPa]	b [mm]	d [mm]	a/d	h [mm]	ρ [%]	f_y [MPa]	V_{test} [kN]
Krefeld et al. (1966)	5CC	35.6	152	252	6.04	305	3.31	378	57.4
	6CC	36.5	152	250	6.09	305	4.35	368	63.2
	C	15.9	203	483	3.16	533	1.57	401	84.6
	OCA	33.9	152	254	6.00	305	2.66	369	48.5
	OCB	33.9	152	254	6.00	305	2.66	368	52.5
	OCA	36.4	254	456	4.01	508	2.20	367	146.9
	OCB	36.4	254	456	4.01	508	2.20	366	133.5
	15A2	19.1	152	316	2.89	381	1.34	386	45.8
	15B2	19.7	152	316	2.89	381	1.34	386	52.1
Podgorniak (1998)	BN50	35.2	300	450	3.00	500	0.81	486	131.9
	BN25	35.2	300	225	3.00	250	0.89	437	73.0
	BN12	35.2	300	110	3.07	125	0.91	458	40.1
Laupa et al. (1953)	S2	25.6	152	269	4.54	305	2.08	284	42.5
	S3	30.7	152	265	4.60	305	2.52	410	53.1
	S4	29.3	152	263	4.61	305	3.21	309	55.6
	S5	28.4	152	262	4.65	305	4.11	315	49.8
	S11	14	152	267	4.56	305	1.90	328	33.8
	S13	24.9	152	262	4.56	305	4.11	304	49.8
Leonhardt et al. (1962)	5l	28	190	270	3.00	320	2.07	465	60.3
	5r	28	190	270	3.00	320	2.07	465	76.5
	6l	28	190	270	4.07	320	2.07	465	60.8
	6r	28	190	270	4.07	320	2.07	465	68.2
	7-1	29.4	190	270	5.00	320	2.07	465	62.3
	7-2	29.4	190	270	5.00	320	2.07	465	68.2
	8-1	29.4	190	270	6.00	320	2.07	465	65.7
Leonhardt et al. (1962)	8-2	29.4	190	270	6.00	320	2.07	465	65.7
	D2/1	35.4	100	140	3.00	160	1.62	427	21.2
	D2/2	35.4	100	140	3.00	160	1.62	427	23.3

Authors	Specimen name	$f_c^{'}$ [MPa]	b [mm]	d [mm]	a/d	h [mm]	ρ [%]	f_y [MPa]	V_{test} [kN]
Leonhardt et al. (1962)	D3/1	36.6	150	210	3.00	240	1.62	413	46.4
	D3/2l	36.6	150	210	3.00	240	1.62	413	41.2
	D3/2r	36.6	150	210	3.00	240	1.62	413	44.5
	D4/1	33.6	200	280	3.00	320	1.62	439	74.1
	D4/2l	33.6	200	280	3.00	320	1.62	439	74.1
	D4/2r	33.6	200	280	3.00	320	1.62	439	68.7
	EA1	19.8	190	270	2.78	320	1.82	439	58.4
	EA2	19.8	190	270	2.78	320	1.78	490	74.6
	C1	37.2	100	150	3.00	180	1.14	425	21.6
	C2	37.2	150	300	3.00	330	1.14	425	64.8
	C3	37.2	200	450	3.00	500	1.14	425	99.1
	C4	37.2	225	600	3.00	670	1.14	425	147.2
Mathey et al. (1963)	I11a-17	27.8	203	403	3.78	457	2.55	505	90.0
	I11a-18	23.9	203	403	3.78	457	2.55	505	82.5
	Va-19	22.3	203	403	3.78	457	0.93	690	64.7
	Va-20	24.3	203	403	3.78	457	0.93	690	67.4
	V1a-24	25	203	403	3.78	457	0.47	696	55.7
	V1a-25	24.5	203	403	3.78	457	0.47	696	51.0
	Vib-21	24.8	203	403	2.84	457	0.84	707	73.0
	Vib-22	24.5	203	403	2.84	457	0.84	707	63.8
	Vib-23	29.0	203	403	2.84	457	0.84	707	76.7
Morrow et al. (1957)	B40 B4	33.0	305	368	2.76	406	1.89	378	159.1
	B56B8	14	305	368	3.86	406	1.89	471	102.2
	B56A4	23.7	305	375	3.80	406	2.45	330	141.1
	B56B4	25.9	305	368	3.86	406	1.89	441	124.8
Morrow et al. (1957)	B56E4	27	305	368	3.86	406	1.28	429	111.0
	B56A6	37.9	308	356	4.00	406	3.88	439	179.5
	B56B6	43.4	305	372	3.83	406	1.87	466	141.6

Authors	Specimen name	$f_c^{'}$ [MPa]	b [mm]	d [mm]	a/d	h [mm]	ρ [%]	f_y [MPa]	V_{test} [kN]
Morrow et al. (1957)	B70B2	15.5	305	365	4.87	406	1.91	462	90.6
	B70A4	25.9	305	368	4.83	406	2.50	436	134.5
	B70A6	42.7	305	356	5.00	406	3.92	435	182.5
	B84B4	25.9	305	363	5.87	406	1.91	465	112.7
Mphonde et al. (1984)	AO-3-3b	20.3	152	298	3.58	337	3.36	414	64.3
	AO-3-3c	36.6	152	298	3.58	337	2.34	414	66.6
	AO-7-3a	36.9	152	298	3.58	337	3.36	414	82.0
	AO-7-3b	40.7	152	298	3.58	337	3.36	414	82.4
Rajagopalan et al. (1968)	S-1	34.7	154	259	4.92	311	1.42	655	35.6
	S-2	31.4	154	265	3.83	311	0.98	655	37.4
	S-3	27.5	152	267	4.19	311	0.81	524	31.1
	S-4	31.4	152	268	4.17	311	0.63	524	28.0
	S-5	36.5	152	262	4.27	311	0.53	1779	33.6
	S-9	23.8	152	262	4.27	311	0.53	1779	24.5
	S-6	29.5	151	268	4.17	311	0.35	1779	27.4
	S-7	27.2	152	268	4.17	311	0.25	1779	30.0
	S-12	28.2	152	268	4.17	311	0.25	1779	24.6
	S-13	22.5	152	265	4.22	311	1.73	655	40.0
Ruesch (1962)	11 X	22.0	90	111	3.60	134	2.63	481	14.6
	11 Y	22.0	120	199	3.60	229	2.64	407	30.1
	11 Z	23.1	180	262	3.62	302	2.64	412	54.7
Taylor (1972)	1A	35.3	203	370	3.02	406	1.03	350	63.1
	2A	40.8	203	370	3.02	406	1.54	350	93.5
	1B	35.3	203	370	3.02	406	1.03	350	77.2
	2B	40.8	203	370	3.02	406	1.54	350	102.6
	3B	38.8	203	370	3.02	406	1.03	350	77.6
	B1	23.0	200	465	3.00	500	1.35	420	104.3

Authors	Specimen name	$f_c^{'}$ [MPa]	b [mm]	d [mm]	a/d	h [mm]	ρ [%]	f_y [MPa]	V_{test} [kN]
Taylor (1972)	B2	20.9	200	465	3.00	500	1.35	420	87.3
	B3	27.0	200	465	3.00	500	1.35	420	85.3
	A1	27.3	400	930	3.00	1000	1.35	420	358.4
	A2	23.9	400	930	3.00	1000	1.35	420	328.4
Thorenfeld et al. (1990)	B11	51.3	150	221	3.00	250	1.82	500	58.0
	B13	51.3	150	207	4.00	250	3.24	500	70.0
	B14	51.3	150	207	3.00	250	3.24	500	83.0
	B16	51.3	150	207	3.00	250	3.24	500	82.6
	B17	51.3	150	207	4.00	250	3.24	500	77.9
	B18	51.3	150	207	3.00	250	3.24	500	82.6
	B19	51.3	150	207	4.00	250	3.24	500	86.0
	B20	51.3	150	207	3.00	250	3.24	500	107.1
Walraven (1978)	A2	22.9	200	420	3.00	450	0.74	440	70.6
	A3	23.2	200	720	3.00	750	0.79	440	100.8
Thorenfeldt (1990)	B33	55.1	150	207	4.00	250	3.23	500	68.0
	B34	55.1	150	207	3.00	250	3.23	500	82.6
Islam et al. (1998)	M60-S0	48.3	150	207	3.86	250	2.02	554	45.5
	M60-S1	48.3	150	207	2.90	250	2.02	554	92.3
	M60-S3	48.3	150	207	2.90	250	2.02	554	90.4
	M60-S4	48.3	150	207	3.86	250	2.02	554	51.9
	M40-S0	32.7	150	205	3.90	250	3.19	320	55
	M40-S1	32.7	150	205	2.93	250	3.19	320	84.6
	M40-S3	32.7	150	205	2.93	250	3.19	320	80.7
	M25-S0	25.3	150	207	3.86	250	2.02	350	47.5
	M25-S3	25.3	150	207	2.90	250	2.02	350	56.5
Lambolle et al. (1990)	NS-1.07	35.3	200	415	3.01	450	0.97	545	127
	NS-1.45	32.3	200	415	3.01	450	1.45	545	180

Authors	Specimen name	$f_c^{'}$ [MPa]	b [mm]	d [mm]	a / d	h [mm]	ρ [%]	f_y [MPa]	V_{test} [kN]
Kulkami et al. (1998)	B4JL20-S	39.8	102	152	5.00	178	1.37	518	19.5
	B3NO15-S	40.9	102	152	4.00	178	1.37	518	22.7
	B3NO30-S	42.8	102	152	3.50	178	1.37	518	24.2
Coderwail et al. (1974)	734-34	28.2	135	234	3.08	260	0.97	818	41.2
Moody et al. (1954)	A1	28.8	178	262	3.06	305	2.17	310	60.1
	A2	29.5	178	267	3.00	305	2.14	310	66.8
	A3	29.5	178	268	2.99	305	2.23	310	75.7
	A4	29.9	178	270	2.96	305	2.37	310	71.2
	B1	20.1	178	267	3.00	305	1.60	310	56.3
	B2	20.5	178	268	2.99	305	1.63	310	60.1
	B3	18.3	178	270	2.96	305	1.60	310	55.6
	B4	15.9	178	272	2.95	305	1.64	310	55.6
	1	34.9	152	268	3.41	305	1.90	310	57.9
	2	15.9	152	268	3.41	305	1.90	310	35.6
	3	24.5	152	268	3.41	305	1.90	310	52.3
	4	14.6	152	268	3.41	305	1.90	310	40.5
	5	29.2	152	268	3.41	305	1.90	310	52.1
	6	15.0	152	268	3.41	305	1.90	310	34.5
	7	29.4	152	268	3.41	305	1.90	310	51.2
	9	39.1	152	268	3.41	305	1.90	310	53.4
	10	22.7	152	268	3.41	305	1.90	310	49.0
	11	36.2	152	268	3.41	305	1.90	310	60.1
	12	19.2	152	268	3.41	305	1.90	310	47.2
	14	21.4	152	268	3.41	305	1.90	310	43.2
	15	35.5	152	268	3.41	305	1.90	310	51.2
	16	15.5	152	268	3.41	305	1.90	310	37.8
Ferguson (1956)	F2	27.8	101	189	3.23	210	2.08	310	22.3

초 록

이 논문은 위험 균열 경로를 고려한 전단철근이 없는 철근 콘크리트 보의 전단강도를 평가하고 선형탄성파괴역학에서의 혼합 파괴모드를 이용하여 크기 효과를 알아보는데 주목적이 있다. 이러한 선형탄성파괴역학은 균열 선단에서의 응력 상태를 균열의 길이의 함수로 표현할 수 있으므로 전단강도에 대한 크기 효과에 대한 이론적인 근거를 제공해준다.

철근콘크리트 부재의 전단강도와 크기효과에 대한 수많은 실험적, 해석적 연구의 노력에도 불구하고 위험 균열 경로를 고려한 전단 철근이 없는 일반 보와 깊은 보에 대해 크기 효과와 전단 파괴를 설명할 수 있는 근본적인 이론이 여전히 제시되지 못하고 있는 실정이다. 기존의 규준과 제시된 많은 모델은 경험에 의존하고 있으며 아울러 통계적인 방법에 기초하고 있다.

전단강도를 결정하고 철근 콘크리트 보의 크기 효과를 알아보기 위해 위험 균열 경로와 균열 길이에 기초한 파괴 메커니즘을 제안하였다. 이 연구에서는 사인장 파괴와 미끄럼 파괴에서 발생하는 대각 위험 균열 선단에서 이축 응력 상태를 가정한다. 보의 중립축을 기준으로 응력의 변화가 생기며 이는 주요 파괴 모드의 변화를 요구한다. 이러한 파괴는 분리파괴와 미끄러짐 파괴와 같은 재료의 파괴로 정의되었다. 변형을 고려한 강도 모델을 제시하기 위해 수정 모어 쿨롱 이론을 이용하였으며 재료의 파괴 이론을 이용해 파괴 메커니즘을 알아보았다. 대각 균열 선단에서의 응력 상태를 알아보기 위해 재료의 파괴 이론에 의해 결정된 극한 응력과 균열 길이로 표현된 모드-I과 모드-II파괴에 대한 크기에 의존하는 임계 응력 확대 계수를 제안하였다. 응력 확장 계수와 임계 응력 확장 계수와의 관계로부터 크기 효과는 모드-I 파괴와 모드-II 파괴 모두 균열 길이에 관

계된다는 것을 알 수 있다.

전단 철근이 없는 일반보의 전단강도를 구하기 위해 파괴 모드를 위험 균열 경로를 기초로 사인장 파괴와 미끄럼 파괴로 구분하였다. 그리고 압축대의 위험 단면에서는 콘크리트 연화효과가 발생한다고 가정하였다. 또한 사인장 파괴와 미끄럼 파괴에 대해 콘크리트 변형률에 기초한 새로운 휨-전단 거동을 제안하였다. 극한 전단 강도는 휨 거동 곡선과 연화효과를 나타내는 전단 곡선이 만나는 지점에서 결정된다.

전단 철근이 없는 깊은 보의 전단력을 결정하기 위해 일축 압축력을 받는 콘크리트 각기둥의 거동에 대해 알아보았다. 이 각기둥에는 수직응력과 전단응력이 모두 존재한다고 가정하였다. 해석결과 깊은 보에서도 유효 깊이에 대한 크기 효과를 보여주었다.

제안된 모델을 철근콘크리트 전단 철근이 없는 일반 보와 깊은 보의 전단 강도를 추정한다. 제안된 이론은 전단응력에 대해 다양한 콘크리트 강도, 절근비, 전단 스팬비 그리고 유효 깊이를 갖는 일반 보와 깊은 보의 실험 결과와 잘 일치하였다.

위험 균열 경로와 균열 길이에 기초한 제안된 이론적인 모델은 이미 제시된 다른 모델들 보다 철근 콘크리트 보의 크기 효과를 설명하는 데 보다 합리적이다.

주요어 : 위험 균열 경로, 전단강도, 크기효과, 임계응력확대계수, 혼합파괴모드, 파괴 메커니즘

학번 : 2007-30163